Reduction in animal abundance and oxygen availability during and after the end-Triassic mass extinction

Abstract

The end-Triassic biodiversity crisis was one of the most severe mass extinctions in the history of animal life. However, the extent to which the loss of taxonomic diversity was coupled with a reduction in organismal abundance remains to be quantified. Further, the temporal relationship between organismal abundance and local marine redox conditions is lacking in carbonate sections. To address these questions, we measured skeletal grain abundance in shallow-marine limestones by point counting 293 thin sections from four stratigraphic sections across the Triassic/Jurassic boundary in the Lombardy Basin and Apennine Platform of western Tethys. Skeletal abundance decreased abruptly across the Triassic/Jurassic boundary in all stratigraphic sections. The abundance of skeletal organisms remained low throughout the lower-middle Hettangian strata and began to rebound during the late Hettangian and early Sinemurian. A two-way ANOVA indicates that sample age ($p<0.01$, $\eta^2=0.30$) explains more of the variation in skeletal abundance than the depositional environment or paleobathymetry ($p<0.01$, $\eta^2=0.15$). Measured I/Ca ratios, a proxy for local shallow-marine redox conditions, show this same pattern with the lowest I/Ca ratios occurring in the early Hettangian. The close correspondence between oceanic water column oxygen levels and skeletal abundance indicates a connection between redox conditions and benthic organismal abundance across the Triassic/Jurassic boundary. These findings indicate that the end-Triassic mass extinction reduced not only the biodiversity but also the carrying capacity for skeletal organisms in early Hettangian ecosystems, adding to evidence that mass extinction of species generally leads to mass rarity among survivors.

1 Introduction

Predicting the responses of marine ecosystems to extreme environmental change is a task of immense importance for the 21st century, as such predictions are needed to guide effective conservation strategies. The major mass extinctions of the geological past provide our best empirical constraints on such predictions (e.g., Harnik et al., 2012; Blois et al., 2013). These biodiversity crises significantly altered the taxonomic composition and ecological structure of marine ecosystems in response to environmental change (e.g., Droser et al., 2000; Bambach et al., 2002; Wagner et al., 2006; Hull and Darroch, 2013).

Mass extinctions have traditionally been recognized by rapid reductions in taxonomic diversity at regional to global scales (e.g., Raup and Sepkoski, 1982; Bambach, 2006). Taxonomic diversity, however, only partially reflects the evolutionary and ecological effects of mass extinctions. Mass extinction events also impact the biogeographic distributions of taxa (Finnegan et al., 2016; Penn et al., 2018), the relative diversities of different ecological guilds (Schubert and Bottjer, 1995; Roopnarine and Angielczyk, 2015; Dineen et al., 2019), body-size distributions within and among species (Payne, 2005; Atkinson et al., 2019), and the abundances of biomineralizing and bioturbating taxa (Twitchett and Barras, 2004; Knaust, 2010; Cribb and Bottjer, 2020). The relative

taxonomic and ecological significances of mass extinction events often differ, meaning that extinction and recovery must be understood through the analysis not only of taxonomic diversity but also of other dimensions of biodiversity and ecosystem function (Droser et al., 2000; Greene et al., 2011; Hull et al., 2011; McGhee et al., 2013). Some of the most taxonomically severe extinction events, such as the Late Ordovician extinction, had comparatively little effect on the structure of ecosystems (Brenchley et al., 2001; Christie et al., 2013). In other cases, the global taxonomic losses do not consistently predict the composition of post-extinction ecosystems. For instance, the end-Permian mass extinction preferentially reduced taxonomic diversity within heavily calcified clades such as corals, brachiopods, and echinoderms relative to moderately calcified clades such as bivalves and gastropods (Sepkoski et al., 1981; Knoll et al., 1996, 2007a), but some earliest Triassic shallow-marine communities remained dominated by crinoids and brachiopods rather than by bivalves and gastropods (Greene et al., 2011; Brosse et al., 2019).

Explaining and predicting differences between the responses of diversity and abundance across intervals of rapid environmental change is one of the most important unsolved problems in the study of mass extinction and the conservation of future biodiversity and ecosystem function. Reduction in animal abundance, either overall or differentially across clades and functional groups, can fundamentally alter the state of an ecosystem even in the absence of extinction. For example, marine defaunation by commercial fishing has caused population blooms of species at lower trophic levels, such as prawns and sea urchins, in some parts of the ocean (Scheffer et al., 2005; Diaz and Rosenberg, 2008; McCauley et al., 2015). On land, the biomass of large mammals has increased over the past several centuries even as their taxonomic diversity has declined due to the enormous increases in the population sizes of humans as well as domestic cattle, pigs, and sheep (Barnosky et al., 2012).

Despite the importance of overall biomass to trophic transfer efficiency and nutrient cycling, the responses of overall biomass within ecosystems to past mass extinction events remains poorly quantified. Only a few studies across the end-Silurian (Bowman et al., 2020), end-Permian (Payne et al., 2006; Jacobsen et al., 2011), and end-Cretaceous (Hull et al., 2011; Sibert et al., 2014) extinctions provide empirical constraint on changes in animal abundance across mass extinction intervals. The key pattern emerging from this work is that changes in organismal abundance vary considerably in both time and space across different extinction intervals. These few studies have demonstrated that quantifying animal abundance across mass extinctions in a biogeochemical framework can provide a robust picture of the ecological severity of mass extinctions (Hull, 2015). From a functional standpoint, mass rarity may be as important or more important than the reduction of biodiversity (Hull, 2015).

The end-Triassic mass extinction, ca. 201.5 Ma (Blackburn et al., 2013), was the most taxonomically severe mass extinction experienced by a marine fauna that is taxonomically similar to its modern counterpart (Sepkoski et al., 1981; Ritterbush et al., 2015a). The ecological severity of the end-Triassic mass extinction trails only the end-Permian and end-Cretaceous mass extinctions (McGhee Jr et al., 2004; McGhee et al., 2013; Bond and Grasby, 2017). It preferentially impacted the diversity of reef-building taxa like scleractinian corals and sphinctozoan sponges (Hautmann, 2004; Kiessling and Aberhan, 2007; Kiessling et al., 2007; Dunhill et al., 2018). Geological and geochemical data indicate many parallels between the circumstances of the end-Triassic extinction and the "deadly trio" (Pörtner et al., 2004) of climate warming, ocean deoxygenation, and ocean acidification that imperil extant marine animals. During the end-Triassic

mass extinction, volcanism in the Central Atlantic Magmatic Province (CAMP) caused the massive injection of isotopically light carbon into the atmosphere (Ruhl and Kürschner, 2011; Bachan et al., 2012; Fox et al., 2020). Sedimentary and geochemical proxy data indicate a resulting drop in the ocean pH (Greene et al., 2011), rise in temperature of about 10 °C in the tropics (Pálfy et al., 2007), and expansion of anoxic and euxinic bottom waters (van de Schootbrugge et al., 2007; Richoz et al., 2012; Kasprak et al., 2015; Jost et al., 2017b; Atkinson and Wignall, 2019; Larina et al., 2019; He et al., 2020).

Although the taxonomic severity and environmental circumstances of the end-Triassic extinction are increasingly well constrained, their impact on the abundances of animals and other well-fossilized taxa (e.g., foraminifera and calcareous algae) remain essentially unknown due to the lack of relevant data. To fill this knowledge gap, here we quantify changes in organismal abundance across the Triassic/Jurassic transition by generating limestone compositional data across four stratigraphic sections spanning the Triassic/Jurassic boundary in the Tethys realm. By standardizing skeletal content relative to rock volume in carbonate-rich depositional environments and by investigating changes in skeletal content across depositional settings, we provide the first estimate of overall changes in the biomass of skeletal animals, calcareous algae, and foraminifera. Because physiological data and evidence from both the modern ocean (Deutsch et al., 2015) and the end-Permian mass extinction (Penn et al., 2018b) indicate that the effects of oxygen availability for aerobic organisms present an important control on extinction and biogeography, we also reconstruct the variation in redox conditions for two of the sections through measurement of I/Ca ratios.

2 Geological setting

2.1 Overview

The shallow-marine carbonate sediments exposed in the southern Alps (Lombardy Basin) and southern Apennines of Italy record sedimentation in two distinct paleogeographic domains of western Tethys during the Mesozoic (Fig.1). These paleogeographic domains reflect the Triassic rifting of Pangaea, which led to closure of the Paleotethys Ocean and expansion of the Neotethys Ocean in the Late Triassic (Haas et al., 1995; Schettino and Turco, 2011). As a result of rifting, a series of fault-controlled, intra-platform basins developed across the western Mediterranean. Shallow-marine carbonate platforms developed during this time in the northern and southern parts of western Tethys (Stampfli et al., 2001; Iannace and Zamparelli, 2002). The platforms exposed in the northern, central, and southern Apennines of Italy developed in connection with the Ionian Arm of Tethys, which opened in the Middle Triassic (Ciarapica and Passeri, 2005). Sedimentary deposits of the Northern Calcareous Alps developed in connection with the Alpine Ocean (also referred to as the Ligurian-Piedmont Ocean), which started opening in the Late Triassic to Early Jurassic (Bertotti et al., 1993; Jadoul et al., 2005) (Fig.1).

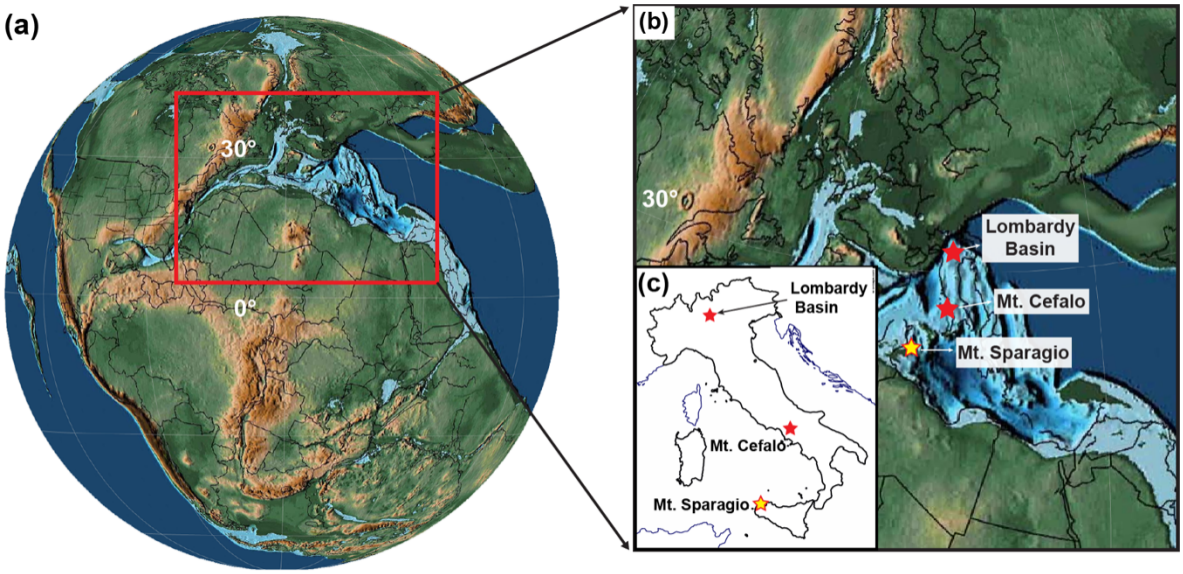

123
124

125 *Figure 1:* ***Paleogeography and study site locations.*** *Panel (a) shows the Early Jurassic*
126 *paleogeography modified using the GPLATES software. Panel (b) indicates the paleogeographic*
127 *locations of the Lombardy Basin (southern Alps), Mt. Cefalo (southern Apennines) and Mt.*
128 *Sparagio (Sicily) sections in the Tethys sea. Panel (c) shows the present-day locations of*
129 *aforementioned sections in Italy. The GPS coordinates for the sections studies in this study are:*
130 *Italcementi:* 45°46′33.83″N 9°31′9.91″E *, Val Adrara:* 45°43′29.33″N 9°57′32.29″E *, Pozzo*
131 *Glaciale:* 45°41′5.99″N 10°2′56.83″E *, Mt. Cefalo:* 41°15′32.05″N 13°32′10.50″E. The
132 approximate location of Mt. Sparagio section was obtained from He et al. (2022a). *The*
133 *paleogeographic maps are from* Scotese, (2016)*. The outline map of Italy was downloaded from*
134 *www.d-maps.com using this link: https://d-maps.com/carte.php?num_car=2322&lang=en*

135

136 **2.2 Lombardy Basin**

137 The Lombardy Basin was in close proximity to the European continent during the Late Triassic
138 and Early Jurassic (Fig. 1) and was a site of sediment accumulation in an active rift basin (Jadoul
139 et al., 1992, 2004; Berra et al., 2010). Rifting led to development of horst and graben structures,
140 which became sites of carbonate sedimentation (Jadoul et al., 1992). During the Norian, shallow-
141 marine carbonates accumulated on structural highs and bedded turbiditic limestones accumulated
142 in deeper intra-platform troughs. Rifting slowed during the late Norian and a west-to-east-dipping
143 homoclinal ramp developed (Jadoul et al., 1992, 2004). The Rhaetian-Hettangian ramp carbonates
144 in the Lombardy Basin increase in thickness from west to east due to differential subsidence
145 associated with rifting. Basin-wide marine transgression during the late Hettangian led to
146 deposition of chert-rich sediments of the Sedrina and Moltrasio limestones. The platform
147 ultimately drowned early in the Sinemurian (McRoberts, 1994; Jadoul et al., 2004).

The Rhaetian-Hettangian sedimentary succession in the Lombardy Basin of the south-western Alps consists of shallow-marine ramp carbonates (Galli et al., 2007). The Rhaetian succession of the Lombardy Basin is represented by the Zu Limestone (Figs. 2(a, b, c), 3, 4). The Zu Limestone is a fossiliferous packstone to framestone with a diverse open marine fauna consisting of bivalves, gastropods, and large benthic foraminifera with subordinate corals, brachiopods, ostracods, and echinoderms (Fig. 2). The Zu Limestone is abruptly overlain by the Malanotte Formation, which has been assigned a Hettangian age based on pollen content and carbon isotope chemostratigraphy (van de Schootbrugge et al., 2008). The lower Malanotte Formation is an unfossiliferous marl (Figs. 3, 4). The marl is overlain by carbonate-rich mudstones and wackestones containing rare mollusks (Fig. 2). The middle-upper Malanotte Formation is composed of oolitic sands and peloidal packstone indicating a shallowing-upward trend (Galli et al., 2007; Jadoul and Galli, 2008). The Albenza Formation overlies the Malanotte Formation and is composed of oolitic grainstone and oncoidal packstone indicating deposition in a shallow-marine environment (Figs. 2-5; Galli et al., 2007; Jadoul and Galli, 2008). The Albenza Formation carbonates also contain some stratigraphically limited intervals exhibiting fabric destructive dolomitization. The Sedrina Limestone, which overlies the Albenza Formation, is a cherty, sponge-rich limestone at the Val Adrara locality. It is composed of thin- to medium-bedded mudstones and wackestones and lacks visible bedforms, thus indicating deposition in a deep-water, distal ramp setting (McRoberts, 1994; Bachan et al., 2012). At the Pozzo Glaciale section, the Sedrina Limestone is composed of oncolitic and oolitic grainstone to packstone, indicating deposition in a subtidal, open-marine environment (McRoberts, 1994; Jadoul and Galli, 2008) (Figs. 3-5). The Pozzo Glaciale section has been interpreted as the eastern margin of the Lombardian Platform (Fig. 5; McRoberts, 1994; Jadoul and Galli, 2008). The Moltrasio Limestone, which overlies the entire Lombardy Basin, is composed of chert-bearing mudstone and marks the final drowning of the Lombardian Platform (Fig. 2; McRoberts, 1994; Jadoul and Galli, 2008).

In this study, we analyzed hand samples from the three measured stratigraphic sections within a broad shallow-to-deep depositional gradient in the Lombardy Basin: Italcementi, Val Adrara, and Pozzo Glaciale (Figs. 3-5). The sections can be correlated based on the formation boundaries, supplemented by carbon isotope chemostratigraphy (Galli et al., 2005; Bachan et al., 2012). Biostratigraphic age assignments are based on Gaetani (1970), Lakew (1990, 1994), McRoberts (1994), and Muttoni et al. (2010).

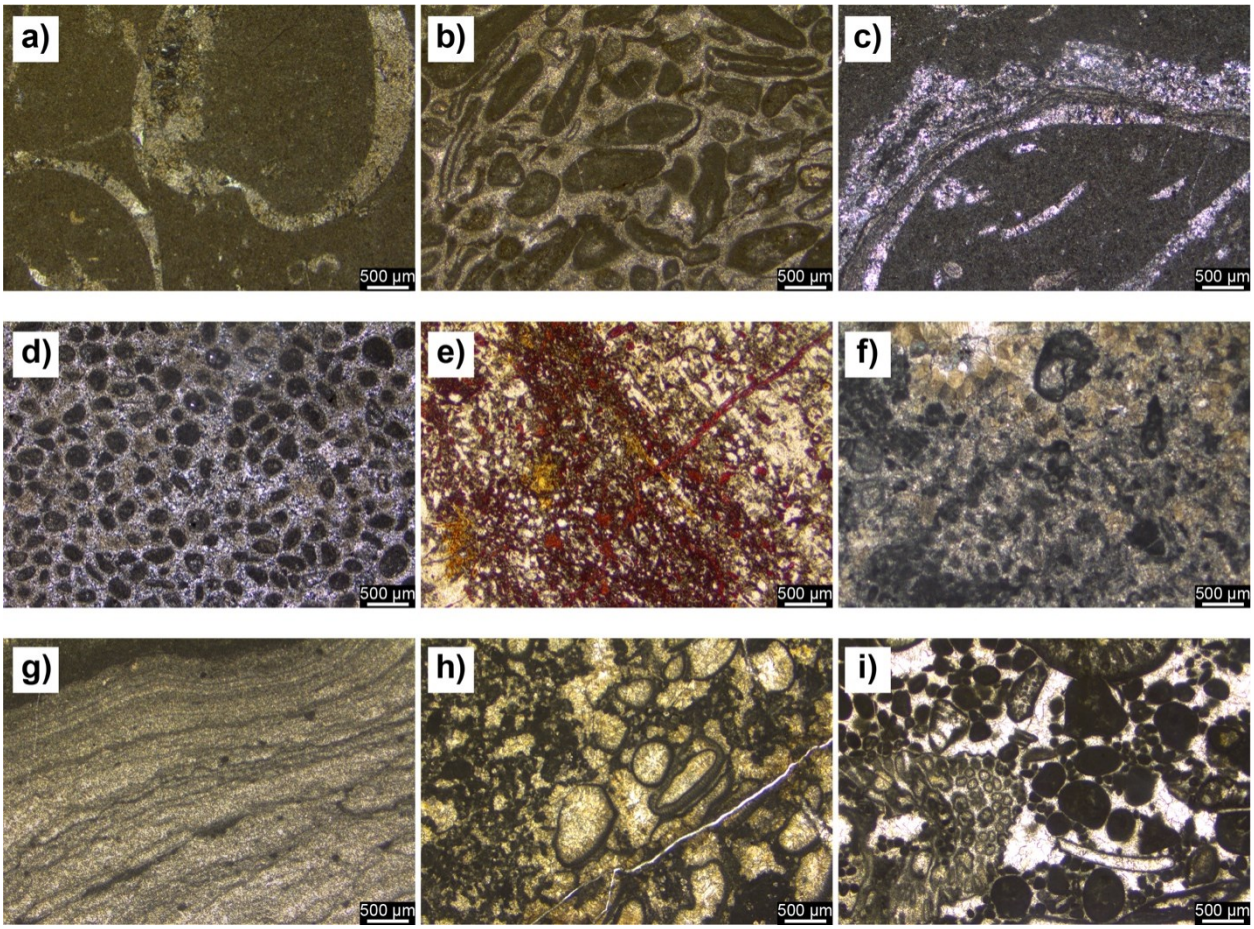

*Figure 2: Thin section photomicrographs illustrating microfacies from the Lombardy Basin and Apennine Platform. (a) Skeletal packstone from the Rhaetian Zu Limestone showing megalodontid bivalve fragments (Italcementi section), (b) Peloidal grainstone from the Rhaetian Zu Limestone (Italcementi section), (c) Bivalve-rich skeletal packstone from the Rhaetian Zu limestone (Val Adrara section), (d) Oolitic grainstone from lower Hettangian Albenza Formation (Val Adrara section), (e) Sponge spicules from early Sinemurian Moltrasio Limestone (Pozzo Glaciale section), (f)The Rhaetian association of dasyclad green algae (*Gryphoporella curvata*) and problematic algae (*Thaumatoporella parvovesiculifera*) from Mt. Cefalo section, (g) Laminar stromatolites from the early Hettangian (Mt. Cefalo section), (h) Problematic algae in a clotted microbial fabric (lower Hettangian, Mt. Cefalo section), (i) Open-marine, subtidal assemblage of calcareous green algae, bivalves, and peloids in upper Sinemurian-lower Pliensbachian Mt. Cefalo section.*

2.3 Apennine Platform

The Mt. Cefalo section is part of the vast, shallow-marine carbonate succession of the Apennine Platform (Fig. 1). It was deposited in the south-western Tethys close to the deep-water, Ionian arm of Tethys. The peritidal sedimentary successions from this shelf are exposed in the central and southern Apennines (Mancinelli et al., 2005; Di Stefano et al., 2015), western Sicily (Todaro et al., 2016, 2017), Greece (Romano et al., 2008), and Turkey (Coskun Tunaboylu et al., 2014).

The measured section is part of a thick Mesozoic carbonate succession deposited from the Late Triassic to Cretaceous in the northern, central, and southern Apennines of Italy (Fig. 6). The sediments from Mt. Cefalo were deposited in a shallow-marine, peritidal environment (Mancinelli et al., 2005, Bachan et al., 2012). The meter-scale cycles at Mt. Cefalo, the shallowest section of our four sections, are typically composed of allochem-rich packstone and grainstone capped by fenestral boundstones (Fig. 2). The cycles alternate between microfacies containing clotted and filamentous microbialites exhibiting fenestral fabrics indicating an intertidal to supratidal depositional environment and microfacies containing calcareous algae and benthic foraminifera and lacking fenestral fabrics, suggesting deposition in a shallow subtidal to restricted lagoon setting (Mancinelli et al., 2005, Bachan et al., 2012). The Rhaetian fossil assemblage is dominated by dasyclad green algae (*Gryphoporella curvata*), large benthic foraminifera (*Triasina hantkeni*), megalodontid bivalves, gastropods, echinoderms, ostracods, and problematic algae (*Thaumatoporella parvovesiculifera*) (Fig. 2). The Hettangian-lower Sinemurian (110-270 m) assemblage is distinguished by an absence of megalodontid bivalves, dasyclad algae, and large benthic foraminifera. The Hettangian-lower Sinemurian biota is dominated by problematic algae with minor mollusks. Dasyclad algae reappear and become more common in the upper Sinemurian-lower Pliensbachian strata (270-325 m) along with a rich assemblage of large benthic foraminifera (Mancinelli et al., 2005) (Fig. 2).

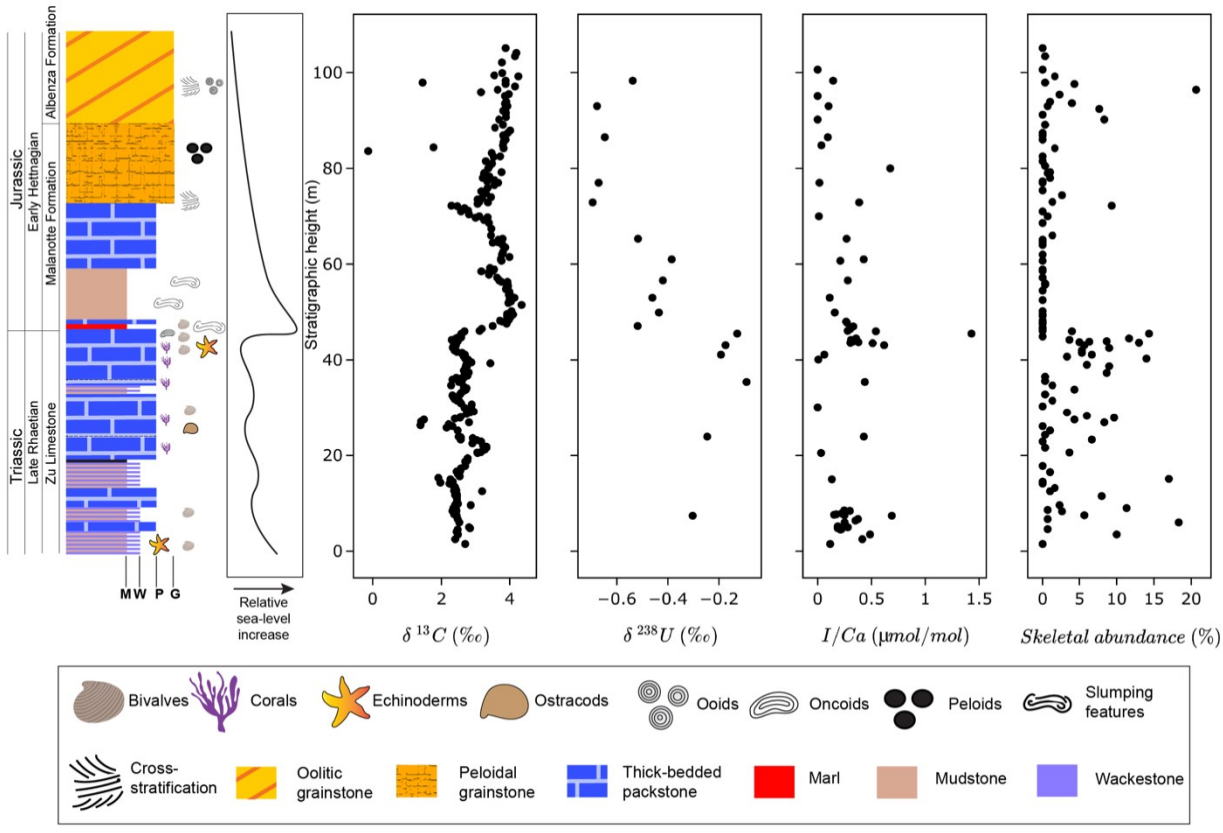

Figure 3: The variations in carbonate carbon isotope ratios ($\delta^{!"}C$; Bachan et al., 2012), uranium isotopes ratios ($\delta^{\#"\$}U$; Jost et al., 2017), I/Ca ratios and skeletal abundance at the Italcementi section in the Lombardy Basin (this study).

3 Materials and Methods

The samples used in this study were collected from four measured stratigraphic sections, three from the Lombardy Basin (Figs. 3-5) in the southern Alps and one (Mt. Cefalo) from the Apennine Platform (Fig. 6) in the southern Apennines. The hand samples were used for the compositional analysis and I/Ca measurements. A total of 370 (Italcementi: 159, Val Adrara: 169, Pozzo Glaciale: 42) samples were studied from the Lombardy Basin, and 67 samples were studied from the Apennine Platform section at Mt. Cefalo. The number of samples analyzed for both composition and I/Ca ratio amounted to 26 and 15 for the Italcementi Val Adrara sections respectively.

3.1 Compositional analysis of marine limestones

In this study, a total of 293 samples: 112, 72, 42 from Italcementi, Val Adrara and Pozzo Glaciale, respectively, and 67 from Mt. Cefalo were chosen for thin sectioning. The proportional content of

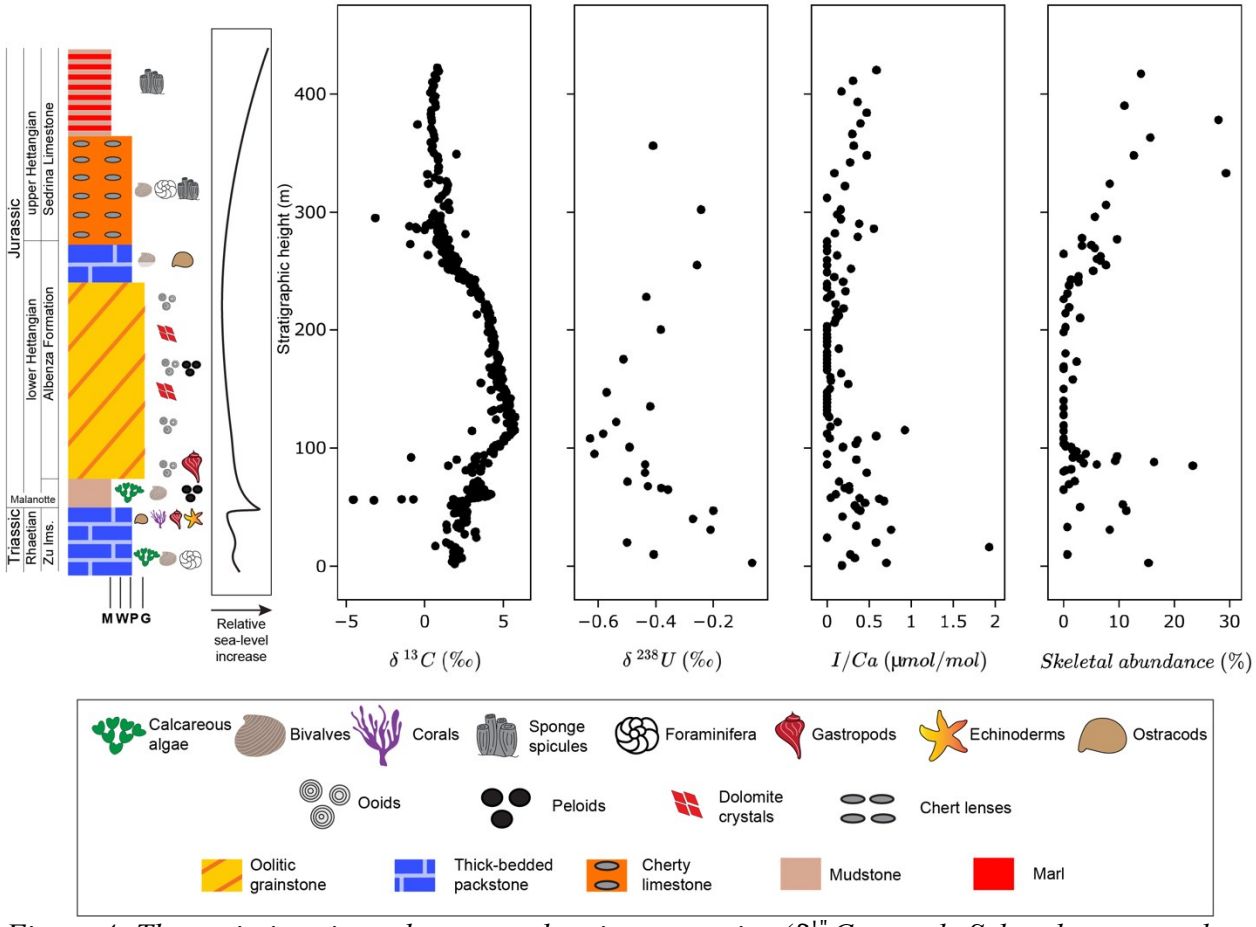

Figure 4: The variations in carbonate carbon isotope ratios ($\delta^{!"}C$; van de Schootbrugge et al., 2008; Bachan et al., 2012), uranium isotopes ratios ($\delta^{\#"\$}U$; Jost et al., 2017), I/Ca ratios and skeletal abundance at the Val Adrara section in the Lombardy Basin (this study). The age model is based on Bachan and Payne (2016).

grains, matrix, cement, and void space was quantified via compositional analysis. Compositional analysis was conducted by counting 300 points per thin section (size: 26mm X 46mm) across the Rhaetian-Hettangian interval in the Lombardy Basin and Mt. Cefalo section from the Apennine Platform (Table S1). Specifically, samples were point-counted using a mechanical stage following the grain-solid method (Flügel, 2010). Skeletal grains were assigned to higher taxonomic groups when identifiable, down to the Linnaean class level where possible. The categories used for compositional analysis were: bivalves, gastropods, brachiopods, echinoderms, ostracods, corals, bryozoans, sponges, foraminifera, red algae, green algae, problematica, unidentified biota, filamentous microbial fabric, clotted microbial fabric, micrite, micrite clasts, peloid, radiaxial fibrous calcite cement, blocky calcite cement, microsparite, dolomite, and ooids. The microbial components were point-counted by the presence of clotted and filamentous fabric in thin sections. Microbial components were not included in the calculation of total skeletal abundance calculation, which focused on enzymatically controlled carbonate skeletons.

The diversity of skeletal components in limestone samples was quantified by a comprehensive survey of each thin section. The diversity of a thin section is represented by the number of distinct taxonomic categories observed (Table S2). The total diversity of a thin section was quantified as the number of distinct categories of enzymatically controlled skeletal grains present in the thin section (see above for the categories used). For instance, if a thin section contained only calcareous algae and bivalves, then its diversity would be noted as two. This approach ensured that a skeletal grain that was not counted while point counting would still be accounted for in the total diversity.

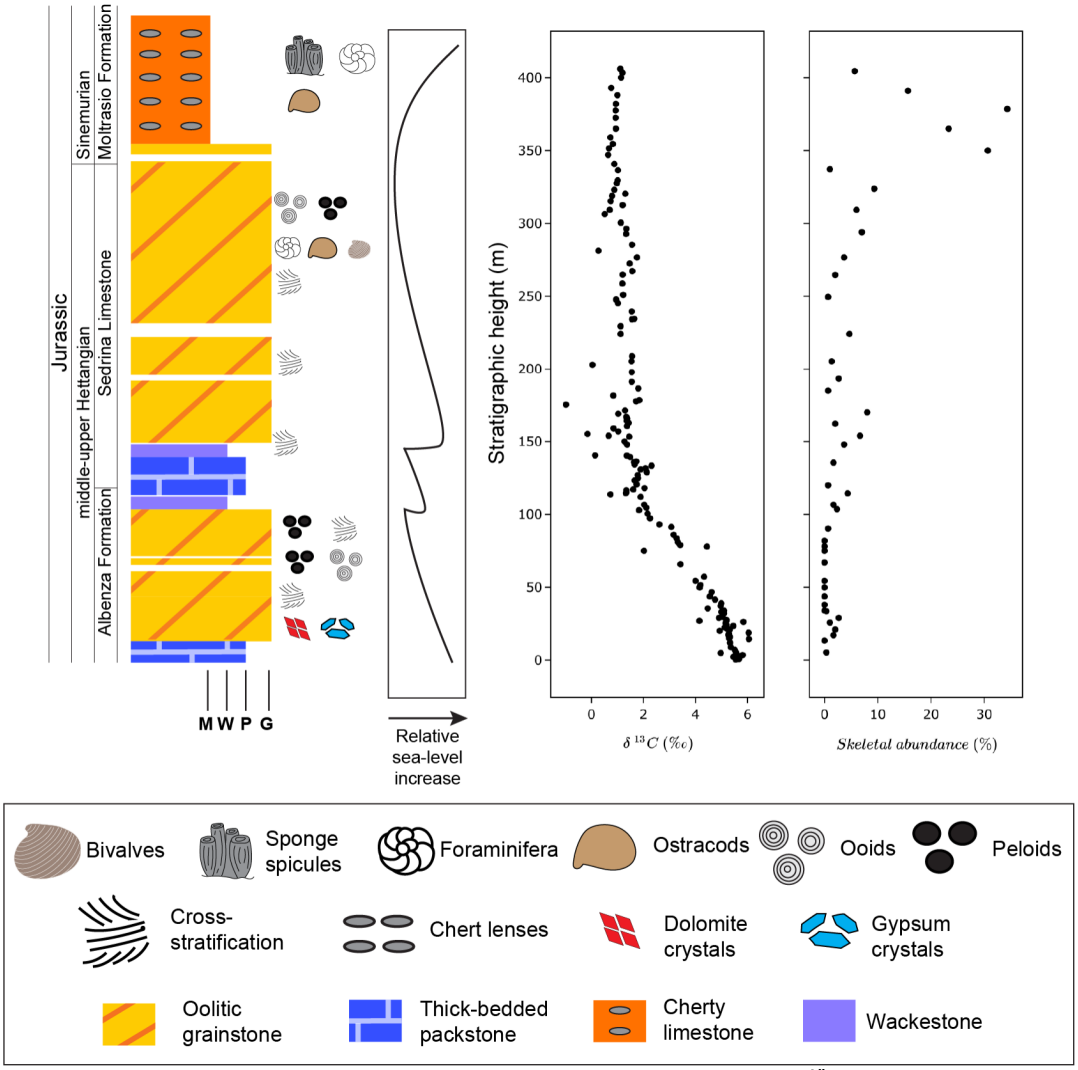

Figure 5: The variations in carbonate carbon isotope ratios ($\delta^{13}C$; van de Schootbrugge et al., 2008; Bachan et al., 2012) and skeletal abundance at the Pozzo Glaciale section in the eastern edge of Lombardy Basin (this study).

3.2 I/Ca as a redox proxy

The I/Ca ratio of marine limestone has been established as a paleo-proxy for shallow-marine redox conditions (Lu et al., 2010, 2018; Zhou et al., 2014, 2015; Hardisty et al., 2017). The residence time of iodine in seawater is ~300 ky, which is much greater than the seawater circulation time (~1 ky). Although the concentration of iodine in the ocean can be assumed to be globally uniform (Chance et al., 2014), its speciation is spatially variable. The dissolved inorganic iodine is dominantly present in its thermodynamically stable forms of iodate (IO_3^-) and iodide (I^-) ions in seawater (Wong and Brewer, 1977). The standard reduction potential of IO_3^-/I^- is very close to that of O_2/H_2O, thus making the speciation of iodine very sensitive to dissolved oxygen concentrations. In oxic conditions, most iodine occurs as iodate and is reduced to iodide in dysoxic to anoxic conditions.

In the modern ocean, the concentration of iodate qualitatively tracks the concentration of dissolved oxygen in seawater (Truesdale et al., 2000; Lu et al., 2016). In the well-oxygenated upper ocean, iodate is the dominant iodine species whereas in anoxic basins and in oxygen minimum zones (OMZs), iodide is dominant (Wong and Brewer, 1977; Emerson et al., 1979). During formation of carbonate sediment, only iodate is incorporated into the carbonate lattice (Lu et al., 2010). Consequently, the concentration of iodine relative to calcium in limestone is sensitive to the dissolved oxygen concentration in the seawater from which it was precipitated (Lu et al., 2010).

In total, 104 samples from the Val Adrara and Italcementi sections of the Lombardy Basin were analyzed for I/Ca ratios following the methods of Lu et al. (2018) (Table S3). The I and Ca concentrations were measured on a Bruker M90 quadrupole inductively-coupled-plasma mass spectrometer (ICP-MS) housed at Syracuse University. For the analysis, 3-5 mg of powdered limestone (extracted using 0.8 mm drill bit) samples were weighed out, thoroughly rinsed with de-ionized water, and then dissolved in 3% HNO_3 acid. The solutions were diluted for analysis to achieve ~50 ppm Ca. To stabilize iodine, 0.5% tertiary amine solution was added to each solution. For analysis, 5 ppb of Sc and Cs were added as internal standards. The detection limit of I/Ca is around 0.1 μmol/mol. The sensitivity of ^{127}I is tuned to about 80–100 kcps for a 1 ppb standard. The precision of ^{127}I is typically better than 1%. The long-term precision is assessed with repeated measurements of the reference material JCp-1 (Lu et al., 2010) and was 3.70 ± 0.27 μmol/mol (1σ) (n=2,280) (Lu et al., 2020). The I/Ca values of samples were corrected by adjusting the value of

294 the adjacent JCp-1 measurements to 4

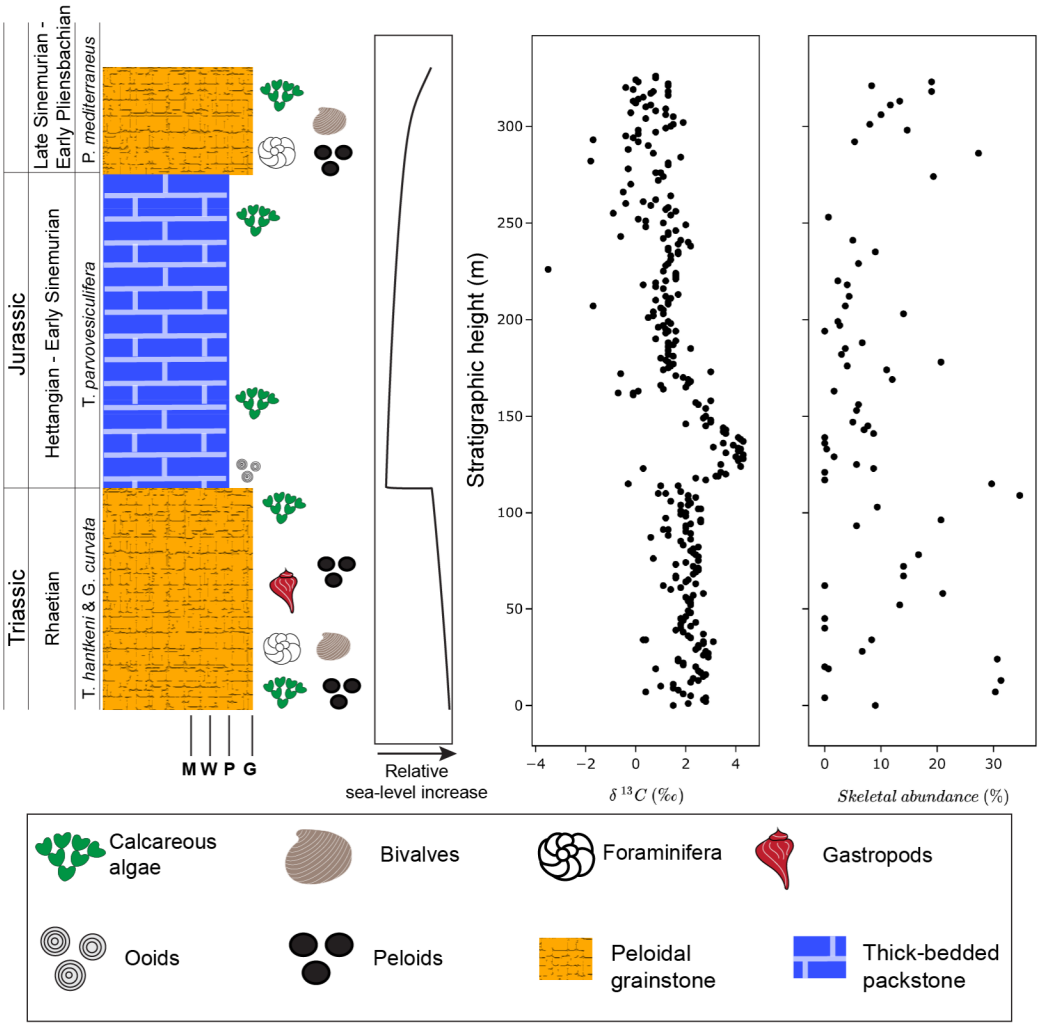

295
296 *Figure 6: The variations in carbonate carbon isotope ratios ($\delta^{13}C$; Bachan et al., 2012) and*
297 *skeletal abundance in the Mt. Cefalo section of the Apennine platform (this study).*
298

299 **4 Results**

300 **4.1 Compositional analysis of marine limestones**

301 The Lombardy Basin and the Apennine Platform both record a drop in skeletal abundance across
302 the Triassic-Jurassic boundary (Figs. 3–6). All three stratigraphic sections indicate a statistically
303 significant change in the skeletal abundance across the Upper Triassic and Lower Jurassic time
304 intervals (binned into time intervals defined by the stratigraphic or biostratigraphic constraints for
305 each stratigraphic section as depicted in Figs. 3-6; one-way ANOVA results: Mt. Cefalo: $p<0.01$,
306 Italcementi: $p<0.01$, Val Adrara: $p=0.01$) (Fig. 7). Furthermore, a two-way ANOVA on all 293
307 samples across the four stratigraphic sections shows that the time interval ($p<0.01$, $\eta^2=0.30$)
308 explains more of the variation in skeletal content than which stratigraphic section the sample is

from (p<0.01, η^2=0.15). To test this finding further, we conducted another two-way ANOVA consisting of samples from the same ramp, but different water depths from the Italcementi and Val Adrara sections. The results again showed similar results with more of the variation in skeletal abundance explained by time interval (p<0.01, η^2=0.37) than by stratigraphic section (p<0.01, η^2=0.12).

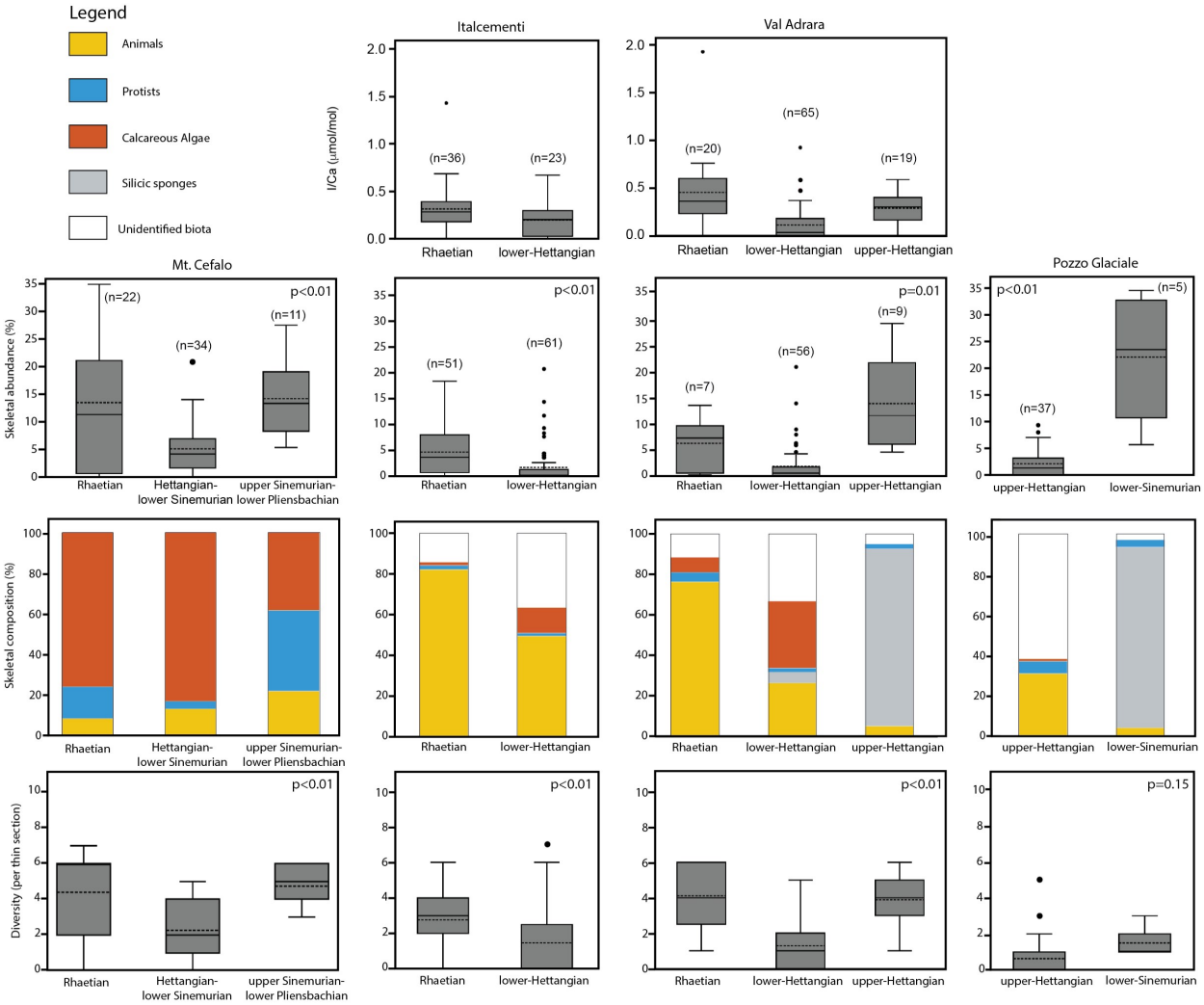

Figure 7: Box plots showing changes in I/Ca ratios, skeletal abundance, skeletal composition, diversity (per thin section) in Upper Triassic and Lower Jurassic limestones from the Lombardy Basin (Italcementi, Val Adrara, Pozzo Glaciale) and Apennine Platform (Mt. Cefalo) sections. "n" indicates the number of samples in each category. The figure broadly depicts significant changes in the skeletal abundance, biotic composition and diversity in marine ecosystems during the Triassic/Jurassic transition along with the redox chemistry as depicted by I/Ca ratios.

The composition of skeletal material across Lombardy Basin and Apennine Platform stratigraphic sections differed significantly depending on the depositional environment and time interval (Fig. 7). The main difference between the Lombardy Basin and Apennine Platform limestones is the dominance of non-poriferan animals as skeleton producers in the Lombardy Basin whereas calcareous algae and protists are the skeletal grains in the Apennine Platform (Fig. 7). The Rhaetian Zu Limestone at Italcementi and Val Adrara is primarily composed of non-poriferan animal

skeletons (~80%) with protists and calcareous algae forming a minor (<5%) component of skeletal material. The proportion of non-poriferan animal skeletal material as a fraction of all skeletal material decreased in the lower Hettangian strata in both Italcementi and Val Adrara sections whereas the proportion of calcareous algae increased. In the upper Hettangian Sedrina limestone, the Val Adrara locality shows evidence of a rapid increase of water depth evident from the well-bedded carbonate mudstone-wackestone facies rich in sponge spicules floating in a micritic matrix (McRoberts, 1994; Bachan et al., 2012). The skeletal component of limestones at this location is primarily hexactinellid sponges (88%) with minor contributions from non-poriferan calcifying animals and protists. This composition contrasts with that of Pozzo Glaciale, where the identifiable skeletal components are entirely composed of non-poriferan animals and protists. The deepening trend continued across the entire Lombardy Basin during the late Sinemurian and led to deposition of the Moltrasio Limestone, which primarily contains hexactinellid sponges (89%) (Fig. 4, 5, 7).

In the Apennine Platform, the peritidal facies at Mt. Cefalo are primarily composed of calcareous algae (>75%) in the Rhaetian and Hettangian-early Sinemurian strata (Fig. 7). The composition of skeletal material changed significantly in the upper Sinemurian and lower Pliensbachian strata with a significant contribution from benthic foraminifera (~40%) and animals (~22%).

Similar to the skeletal abundance trends, the mean (and median) diversity per sample dropped significantly across the Triassic-Jurassic boundary in both Lombardy Basin and Apennine Platform sections (one-way ANOVA analysis, Mt. Cefalo: $p<0.01$, Italcementi: $p<0.01$, Val Adrara: $p<0.01$) (Fig. 7). The variations in taxonomic diversity across the four stratigraphic sections are more strongly associated with changes in time interval (two-way ANOVA: $p<0.01$, $\eta^2=0.19$) than with the identity of the stratigraphic section (two-way ANOVA: $p<0.01$, $\eta^2=0.09$). Furthermore, the frequency with which biota from dominant taxonomic categories occurred in samples also decreased sharply across the Triassic-Jurassic boundary (Fig. S1).

4.2 I/Ca ratios of bulk carbonate samples

Iodine/calcium background values in both sections are generally low (< 2 μmol/mol). The I/Ca ratios decline between the Rhaetian and Hettangian at both Italcementi and Val Adrara (Figs. 3, 4, 7). These declines are statistically significant or marginally significant in both the Val Adrara (one-way ANOVA: $p<0.01$) and Italcementi (one-way ANOVA: $p=0.05$) sections (Fig. 7). The limestone samples from the Rhaetian (Zu Limestone) of the Lombardy Basin show I/Ca ratios in the range of <0.01 to 0.70 μmol/mol (Figs. 3, 4). In the Italcementi section, the mean I/Ca ratio is 0.30 ± 0.25 μmol/mol (1$\boldsymbol{\sigma}$, n=36) whereas the Val Adrara section shows a slightly higher mean I/Ca ratio of 0.45 ± 0.40 μmol/mol (1$\boldsymbol{\sigma}$, n=20; Figs. 2, 3). Overall, the I/Ca ratios in the Rhaetian Zu Limestone of Lombardy Basin decrease towards the Rhaetian-Hettangian boundary. The decreasing trend continues into the lower Hettangian Malanotte and Albenza formations. At the Italcementi section, the mean I/Ca ratio is 0.20 ± 0.16 μmol/mol (1$\boldsymbol{\sigma}$, n=23) whereas in the Val Adrara section, the mean I/Ca ratio is 0.10 ± 0.17 μmol/mol (1$\boldsymbol{\sigma}$, n=65) in the lower-Hettangian strata. In the upper Hettangian Sedrina limestone exposed only at Val Adrara locality, the I/Ca ratio shows a slight increasing trend towards the top of the section and reaches a mean ratio of 0.28 ± 0.16 μmol/mol (1$\boldsymbol{\sigma}$, n=19) (Figs. 3, 4).

5 Discussion

5.1 Ecological changes across the Triassic/Jurassic boundary in the Lombardy Basin

The compositional changes in shallow-marine carbonates across the Triassic-Jurassic boundary in the Lombardy Basin and Apennine Platform indicate a significant decrease in the abundance and diversity of marine organisms in shallow-marine ecosystems across the extinction interval that cannot be explained by local facies variation (Fig. 8). The decrease in skeletal abundance and diversity occurs across a variety of depositional environments ranging from proximal to distal ramp environments of the Lombardy Basin and to peritidal environments of the Apennine Platform. In addition, variation in skeletal content among time intervals is larger than variation among stratigraphic sections. Thus, the observed variations in the skeletal abundance are best interpreted to reflect an external control acting across all sampled locations irrespective of the depositional setting.

The decrease in skeletal content across the Triassic/Jurassic boundary cannot be explained by related changes in the depositional environments represented across the two basins (Fig. 8). In the Lombardy Basin, the Rhaetian Zu Limestone is dominantly composed of open-marine fauna deposited in a shallow-marine environment in both the proximal ramp section at Italcementi and the more distal section at Val Adrara. The overlying Malanotte Formation is composed of marls overlain by thin-bedded carbonate mudstones indicating a rise in relative sea level (Bachan et al., 2012). This abrupt change in carbonate sedimentation has been interpreted as a transgressive event that can be traced across the Lombardy Basin and into the Northern Calcareous Alps of western Tethys (McRoberts et al., 1997). The subsequent shallowing indicated by deposition of cross-bedded oolitic and peloidal limestones of the Albenza Formation did not, however, coincide with an increase in skeletal grain abundance. Instead, the skeletal abundance decreased sharply in the lower-middle Hettangian Malanotte Formation and stayed low throughout the lower-middle Hettangian Albenza Formation. The low skeletal abundance at both Italcementi (proximal ramp) and Val Adrara (distal ramp) sections indicates that this pattern is not an artifact of local high-energy environments but was a common occurrence across the entire ramp of Lombardy Basin during that time.

This pattern of reduced skeletal abundance and a shift to a non-skeletal carbonate factory also occurs at the Mt. Cefalo section and across the entire Apennine Platform (Barattolo and Romano, 2005; Mancinelli et al., 2005; Brandano et al., 2016; Todaro et al., 2017). The skeletal content at Mt. Cefalo is consistent with observations of physical sedimentary structures that indicate deposition in a peritidal environment across the Rhaetian/Hettangian transition (see Bachan et al. (2012) for detailed stratigraphy). The Rhaetian intertidal facies are composed of stromatolitic laminites whereas the subtidal facies are composed of bioturbated limestones rich in large benthic foraminifera (*T. hantkeni*) and calcareous algae (*G. curvata*). The Triassic/Jurassic boundary is marked by a subaerial exposure surface associated with a sea-level drop that can be traced across the entire Apennine Platform (Berra, 2012; Cirilli et al., 2015; Todaro et al., 2017). The limestone immediately above the exposure surface is oolitic grainstone containing very little skeletal material, indicating the demise of the biological carbonate factory and a shift to a non-skeletal mode of carbonate precipitation. The oolitic limestones are overlain by laminated fenestral boundstones indicating a microbial mode of carbonate precipitation with few intervals rich in calcareous algae but almost devoid of animals and protists. The compositional data from Mt. Cefalo indicates that ecosystems in peritidal environments contained few skeletal animals following the end-Triassic mass extinction and that carbonate precipitation was dominantly abiotic

and microbially induced. This shift from metazoan-dominated to microbial and abiotic modes of carbonate precipitation in early-Hettangian is not unique to Mt. Cefalo: compositional data from northern and central Apennines (Brandano et al., 2016) show similar shifts in limestone composition across the Triassic/Jurassic boundary. This finding further supports the interpretation that the facies shifts at Mt. Cefalo are indicative of a more widespread pattern in carbonate deposition rather than a local shift in the depositional environment. The facies pattern in upper Hettangian-lower Sinemurian at Mt. Cefalo records a shift in sedimentation in an open marine peritidal environment with thicker subtidal intervals. However, the overall metazoan abundance remained low throughout the Hettangian and early Sinemurian indicating that the changes in biotic abundance transcended the shift in depositional environment (Fig. 6).

Like the abundance patterns, the diversity data is also indicative of a biotic crisis at the end of the Triassic period in Lombardy Basin and Apennine platform. The overall diversity of taxa per sample decreased sharply across the Triassic-Jurassic transition. The fossil occurrences of dominant taxonomic categories when plotted as the percentage of samples in which they appear indicates not only that the taxa became less abundant but also that the frequency with which they occurred decreased substantially (Fig. S1).

The close similarities in skeletal abundance and diversity patterns across the Triassic/Jurassic boundary between the widely separated regions (~500 km) of the Lombardy Basin and the Apennine Platform are also representative of a more general pattern across the western Tethys. This pattern of reduced animal abundance across the Triassic/Jurassic boundary followed by establishment of abiotic and microbial carbonate factories during the Early Jurassic occurred also in the Northern Calcareous Alps in Austria (McRoberts et al., 1997), the Transdanubian Range in Hungary (Palfy et al., 2021), the central and northern Apennines of Italy (Barattolo and Romano, 2005; Mancinelli et al., 2005; Brandano et al., 2016), western Sicily (Todaro et al., 2017, 2018), Greece (Romano et al., 2008) and Turkey (Coskun Tunaboylu et al., 2014). The recovery of skeletal abundance to pre-extinction levels in shallow-marine environments across western Tethyan carbonate platforms occurred in upper Hettangian-Sinemurian limestones with an increase in skeletal contribution from protists and mollusks. Overall, the Early Jurassic ecosystems of western Tethys supported far less benthic biomass and diversity than their Late Triassic counterparts.

The changes in shallow-marine ecosystems in the western Tethys are also representative of a global biotic crisis that unfolded at the end of the Triassic. In the southern Tethys, the shallow-marine platforms of the Arabian plate record a decrease in skeletal abundance across the Triassic/Jurassic boundary and a shift to an abiotic carbonate factory dominated by ooids (Al-Suwaidi et al., 2016, Ge et al., 2018). Evidence from eastern Panthalassa indicates a different extinction pattern than Tethyan sections. During the Early Jurassic, calcifying organisms decreased in abundance and were replaced by silicic demosponges in middle- to inner-ramp environments in Peru (Ritterbush et al., 2014, 2015b; Corsetti et al., 2015) and Nevada (Ritterbush et al., 2015b, 2016). The post-extinction facies in the Lombardy Basin (this study) and the Eiberg Basin of western Tethys (Delecat and Reitner, 2005) show a similar increase in silicifying hexactinellid sponges in upper Hettangian and lower Sinemurian strata. However, it is challenging to compare them with the Panthalassic ramp sections because the intra-platform basins in the Northern Calcareous Alps experienced a rise in relative sea level beginning in middle-late Hettangian that coincided with an increase in the sponge abundance. Hence, it is unclear whether the increase in abundance of

sponges in the Lombardy and Eiberg Basins was a response to the end-Triassic biotic crisis or a response to expansion of deeper marine benthic habitats associated with the rise in relative sea level.

The decrease in the abundance of shell-forming organisms suggests that overall ecological activity decreased sharply across the Triassic/Jurassic transition. The evidence provided above focuses mainly on the composition of carbonate sediments deposited in shallow-marine environments. In theory, the ecological and evolutionary dynamics of shell-forming organisms in carbonate environments could differ from those of skeletal organisms in different environments or from those of non-skeletal organisms. However, evidence of decreased metazoan activity across the Triassic/Jurassic transition is also evident in ichnofacies patterns from both siliciclastic and carbonate environments. The number of ichnotaxa, depth of bioturbation and size of burrows decreased sharply during late Rhaetian-early Hettangian time in Panthalassic (New York Canyon), Tethyan (Austria) and adjacent ocean basins (southern England) (Twitchett and Barras, 2004; Barras and Twitchett, 2007). A sharp decrease in the bioturbation-associated porosity in limestones also occurred in peritidal carbonates of western Tethys (Todaro et al., 2016). The presence of wrinkle structures in shallow-marine sediments has been associated with reduced metazoan activity in post-extinction environments (Pruss et al., 2004; Mata and Bottjer, 2009; Mariotti et al., 2014). Similar wrinkle structures occur in siliciclastic subtidal environments during the Hettangian (Häntzschel and Reineck, 1968; Peterffy et al., 2016).

The reduction in ecological functioning due to biogeochemical disturbance has occurred multiple times during the Phanerozoic (Droser et al., 2002; Aberhan and Kiessling, 2015; Hull, 2015). The mean total skeletal abundance in comparable peritidal environments was reduced by more than 90% across Permian-Triassic strata (from six stratigraphic sections in South China; Payne et al., 2006) as compared to a ~60 % decrease across the Triassic/Jurassic strata (Fig. 9). Of the total skeletal abundance, the calcareous algae show an especially interesting response to the end-Permian and end-Triassic extinction events (Fig. 8). Macroscopic green algae were ecologically important primary producers during the Paleozoic and early Mesozoic (Wray, 1977; Knoll et al., 2007; Payne and van de Schootbrugge, 2007; Hull, 2017). Lower Triassic strata from shallow-marine environments were nearly devoid of calcareous algae in the aftermath of the end-Permian extinction (Bucur, 1999, Payne et al., 2006). Conversely, the calcareous algal abundance in the Lower Jurassic strata decreased only slightly across the Triassic/Jurassic transition (Fig. 9). This difference in algal abundance in the aftermaths of the two mass extinctions could indicate that the end-Permian mass extinction was much more severe for calcifying primary producers than the end-Triassic extinction (Bucur, 1999).

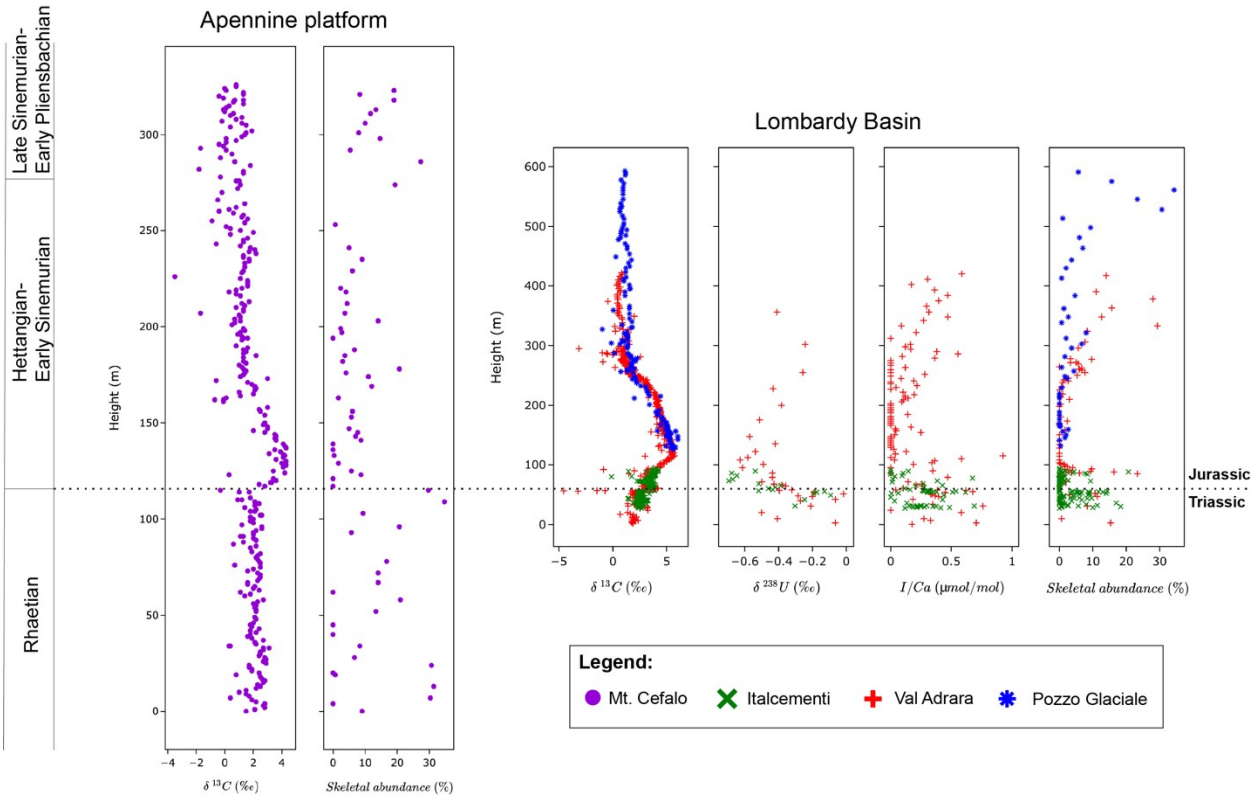

Figure 8: A composite plot of variations in stable isotope proxies, I/Ca ratios and skeletal abundance in Lombardy basin and Apennine platform. See figures 3-6 for data sources. The figure indicates broad scale spatial and temporal changes in the abundance of skeleton-forming organisms across the Triassic/Jurassic boundary in context of local (I/Ca) and global ($\delta^{\#"\$}U$) redox proxies and carbon isotope ratios. The local and global redox proxies indicate a shift to reducing redox conditions in the Lower Jurassic. The negative and positive carbon isotope excursions in Lower Jurassic are global in extent and can be tracked across multiple basins. See Bachan et al. (2012) for detailed description of carbon cycle changes across the Triassic/Jurassic boundary.

5.2 Marine redox conditions and environmental dynamics across the T/J boundary

The I/Ca ratios from the Lombardy Basin most likely record Triassic/Jurassic variations in marine redox conditions. Typical carbonate diagenesis processes, such as alteration by meteoric fluids and dolomitization, can decrease the concentrations of iodate in the carbonate crystal lattice (Hardisty et al., 2017). The elemental ratios of Mg/Ca and Mn/Sr indicate low likelihood of substantial diagenetic alteration in our samples. In the Lombardy Basin samples, there is weak correlation of I/Ca with $\delta^{!\$}O$ (Pearson corr.(r), Italcementi: r=0.27, p=0.04, n=54; Val Adrara: r=0.28, p=0.01, n=81), of I/Ca with Mg/Ca (Pearson corr.(r), Italcementi: r=0.33, p=0.01, n=54; Val Adrara: r=-0.03, p=0.75, n=81) and of I/Ca with Mn/Sr (Pearson corr.(r), Italcementi: r=0.11, p=0.69, n=13; Val Adrara: r=0.12, p=0.43, n=42) (Fig. S2). The Mn/Sr ratio, in particular, is indicative of the degree of alteration through meteoric diagenesis (Brand and Veizer, 1980). In theory, the Mn/Sr and I/Ca ratios should be inversely correlated in case of significant diagenesis in the meteoric zone (Hardisty et al., 2017). However, the samples from the Lombardy Basin do not indicate significant

inverse correlation between the two ratios. Furthermore, He et al. (2022a) reported a sharp drop in carbonate I/(Ca+Mg) ratios from a mean of 3.5 μmol/mol during pre-extinction period to 1.4 μmol/mol across the extinction horizon in another Italian section (Mt. Sparagio, Fig. 1), independently supporting the temporal trend in local redox conditions observed in this study.

The lithology of the limestones also does not appear to play a major role in governing I/Ca ratios. A one-way ANOVA ($p<0.05$, $\eta^2=0.16$) on the I/Ca ratios of different lithologies encountered in our data indicates that although there are statistically significant differences in the means of different lithologies, this factor overall explains only a minor percentage of variance in the I/Ca ratios (Fig. S3). A two-way ANOVA of the Val Adrara section data, with age and lithology as the independent variables, indicates that time period ($p=0.04$, $\eta^2=0.07$) is a significant predictor of I/Ca ratios whereas the lithology is not ($p=0.62$, $\eta^2=0.02$). In the Italcementi section, the lithology ($p=0.07$, $\eta^2=0.45$) similarly explains more of the variation in I/Ca than does the time period ($p=0.45$, $\eta^2=0.01$) but overall neither time period nor lithology is significantly associated with I/Ca ratios in the two-way ANOVA. The small effect size and lack of statistically significant associations could indicate that I/Ca ratios at Italcementi section have a higher noise/signal ratio than at Val Adrara. The source of noise could be diagenetic and/or lithologic factors. However, the weight of the evidence points to temporal changes in primary I/Ca ratios across the Triassic/Jurassic boundary.

The I/Ca values found in this study are relatively low (< 2 μmol/mol), whereas the Rhaetian peritidal limestones from the southwestern Tethys (He et al., 2022a) have higher I/Ca values. These observations can be explained in two ways: (1) the low I/Ca values in the Lombardy Basin are largely primary signals indicating a low-oxygen water mass in close proximity to the sample locations; or (2) post-depositional diagenetic alteration lowered the primary I/Ca of the rocks after deposition. Support for a low-oxygen water mass (and a primary signal) comes from the argument that the organic matter remineralization depth in the oceanic water column deepened during the Mesozoic, which reduced the prevalence of shallow oxygen minimum zones compared to the Paleozoic (Lu et. al, 2018). Although the exact timing of this transition is still unclear, a shallower OMZ in the Triassic is consistent with current evidence, including previously published I/Ca data from the Rhaetian (Lu et al., 2018). For instance, our mean I/Ca values during the Rhaetian (0.30 μmol/mol and 0.45 μmol/mol for Italcementi and Val Adrara respectively) are close to values (0.22 μmol/mol) from the adjacent Lagonegro Basin (Lu et al., 2018). On the other hand, the Rhaetian peritidal limestones from the southwestern Tethys exhibit high I/Ca ratios, around 3.5 μmol/mol (He et al., 2022a). Therefore, it is possible that some low oxygen waters were close to the Lombardy Basin sections throughout the study interval. Diagenetic loss of carbonate-associated iodine during later diagenesis cannot be completely ruled out, but there is no evidence to suggest that the stratigraphic trend in I/Ca is dominated by diagenesis based on relationships with $\delta^{!\$}O$, Mg/Ca, and Mn/Sr (Fig. S2).

The I/Ca data (0.00-0.70 μmol/mol) from the Upper Triassic of the Lombardy Basin suggest a water column where oxygen was present and relatively stable but not abundant (Fig. 8). The sub-surface marine redox conditions at the end of the Triassic shifted toward anoxic/hypoxic conditions based on a decrease in I/Ca (Fig. 8). Variation in I/Ca ratios indicating an expansion of local dysoxic and anoxic waters across the Triassic/Jurassic boundary is consistent with other lines of evidence for globally widespread anoxic and euxinic water column conditions in shallow marine environments during the Early Jurassic (He et al., 2022a, 2022b). The uranium isotope ratios

($\delta^{238}U$) from the Lombardy Basin record a negative excursion of 0.7 ‰, indicating a 30-fold increase in anoxic seafloor area in a span of ~45 kyr at the Triassic/Jurassic boundary (Jost et al., 2017a). Anoxia-driven isotopic excursions have also been interpreted from carbonate-associated sulphate ($\delta^{34}S$) isotope ratios (He et al., 2020). The evidence of photic zone euxinia in shallow-marine environments across the Triassic/Jurassic boundary has also been reported from changes in nitrogen isotope ratios and fossil biomarker studies from Tethyan and Panthalassic sections (Richoz et al., 2012; Jaraula et al., 2013; Kasprak et al., 2015; Fujisaki et al., 2020). The reducing redox conditions remained prevalent in global oceans through the middle-late Hettangian with first signs of shifts towards oxic environments occurring in the early Sinemurian (Richoz et al., 2012; Ritterbush et al., 2015b; Thibodeau et al., 2016).

The fluctuating local redox conditions across the Triassic/Jurassic boundary and their close correspondence with skeletal abundance indicate a connection between water-column anoxia and the reduction in benthic faunal abundance across the extinction boundary. The fluctuating local redox conditions well corresponded to changes in skeletal abundance, indicating water column anoxia as a candidate controlling the benthic faunal abundance through the restriction of aerobic habitat (Fig. 10). However, an overarching control, such as climate, which drove increased anoxia in the Jurassic, could also have shaped variation in skeletal abundance. For instance, interaction between temperature and oxygen availability explain the biogeography of many living species through their influences on the ratio of oxygen supply to metabolic demand (Deutsch et al., 2015). In this latter case, redox conditions may not have been directly or entirely responsible for the changes in skeletal abundance but may have remained correlated with skeletal changes due to shared controls (Fig. 10).

Geological evidence from the Triassic/Jurassic boundary interval supports the scenario involving shared controls on abundance and redox conditions, for the study sites in the Lombardy Basin and at Mt. Cefalo. Peritidal facies at Mt. Cefalo and shallow-marine facies including oolites in the Lombardy Basin suggest that much of the deposition in the studied sections occurred above fair-weather wave base and that the local water column would have been oxygenated by wind mixing even if the I/Ca proxy recorded the mixing of more poorly oxygenated waters from deeper in the basin due to the slower kinetics of iodide oxidation. Emplacement of the Central Atlantic Magmatic Province (CAMP) at the Triassic/Jurassic boundary is a well-supported candidate for the shared control on skeletal abundance and redox conditions. Carbon dioxide emissions from CAMP led to an increase in atmospheric CO_2 (Bachan et al., 2012). Resultant warming (McElwain et al., 1999; Ruhl and Kürschner, 2011) could have driven deoxygenation as evident from observations in modern oceans (Levin, 2018). This warming would have increased the basal metabolic demands of marine organisms and the elevated carbon dioxide concentrations and reduced pH of marine waters would have added to physiological stresses (Pörtner et al., 2004; Gazeau et al., 2013; Deutsch et al., 2015) (Fig. 10). The combined effects of multiple stressors, especially warming and deoxygenation (Reddin et al., 2020), can potentially account for the lower abundance of skeletal (and non-skeletal) animals in the aftermath of the mass extinction event.

Irrespective of the control, the geochemical proxy evidence indicates multiple episodes of carbon dioxide release during the early Hettangian created deleterious environmental conditions by sustaining high temperatures (McElwain et al., 1999; Huynh and Poulsen, 2005) and creating unstable oceanic redox conditions in shallow-marine environments in Early Jurassic. The

prolonged hyperthermal and anoxic conditions could have reduced the carrying capacity of Early Jurassic marine ecosystems and delayed recovery until early Sinemurian time.

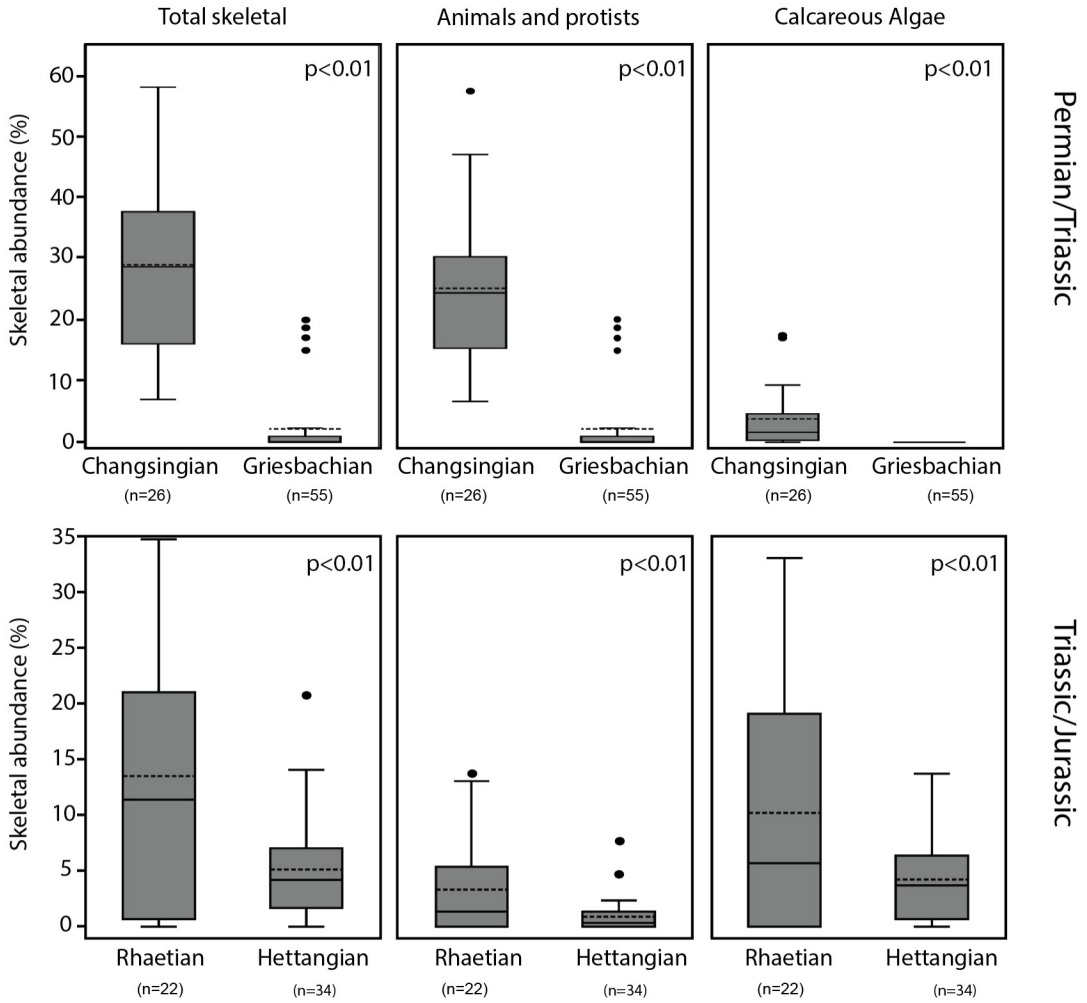

Figure 9: Box plots showing skeletal abundance variations in shallow marine environments across two major mass extinction boundaries: end-Permian mass extinction and end-Triassic mass extinction. In the top panel: the leftmost plot shows total skeletal abundance change across Changsingian (Upper Permian)- Griesbachian (Lower Triassic) boundary. The plots in the center and right show a breakdown of total skeletal abundance in animals and protists, and calcareous algae, respectively. The lower panel from left to right: total skeletal, animal & protists and calcareous algae abundance variations across the Rhaetian (Upper Triassic) - Hettangian (Lower Jurassic) boundary. The data for the end-Permian mass extinction was obtained from Payne et al. (2006). "n" indicates the number of thin sections in each category.

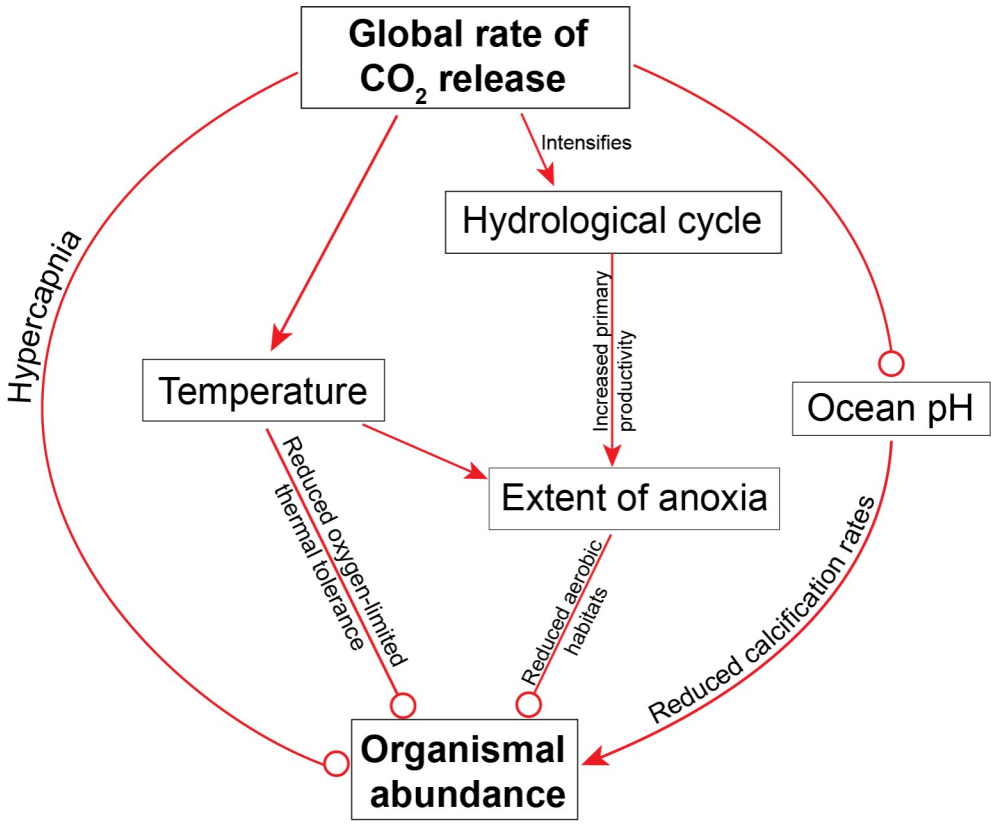

Figure 10: A systems analysis model showing the ocean biogeochemical changes associated with CAMP volcanism and its relationship with the Triassic/Jurassic biotic crisis. The parameters connected by arrows indicate a positive coupling between them and a negative coupling between those connected by open circles. For example, physiological effects due to increase in pCO_2 will lead to a decrease in skeletal abundance indicating an inverse relationship. Thus, this feedback is represented by an open circle.

6 Conclusions

In this study, we measured skeletal abundance and I/Ca ratios in marine limestones in four Tethyan sections to reconstruct changes in faunal abundance and redox conditions across the Triassic/Jurassic boundary. We find evidence of a significant reduction in skeletal abundance across the end-Triassic extinction event that is reproducible among sections and cannot be explained by changes in depositional environment. I/Ca ratios indicate that the drop in skeletal abundance across the Triassic/Jurassic boundary was accompanied by an expansion of reducing conditions in shallow-marine environments in the regions of deposition. The eventual increase in skeletal abundance in the late Hettangian-Sinemurian is also associated with an increase in I/Ca. This correlation between skeletal abundance and I/Ca ratio indicates that the prevalence of dysoxic to anoxic environments during the early Hettangian was an important factor contributing to the decline in skeletal abundance. We hypothesize that physiological constraints posed by high oceanic temperatures and changing ocean pH resulting from carbon dioxide release during CAMP

volcanism acted in tandem with reduced oxygen availability to limit the abundance of skeletal benthic organisms in Hettangian ecosystems.

Changes in abundance of benthic organisms, which are critical to understanding energy flow in ecosystems, have remained among the most difficult to assess across mass extinctions. Studies like this one provide a novel perspective for understanding the ecological severity of mass extinctions, complementary to taxonomic diversity, counts of ecological modes of life, and food-web reconstructions. They also provide a different perspective in directly assessing effects of ongoing, human-induced mass rarity currently underway in modern oceans (Hull, 2015).

References

Aberhan, M., and Kiessling, W., 2015, Persistent ecological shifts in marine molluscan assemblages across the end-Cretaceous mass extinction: Proceedings of the National Academy of Sciences, v. 112, p. 7207–7212, doi:10.1073/pnas.1422248112.

Atkinson, J.W., and Wignall, P.B., 2019, How quick was marine recovery after the end-Triassic mass extinction and what role did anoxia play? Palaeogeography, Palaeoclimatology, Palaeoecology, v. 528, p. 99–119, doi:10.1016/j.palaeo.2019.05.011.

Atkinson, J.W., Wignall, P.B., Morton, J.D., and Aze, T., 2019, Body size changes in bivalves of the family Limidae in the aftermath of the end-Triassic mass extinction: the Brobdingnag effect: Palaeontology, v. 62, p. 561–582.

Bachan, A., and Payne, J.L., 2016, Modelling the impact of pulsed CAMP volcanism on pCO2 and δ13C across the Triassic-Jurassic transition: Geological Magazine, v. 153, p. 252–270, doi:10.1017/S0016756815000126.

Bachan, A., Van De Schootbrugge, B., Fiebig, J., McRoberts, C.A., Ciarapica, G., and Payne, J.L., 2012, Carbon cycle dynamics following the end-Triassic mass extinction: Constraints from paired δ13Ccarb and δ13Corg records: Geochemistry, Geophysics, Geosystems, v. 13, p. 1–24, doi:10.1029/2012GC004150.

Bambach, R.K., 2006, Phanerozoic biodiversity mass extinctions: Annu. Rev. Earth Planet. Sci., v. 34, p. 127–155.

Bambach, R.K., Knoll, A.H., and Sepkoski, J.J., 2002, Anatomical and ecological constraints on Phanerozoic animal diversity in the marine realm: Proceedings of the National Academy of Sciences, v. 99, p. 6854–6859.

Barattolo, F., and Romano, R., 2005, Shallow carbonate platform bioevents during the Upper Triassic-Lower Jurassic: An evolutive interpretation: Bollettino della Societa Geologica Italiana, v. 124, p. 123–142.

Barnosky, A.D. et al., 2012, Approaching a state shift in Earth's biosphere: Nature, v. 486, p. 52–58.

Barras, C.G., and Twitchett, R.J., 2007, Response of the marine infauna to Triassic-Jurassic environmental change: Ichnological data from southern England: Palaeogeography, Palaeoclimatology, Palaeoecology, v. 244, p. 223–241, doi:10.1016/j.palaeo.2006.06.040.

Berra, F., 2012, Sea-level fall, carbonate production, rainy days: How do they relate? Insight from Triassic carbonate platforms (Western Tethys, Southern Alps, Italy): Geology, v. 40, p. 271–274, doi:10.1130/G32803.1.

Berra, F., Jadoul, F., and Anelli, A., 2010, Environmental control on the end of the Dolomia Principale/Hauptdolomit depositional system in the central Alps: Coupling sea-level and climate changes: Palaeogeography, Palaeoclimatology, Palaeoecology, v. 290, p. 138–150, doi:https://doi.org/10.1016/j.palaeo.2009.06.037.

684 Bertotti, G., Siletto, G.B., and Spalla, M.I., 1993, Deformation and metamorphism associated
685 with crustal rifting: The Permian to Liassic evolution of the Lake Lugano-Lake Como area
686 (Southern Alps): Tectonophysics, v. 226, p. 271–284, doi:https://doi.org/10.1016/0040-687
1951(93)90122-Z.

688 Blackburn, T.J., Olsen, P.E., Bowring, S.A., McLean, N.M., Kent, D. V, Puffer, J., McHone, G.,
689 Rasbury, E.T., and Et-Touhami, M., 2013, Zircon U-Pb geochronology links the end-
690 Triassic extinction with the Central Atlantic Magmatic Province: Science, v. 340, p. 941–
691 945.

692 Blois, J.L., Zarnetske, P.L., Fitzpatrick, M.C., and Finnegan, S., 2013, Climate change and the
693 past, present, and future of biotic interactions: Science, v. 341, p. 499–504.

694 Bond, D.P.G., and Grasby, S.E., 2017, On the causes of mass extinctions: Palaeogeography,
695 Palaeoclimatology, Palaeoecology, v. 478, p. 3–29, doi:10.1016/j.palaeo.2016.11.005.

696 Bowman, C.N., Lindskog, A., Kozik, N.P., Richbourg, C.G., Owens, J.D., and Young, S.A.,
697 2020, Integrated sedimentary, biotic, and paleoredox dynamics from multiple localities in
698 southern Laurentia during the late Silurian (Ludfordian) extinction event: Palaeogeography,
699 Palaeoclimatology, Palaeoecology, v. 553, doi:10.1016/j.palaeo.2020.109799.

700 Brand, U., and Veizer, J., 1980, Chemical diagenesis of a multicomponent carbonate system; 1,
701 Trace elements: Journal of Sedimentary Research, v. 50, p. 1219–1236,
702 doi:10.1306/212F7BB7-2B24-11D7-8648000102C1865D.

703 Brandano, M., Corda, L., Tomassetti, L., and Tagliavento, M., 2016, Frequency analysis across
704 the drowning of a Lower Jurassic carbonate platform: The Calcare Massiccio Formation
705 (Apennines, Italy): Marine and Petroleum Geology, v. 78, p. 606–620,
706 doi:https://doi.org/10.1016/j.marpetgeo.2016.09.013.

707 Brenchley, P.J., Marshall, J.D., and Underwood, C.J., 2001, Do all mass extinctions represent an
708 ecological crisis? Evidence from the Late Ordovician: Geological Journal, v. 36, p. 329–
709 340.

710 Brosse, M., Bucher, H., Baud, A., Frisk, Å.M., Goudemand, N., Hagdorn, H., Nützel, A., Ware,
711 D., and Hautmann, M., 2019, New data from Oman indicate benthic high biomass
712 productivity coupled with low taxonomic diversity in the aftermath of the Permian--
713 Triassic Boundary mass extinction: Lethaia, v. 52, p. 165–187.

714 Bucur, I.I., 1999, Stratigraphic significance of some skeletal algae (Dasycladales, Caulerpales) of
715 the Phanerozoic: Depositional episodes and bioevents, p. 53–104.

716 Chance, R., Baker, A.R., Carpenter, L., and Jickells, T.D., 2014, The distribution of iodide at the
717 sea surface: Environ. Sci.: Processes Impacts, v. 16, p. 1841–1859,
718 doi:10.1039/C4EM00139G.

719 Christie, M., Holland, S.M., and Bush, A.M., 2013, Contrasting the ecological and taxonomic
720 consequences of extinction: Paleobiology, v. 39, p. 538–559.

721 Ciarapica, G., and Passeri, L., 2005, Late Triassic and Early Jurassic sedimentary evolution of

722 the Northern Apennines: An overview: Bollettino della Societa Geologica Italiana, v. 124,
723 p. 189–201.

724 Cirilli, S., Buratti, N., Gugliotti, L., and Frixa, A., 2015, Palynostratigraphy and palynofacies of
725 the Upper Triassic Streppenosa Formation (SE Sicily, Italy) and inference on the main
726 controlling factors in the organic rich shale deposition: Review of Palaeobotany and
727 Palynology, v. 218, p. 67–79, doi:https://doi.org/10.1016/j.revpalbo.2014.10.009.

728 Corsetti, F.A. et al., 2015, Investigating the Paleoecological Consequences of Supercontinent
729 Breakup: Sponges Clean Up in the Early Jurassic: The Sedimentary Record, v. 13, p. 4–10,
730 doi:10.2110/sedred.2015.2.4.

731 Coskun Tunaboylu, B., Altiner, D., Isintek, I., and Demirci, D., 2014, Foraminiferal
732 biostratigraphy and sequence stratigraphy of peritidal carbonates at the Triassic-Jurassic
733 boundary (Karaburun Peninsula, Western Turkey): Journal of Asian Earth Sciences, v. 90,
734 p. 61–76, doi:10.1016/j.jseaes.2014.04.015.

735 Cribb, A.T., and Bottjer, D.J., 2020, Complex marine bioturbation ecosystem engineering
736 behaviors persisted in the wake of the end-Permian mass extinction: Scientific reports, v.
737 10, p. 1–8.

738 Delecat, S., and Reitner, J., 2005, Sponge communities from the Lower Liassic of Adnet
739 (Northern Calcareous Alps, Austria): Facies, v. 51, p. 385–404, doi:10.1007/s10347-005-
740 0045-x.

741 Deutsch, C., Ferrel, A., Seibel, B., Pörtner, H.-O., and Huey, R.B., 2015, Climate change
742 tightens a metabolic constraint on marine habitats: Science, v. 348, p. 1132–1135,
743 doi:10.1126/science.aaa1605.

744 Di Stefano, P., Favara, R., Luzio, D., Renda, P., Cacciatore, M.S., Calò, M., Napoli, G., Parisi,
745 L., Todaro, S., and Zarcone, G., 2015, A regional-scale discontinuity in western Sicily
746 revealed by a multidisciplinary approach: A new piece for understanding the geodynamic
747 puzzle of the southern Mediterranean: Tectonics, v. 34, p. 2067–2085,
748 doi:10.1002/2014TC003759.

749 Diaz, R.J., and Rosenberg, R., 2008, Spreading dead zones and consequences for marine
750 ecosystems: science, v. 321, p. 926–929.

751 Dineen, A.A., Roopnarine, P.D., and Fraiser, M.L., 2019, Ecological continuity and
752 transformation after the Permo-Triassic mass extinction in northeastern Panthalassa:
753 Biology Letters, v. 15, doi:10.1098/rsbl.2018.0902.

754 Droser, M.L., Bottjer, D.J., Sheehan, P.M., and McGhee Jr, G.R., 2000, Decoupling of
755 taxonomic and ecologic severity of Phanerozoic marine mass extinctions: Geology, v. 28, p.
756 675–678.

757 Droser, M.L., Jensen, S., and Gehling, J.G., 2002, Trace fossils and substrates of the terminal
758 Proterozoic-Cambrian transition: Implications for the record of early bilaterians and
759 sediment mixing: Proceedings of the National Academy of Sciences, v. 99, p. 12572–

12576, doi:10.1073/pnas.202322499.

Dunhill, A.M., Foster, W.J., Azaele, S., Sciberras, J., and Twitchett, R.J., 2018, Modelling determinants of extinction across two Mesozoic hyperthermal events: Proceedings of the Royal Society B: Biological Sciences, v. 285, doi:10.1098/rspb.2018.0404.

Emerson, S., Cranston, R.E., and Liss, P.S., 1979, Redox species in a reducing fjord: equilibrium and kinetic considerations: Deep Sea Research Part A. Oceanographic Research Papers, v. 26, p. 859–878, doi:https://doi.org/10.1016/0198-0149(79)90101-8.Bond, D.P.G., and Grasby, S.E., 2017, On the causes of mass extinctions: Palaeogeography, Palaeoclimatology, Palaeoecology, v. 478, p. 3–29, doi:10.1016/j.palaeo.2016.11.005.

Bowman, C.N., Lindskog, A., Kozik, N.P., Richbourg, C.G., Owens, J.D., and Young, S.A., 2020, Integrated sedimentary, biotic, and paleoredox dynamics from multiple localities in southern Laurentia during the late Silurian (Ludfordian) extinction event: Palaeogeography, Palaeoclimatology, Palaeoecology, v. 553, doi:10.1016/j.palaeo.2020.109799.

Brand, U., and Veizer, J., 1980, Chemical diagenesis of a multicomponent carbonate system; 1, Trace elements: Journal of Sedimentary Research, v. 50, p. 1219–1236, doi:10.1306/212F7BB7-2B24-11D7-8648000102C1865D.

Deutsch, C., Ferrel, A., Seibel, B., Pörtner, H.-O., and Huey, R.B., 2015, Climate change tightens a metabolic constraint on marine habitats: Science, v. 348, p. 1132–1135, doi:10.1126/science.aaa1605.

Finnegan, S., Rasmussen, C.M., and Harper, D.A.T., 2016, Biogeographic and bathymetric determinants of brachiopod extinction and survival during the Late Ordovician mass extinction: Proceedings of the Royal Society B: Biological Sciences, v. 283, p. 20160007.

Gazeau, F., Parker, L.M., Comeau, S., Gattuso, J.-P., O'Connor, W.A., Martin, S., Pörtner, H.-O., and Ross, P.M., 2013, Impacts of ocean acidification on marine shelled molluscs: Marine Biology, v. 160, p. 2207–2245, doi:10.1007/s00227-013-2219-3.

He, T. et al., 2022a, Shallow ocean oxygen decline during the end-Triassic mass extinction: Global and Planetary Change, v. 210, p. 103770, doi:https://doi.org/10.1016/j.gloplacha.2022.103770.

He, T., Wignall, P.B., Newton, R.J., Atkinson, J.W., Keeling, J.F.J., Xiong, Y., and Poulton, S.W., 2022b, Extensive marine anoxia in the European epicontinental sea during the end-Triassic mass extinction: Global and Planetary Change, v. 210, p. 103771, doi:https://doi.org/10.1016/j.gloplacha.2022.103771.

Huynh, T.T., and Poulsen, C.J., 2005, Rising atmospheric CO2 as a possible trigger for the end-Triassic mass extinction: Palaeogeography, Palaeoclimatology, Palaeoecology, v. 217, p. 223–242, doi:https://doi.org/10.1016/j.palaeo.2004.12.004.

Levin, L.A., 2018, Manifestation, Drivers, and Emergence of Open Ocean Deoxygenation: Annual Review of Marine Science, v. 10, p. 229–260, doi:10.1146/annurev-marine-121916-063359.

798 Lu, Z., Lu, W., Rickaby, R.E.M., and Thomas, E., 2020, Earth History of Oxygen and the
799 iprOxy: Cambridge University Press, Elements in Geochemical Tracers in Earth System
800 Science, doi:10.1017/9781108688604.

801 McElwain, J.C., Beerling, D.J., and Woodward, F.I., 1999, Fossil Plants and Global Warming at
802 the Triassic-Jurassic Boundary: Science, v. 285, p. 1386–1390,
803 doi:10.1126/science.285.5432.1386.

804 Pörtner, H.O., Langenbuch, M., and Reipschläger, A., 2004, Biological impact of elevated ocean
805 CO 2 concentrations: lessons from animal physiology and earth history: Journal of
806 Oceanography, v. 60, p. 705–718.

807 Flügel, E., 2010, Quantitative Microfacies Analysis, *in* Microfacies of Carbonate Rocks:
808 Analysis, Interpretation and Application, Berlin, Heidelberg, Springer Berlin Heidelberg, p.
809 243–266, doi:10.1007/978-3-642-03796-2_6.

810 Fox, C.P., Cui, X., Whiteside, J.H., Olsen, P.E., Summons, R.E., and Grice, K., 2020, Molecular
811 and isotopic evidence reveals the end-Triassic carbon isotope excursion is not from massive
812 exogenous light carbon: Proceedings of the National Academy of Sciences of the United
813 States of America, v. 117, p. 30171–30178, doi:10.1073/pnas.1917661117.

814 Fujisaki, W., Fukami, Y., Matsui, Y., Sato, T., Sawaki, Y., and Suzuki, K., 2020, Redox
815 conditions and nitrogen cycling during the Triassic-Jurassic transition: A new perspective
816 from the mid-Panthalassa: Earth-Science Reviews, v. 204,
817 doi:10.1016/j.earscirev.2020.103173.

818 Gaetani, M., 1970, Faune Hettangiane della parte orientale della provincia di Bergamo: Riv.
819 Italiana Paleontologia Stratigrafia, v. 76, p. 355–442.

820 Galli, M.T., Jadoul, F., Bernasconi, S.M., Cirilli, S., and Weissert, H., 2007, Stratigraphy and
821 palaeoenvironmental analysis of the Triassic-Jurassic transition in the western Southern
822 Alps (Northern Italy): Palaeogeography, Palaeoclimatology, Palaeoecology, v. 244, p. 52–
823 70, doi:10.1016/j.palaeo.2006.06.023.

824 Galli, M.T., Jadoul, F., Bernasconi, S.M., and Weissert, H., 2005, Anomalies in global carbon
825 cycling and extinction at the Triassic/Jurassic boundary: evidence from a marine C-isotope
826 record: Palaeogeography, Palaeoclimatology, Palaeoecology, v. 216, p. 203–214,
827 doi:https://doi.org/10.1016/j.palaeo.2004.11.009.

828 Gazeau, F., Parker, L.M., Comeau, S., Gattuso, J.-P., O'Connor, W.A., Martin, S., Pörtner, H.-
829 O., and Ross, P.M., 2013, Impacts of ocean acidification on marine shelled molluscs:
830 Marine Biology, v. 160, p. 2207–2245, doi:10.1007/s00227-013-2219-3.

831 Greene, S.E., Bottjer, D.J., Hagdorn, H., and Zonneveld, J.-P., 2011, The Mesozoic return of
832 Paleozoic faunal constituents: A decoupling of taxonomic and ecological dominance during
833 the recovery from the end-Permian mass extinction: Palaeogeography, Palaeoclimatology,
834 Palaeoecology, v. 308, p. 224–232.

835 Haas, J., Kovács, S., Krystyn, L., and Lein, R., 1995, Significance of Late Permian-Triassic

facies zones in terrane reconstructions in the Alpine-North Pannonian domain: Tectonophysics, v. 242, p. 19–40, doi:https://doi.org/10.1016/0040-1951(94)00157-5.

Häntzschel, W., and Reineck, H.E., 1968, Fazies-Untersuchungen im Hettangium von Helmstedt (Niedersachsen): Mitteilungen aus dem Geologischen Staatsinstitut in Hamburg, v. 37, p. 5–39.

Hardisty, D.S. et al., 2017, Perspectives on Proterozoic surface ocean redox from iodine contents in ancient and recent carbonate: Earth and Planetary Science Letters, v. 463, p. 159–170, doi:https://doi.org/10.1016/j.epsl.2017.01.032.

Harnik, P.G., Simpson, C., and Payne, J.L., 2012, Long-term differences in extinction risk among the seven forms of rarity: Proceedings of the Royal Society B: Biological Sciences, v. 279, p. 4969–4976.

Hautmann, M., 2004, Effect of end-Triassic CO 2 maximum on carbonate sedimentation and marine mass extinction: Facies, v. 50, p. 257–261.

He, T. et al., 2020, An enormous sulfur isotope excursion indicates marine anoxia during the end-Triassic mass extinction: Science Advances, v. 6, p. eabb6704, doi:10.1126/sciadv.abb6704.

He, T. et al., 2022a, Shallow ocean oxygen decline during the end-Triassic mass extinction: Global and Planetary Change, v. 210, p. 103770, doi:https://doi.org/10.1016/j.gloplacha.2022.103770.

He, T., Wignall, P.B., Newton, R.J., Atkinson, J.W., Keeling, J.F.J., Xiong, Y., and Poulton, S.W., 2022b, Extensive marine anoxia in the European epicontinental sea during the end-Triassic mass extinction: Global and Planetary Change, v. 210, p. 103771, doi:https://doi.org/10.1016/j.gloplacha.2022.103771.

Hull, P.M., 2017, Emergence of modern marine ecosystems: Current Biology, v. 27, p. R466–R469, doi:https://doi.org/10.1016/j.cub.2017.04.041.

Hull, P., 2015, Life in the aftermath of mass extinctions: Current Biology, v. 25, p. R941–R952, doi:10.1016/j.cub.2015.08.053.

Hull, P.M., and Darroch, S.A.F., 2013, Mass extinctions and the structure and function of ecosystems: The Paleontological Society Papers, v. 19, p. 115–156.

Hull, P.M., Norris, R.D., Bralower, T.J., and Schueth, J.D., 2011, A role for chance in marine recovery from the end-Cretaceous extinction: Nature Geoscience, v. 4, p. 856–860.

Huynh, T.T., and Poulsen, C.J., 2005, Rising atmospheric CO2 as a possible trigger for the end-Triassic mass extinction: Palaeogeography, Palaeoclimatology, Palaeoecology, v. 217, p. 223–242, doi:https://doi.org/10.1016/j.palaeo.2004.12.004.

Iannace, A., and Zamparelli, V., 2002, Upper Triassic platform margin biofacies and the paleogeography of Southern Apennines: Palaeogeography, Palaeoclimatology, Palaeoecology, v. 179, p. 1–18, doi:https://doi.org/10.1016/S0031-0182(01)00362-5.

873 Jacobsen, N.D., Twitchett, R.J., and Krystyn, L., 2011, Palaeoecological methods for assessing
874 marine ecosystem recovery following the Late Permian mass extinction event:
875 Palaeogeography, Palaeoclimatology, Palaeoecology, v. 308, p. 200–212,
876 doi:10.1016/j.palaeo.2010.04.024.

877 Jadoul, F., Berra, F., and Frisia, S., 1992, Stratigraphic and paleogeographic evolution of a
878 carbonate platform in an extensional tectonic regime: the example of the Dolomia
879 Principale in Lombardy (Italy): Rivista Italiana di Paleontologia e Stratigrafia, v. 98, p. 29–
880 44, doi:10.13130/2039-4942/8939.

881 Jadoul, F., and Galli, M.T., 2008, The hettangian shallow water carbonates after the
882 triassic/jurassic biocalcification crisis: The albenza formation in the Western Southern
883 ALPS: Rivista Italiana di Paleontologia e Stratigrafia, v. 114, p. 453–470,
884 doi:10.13130/2039-4942/5911.

885 Jadoul, F., Galli, M.T., Berra, F., Cirilli, S., Ronchi, P., and Paganoni, A.M., 2004, The Late
886 Triassic-Early Jurassic of the Lombardy Basin: stratigraphy, palaeogeography and
887 palaeontology. Field guide book escursion P86.

888 Jadoul, F., Galli, M.T., Calabrese, L., and Gnaccolini, M., 2005, Stratigraphy of Rhaetian to
889 lower Sinemurian carbonate platforms in western Lombardy (southern alps, Italy):
890 paleogeographic implications: v. 111, p. 285–303.

891 Jaraula, C.M.B., Grice, K., Twitchett, R.J., Böttcher, M.E., LeMetayer, P., Dastidar, A.G., and
892 Opazo, L.F., 2013, Elevated pCO2 leading to Late Triassic extinction, persistent photic
893 zone euxinia, and rising sea levels: Geology, v. 41, p. 955–958, doi:10.1130/G34183.1.

894 Jost, A.B., Bachan, A., van de Schootbrugge, B., Brown, S.T., DePaolo, D.J., and Payne, J.L.,
895 2017a, Additive effects of acidification and mineralogy on calcium isotopes in
896 Triassic/Jurassic boundary limestones: Geochemistry, Geophysics, Geosystems, v. 18, p.
897 113–124, doi:10.1002/2016GC006724.

898 Jost, A.B., Bachan, A., van de Schootbrugge, B., Lau, K. V., Weaver, K.L., Maher, K., and
899 Payne, J.L., 2017b, Uranium isotope evidence for an expansion of marine anoxia during the
900 end-Triassic extinction: Geochemistry, Geophysics, Geosystems, v. 18, p. 3093–3108,
901 doi:10.1002/2017GC006941.

902 Kasprak, A.H., Sepúlveda, J., Price-Waldman, R., Williford, K.H., Schoepfer, S.D., Haggart,
903 J.W., Ward, P.D., Summons, R.E., and Whiteside, J.H., 2015, Episodic photic zone euxinia
904 in the northeastern Panthalassic Ocean during the end-Triassic extinction: Geology, v. 43, p.
905 307–310, doi:10.1130/G36371.1.

906 Kiessling, W., and Aberhan, M., 2007, Environmental determinants of marine benthic
907 biodiversity dynamics through Triassic--Jurassic time: Paleobiology, v. 33, p. 414–434.

908 Kiessling, W., Aberhan, M., Brenneis, B., and Wagner, P.J., 2007, Extinction trajectories of
909 benthic organisms across the Triassic--Jurassic boundary: Palaeogeography,
910 Palaeoclimatology, Palaeoecology, v. 244, p. 201–222.

911 Knaust, D., 2010, The end-Permian mass extinction and its aftermath on an equatorial carbonate
912 platform: insights from ichnology: Terra Nova, v. 22, p. 195–202.

913 Knoll, A.H., Bambach, R.K., Canfield, D.E., and Grotzinger, J.P., 1996, Comparative Earth
914 history and Late Permian mass extinction: Science, v. 273, p. 452–457.

915 Knoll, A.H., Bambach, R.K., Payne, J.L., Pruss, S., and Fischer, W.W., 2007a, Paleophysiology
916 and end-Permian mass extinction: Earth and Planetary Science Letters, v. 256, p. 295–313,
917 doi:10.1016/j.epsl.2007.02.018.

918 Knoll, A.H., Summons, R.E., Waldbauer, J.R., and Zumberge, J.E., 2007b, CHAPTER 8 - The
919 Geological Succession of Primary Producers in the Oceans, *in* Falkowski, P.G. and Knoll,
920 A.H. eds., Evolution of Primary Producers in the Sea, Burlington, Academic Press, p. 133–
921 163, doi:https://doi.org/10.1016/B978-012370518-1/50009-6.

922 Lakew, T., 1994, Diagenesis of a Rhaetian Patch Reef (Lombardian Basin, southern Alps):
923 Rivista Italiana di Paleontologia e Stratigrafia, v. 100.

924 Lakew, T., 1990, Microfacies and cyclic sedimentation of the Upper Triassic (Rhaetian) Calcare
925 di zu (Southern Alps): Facies, v. 22, p. 187–231, doi:10.1007/BF02536952.

926 Larina, E., Bottjer, D.J., Corsetti, F.A., Zonneveld, J.P., Celestian, A.J., and Bailey, J. V., 2019,
927 Uppermost Triassic phosphorites from Williston Lake, Canada: link to fluctuating euxinic-928
anoxic conditions in northeastern Panthalassa before the end-Triassic mass extinction:
929 Scientific Reports, v. 9, doi:10.1038/s41598-019-55162-2.

930 Levin, L.A., 2018, Manifestation, Drivers, and Emergence of Open Ocean Deoxygenation:
931 Annual Review of Marine Science, v. 10, p. 229–260, doi:10.1146/annurev-marine-121916-
932 063359.

933 Lu, W. et al., 2018, Late inception of a resiliently oxygenated upper ocean: Science, v. 361, p.
934 174–177, doi:10.1126/science.aar5372.

935 Lu, Z., Hoogakker, B.A.A., Hillenbrand, C.-D., Zhou, X., Thomas, E., Gutchess, K.M., Lu, W.,
936 Jones, L., and Rickaby, R.E.M., 2016, Oxygen depletion recorded in upper waters of the
937 glacial Southern Ocean: Nature Communications, v. 7, p. 11146,
938 doi:10.1038/ncomms11146.

939 Lu, Z., Jenkyns, H.C., and Rickaby, R.E.M., 2010, Iodine to calcium ratios in marine carbonate
940 as a paleo-redox proxy during oceanic anoxic events: Geology, v. 38, p. 1107–1110,
941 doi:10.1130/G31145.1.

942 Lu, Z., Lu, W., Rickaby, R.E.M., and Thomas, E., 2020, Earth History of Oxygen and the
943 iprOxy: Cambridge University Press, Elements in Geochemical Tracers in Earth System
944 Science, doi:10.1017/9781108688604.

945 Mancinelli, A., Chiocchini, M., Chiocchini, R.A., and Romano, A., 2005, Biostratigraphy of
946 Upper Triassic-Lower Jurassic carbonate platform sediments of the central-southern
947 Apennines (Italy): Rivista Italiana di Paleontologia e Stratigrafia, v. 111, p. 271–283,
948 doi:10.13130/2039-4942/6314.

949 Mariotti, G., Pruss, S.B., Perron, J.T., and Bosak, T., 2014, Microbial shaping of sedimentary
950 wrinkle structures: Nature Geoscience, v. 7, p. 736–740, doi:10.1038/ngeo2229.

951 Mata, S.A., and Bottjer, D.J., 2009, The paleoenvironmental distribution of Phanerozoic wrinkle
952 structures: Earth-Science Reviews, v. 96, p. 181–195,
953 doi:https://doi.org/10.1016/j.earscirev.2009.06.001.

954 McCauley, D.J., Pinsky, M.L., Palumbi, S.R., Estes, J.A., Joyce, F.H., and Warner, R.R., 2015,
955 Marine defaunation: animal loss in the global ocean: Science, v. 347.

956 McElwain, J.C., Beerling, D.J., and Woodward, F.I., 1999, Fossil Plants and Global Warming at
957 the Triassic-Jurassic Boundary: Science, v. 285, p. 1386–1390,
958 doi:10.1126/science.285.5432.1386.

959 McGhee, G.R., Clapham, M.E., Sheehan, P.M., Bottjer, D.J., and Droser, M.L., 2013, A new
960 ecological-severity ranking of major Phanerozoic biodiversity crises: Palaeogeography,
961 Palaeoclimatology, Palaeoecology, v. 370, p. 260–270, doi:10.1016/j.palaeo.2012.12.019.

962 McGhee Jr, G.R., Sheehan, P.M., Bottjer, D.J., and Droser, M.L., 2004, Ecological ranking of
963 Phanerozoic biodiversity crises: ecological and taxonomic severities are decoupled:
964 Palaeogeography, Palaeoclimatology, Palaeoecology, v. 211, p. 289–297.

965 McRoberts, C.A., 1994, The Triassic-Jurassic ecostratigraphic transition in the Lombardian Alps,
966 Italy: Palaeogeography, Palaeoclimatology, Palaeoecology, v. 110, p. 145–166,
967 doi:10.1016/0031-0182(94)90114-7.

968 McRoberts, C.A., Furrer, H., and Jones, D.S., 1997, Palaeoenvironmental interpretation of a
969 Triassic-Jurassic boundary section from Western Austria based on palaeoecological and
970 geochemical data: Palaeogeography, Palaeoclimatology, Palaeoecology, v. 136, p. 79–95,
971 doi:https://doi.org/10.1016/S0031-0182(97)00074-6.

972 Muttoni, G., Kent, D. V, Jadoul, F., Olsen, P.E., Rigo, M., Galli, M.T., and Nicora, A., 2010,
973 Rhaetian magneto-biostratigraphy from the Southern Alps (Italy): Constraints on Triassic
974 chronology: Palaeogeography, Palaeoclimatology, Palaeoecology, v. 285, p. 1–16,
975 doi:https://doi.org/10.1016/j.palaeo.2009.10.014.

976 Pálfy, J. et al., 2007, Triassic–Jurassic boundary events inferred from integrated stratigraphy of
977 the Csővár section, Hungary: Palaeogeography, Palaeoclimatology, Palaeoecology, v. 244,
978 p. 11–33, doi:https://doi.org/10.1016/j.palaeo.2006.06.021.

979 Payne, J.L., 2005, Evolutionary dynamics of gastropod size across the end-Permian extinction
980 and through the Triassic recovery interval: Paleobiology, v. 31, p. 269–290,
981 doi:10.1666/0094-8373(2005)031[0269:EDOGSA]2.0.CO;2.

982 Payne, J.L., Lehrmann, D.J., Wei, J., and Knoll, A.H., 2006, The pattern and timing of biotic
983 recovery from the end-Permian extinction on the Great Bank of Guizhou, Guizhou
984 province, China: Palaios, v. 21, p. 63–85, doi:10.2110/palo.2005.p05-12p.

985 Payne, J.L., and Van De Schootbrugge, B., 2007, CHAPTER 9 - Life in Triassic Oceans: Links
986 Between Planktonic and Benthic Recovery and Radiation, *in* Falkowski, P.G. and Knoll,

A.H. eds., Evolution of Primary Producers in the Sea, Burlington, Academic Press, p. 165–189, doi:https://doi.org/10.1016/B978-012370518-1/50010-2.

Penn, J.L., Deutsch, C., Payne, J.L., and Sperling, E.A., 2018b, Temperature-dependent hypoxia explains biogeography and severity of end-Permian marine mass extinction: Science, v. 362, doi:10.1126/science.aat1327.

Peterffy, O., Calner, M., and Vajda, V., 2016, Early Jurassic microbial mats—A potential response to reduced biotic activity in the aftermath of the end-Triassic mass extinction event: Palaeogeography, Palaeoclimatology, Palaeoecology, v. 464, p. 76–85, doi:https://doi.org/10.1016/j.palaeo.2015.12.024.

Pörtner, H.O., Langenbuch, M., and Reipschläger, A., 2004, Biological impact of elevated ocean CO 2 concentrations: lessons from animal physiology and earth history: Journal of Oceanography, v. 60, p. 705–718.

Pruss, S., Fraiser, M., and Bottjer, D.J., 2004, Proliferation of Early Triassic wrinkle structures: Implications for environmental stress following the end-Permian mass extinction: Geology, v. 32, p. 461–464, doi:10.1130/G20354.1.

Raup, D.M., and Sepkoski, J.J., 1982, Mass extinctions in the marine fossil record: Science, v. 215, p. 1501–1503.

Reddin, C.J., Nätscher, P.S., Kocsis, Á.T., Pörtner, H.O., and Kiessling, W., 2020, Marine clade sensitivities to climate change conform across timescales: Nature Climate Change, v. 10, p. 249–253, doi:10.1038/s41558-020-0690-7.

Richoz, S. et al., 2012, Hydrogen sulphide poisoning of shallow seas following the end-Triassic extinction: Nature Geoscience, v. 5, p. 662–667, doi:10.1038/ngeo1539.

Ritterbush, K.A., Bottjer, D.J., Corsetti, F.A., and Rosas, S., 2014, New evidence on the role of siliceous sponges in ecology and sedimentary facies development in eastern Panthalassa following the Triassic–Jurassic mass extinction: PALAIOS, v. 29, p. 652–668, doi:10.2110/palo.2013.121.

Ritterbush, K.A., Ibarra, Y., and Tackett, L.S., 2016, Post-extinction biofacies of the first carbonate ramp of the early Jurassic (Sinemurian) in NE Panthalassa (New York canyon, Nevada, USA): PALAIOS, v. 31, p. 141–160, doi:10.2110/palo.2015.021.

Ritterbush, K.A., Rosas, S., Corsetti, F.A., Bottjer, D.J., and West, A.J., 2015a, Andean sponges reveal long-term benthic ecosystem shifts following the end-Triassic mass extinction: Palaeogeography, Palaeoclimatology, Palaeoecology, v. 420, p. 193–209, doi:10.1016/j.palaeo.2014.12.002.

Romano, R., Masett, D., Carras, N., Barattolo, F., and Roghi, G., 2008, The triassic/jurassic boundary in a peritidal carbonate platform of the pelagonian domain: The mount messapion section (Chalkida, Greece): Rivista Italiana di Paleontologia e Stratigrafia, v. 114, p. 431–452, doi:10.13130/2039-4942/5910.

Roopnarine, P.D., and Angielczyk, K.D., 2015, Community stability and selective extinction

during the Permian-Triassic mass extinction: Science, v. 350, p. 90–93.

Ruhl, M., and Kürschner, W.M., 2011, Multiple phases of carbon cycle disturbance from large igneous province formation at the Triassic-Jurassic transition: Geology, v. 39, p. 431–434, doi:10.1130/G31680.1.

Scheffer, M., Carpenter, S., and de Young, B., 2005, Cascading effects of overfishing marine systems: Trends in ecology \& evolution, v. 20, p. 579–581.

Schettino, A., and Turco, E., 2011, Tectonic history of the western Tethys since the Late Triassic: GSA Bulletin, v. 123, p. 89–105, doi:10.1130/B30064.1.

Van De Schootbrugge, B., Payne, J.L., Tomasovych, A., Pross, J., Fiebig, J., Benbrahim, M., Föllmi, K.B., and Quan, T.M., 2008, Carbon cycle perturbation and stabilization in the wake of the Triassic-Jurassic boundary mass-extinction event: Geochemistry, Geophysics, Geosystems, v. 9, doi:10.1029/2007GC001914.

van de Schootbrugge, B., Tremolada, F., Rosenthal, Y., Bailey, T.R., Feist-Burkhardt, S., Brinkhuis, H., Pross, J., Kent, D. V., and Falkowski, P.G., 2007, End-Triassic calcification crisis and blooms of organic-walled “disaster species”: Palaeogeography, Palaeoclimatology, Palaeoecology, v. 244, p. 126–141, doi:10.1016/j.palaeo.2006.06.026.

Schubert, J.K., and Bottjer, D.J., 1995, Aftermath of the Permian-Triassic mass extinction event: Paleoecology of Lower Triassic carbonates in the western USA: Palaeogeography, Palaeoclimatology, Palaeoecology, v. 116, p. 1–39.

Scotese, C.R., 2016, Tutorial: PALEOMAP PaleoAtlas for GPlates and the PaleoData Plotter Program, PALEOMAP Project:, doi:10.13140/RG2.2.34367.00166.

Sepkoski, J.J., Bambach, R.K., Raup, D.M., and Valentine, J.W., 1981, Phanerozoic marine diversity and the fossil record: Nature, v. 293, p. 435–437.

Sibert, E.C., Hull, P.M., and Norris, R.D., 2014, Resilience of Pacific pelagic fish across the Cretaceous/Palaeogene mass extinction: Nature Geoscience, v. 7, p. 667–670, doi:10.1038/ngeo2227.

Stampfli, G.M., Borel, G.D., Cavazza, W., Mosar, J., and Ziegler, P.A., 2001, Palaeotectonic and palaeogeographic evolution of the western Tethys and PeriTethyan domain (IGCP Project 369): Episodes, v. 24, p. 222–227, doi:10.18814/epiiugs/2001/v24i4/001.

Thibodeau, A.M., Ritterbush, K., Yager, J.A., West, A.J., Ibarra, Y., Bottjer, D.J., Berelson, W.M., Bergquist, B.A., and Corsetti, F.A., 2016, Mercury anomalies and the timing of biotic recovery following the end-Triassic mass extinction: Nature Communications, v. 7, p. 11147, doi:10.1038/ncomms11147.

Todaro, S., Hollis, C., and Di Stefano, P., 2016, Spongy-like porosity in peritidal carbonates: An interaction of cyclic sea-level oscillations, fresh water supply and sediment texture: Sedimentary Geology, v. 333, p. 70–83, doi:10.1016/j.sedgeo.2015.12.005.

Todaro, S., Rigo, M., Randazzo, V., and Di Stefano, P., 2018, The end-Triassic mass extinction:

A new correlation between extinction events and δ13C fluctuations from a Triassic-Jurassic peritidal succession in western Sicily: Sedimentary Geology, v. 368, p. 105–113, doi:https://doi.org/10.1016/j.sedgeo.2018.03.008.

Todaro, S., Di Stefano, P., Zarcone, G., and Randazzo, V., 2017, Facies stacking and extinctions across the Triassic–Jurassic boundary in a peritidal succession from western Sicily: Facies, v. 63, p. 1–21, doi:10.1007/s10347-017-0500-5.

Truesdale, V.W., Bale, A.J., and Woodward, E.M.S., 2000, The meridional distribution of dissolved iodine in near-surface waters of the Atlantic Ocean: Progress in Oceanography, v. 45, p. 387–400, doi:https://doi.org/10.1016/S0079-6611(00)00009-4.

Twitchett, R.J., and Barras, C.G., 2004, Trace fossils in the aftermath of mass extinction events: Geological Society, London, Special Publications, v. 228, p. 397–418.

Wagner, P.J., Kosnik, M.A., and Lidgard, S., 2006, Abundance distributions imply elevated complexity of post-Paleozoic marine ecosystems: Science, v. 314, p. 1289–1292.

Wong, G.T.F., and Brewer, P.G., 1977, The marine chemistry of iodine in anoxic basins: Geochimica et Cosmochimica Acta, v. 41, p. 151–159, doi:https://doi.org/10.1016/0016-7037(77)90195-8.

Wray, J.J., 1977, Late Paleozoic Calcareous Red Algae, *in* Flügel, E. ed., Fossil Algae, Berlin, Heidelberg, Springer Berlin Heidelberg, p. 167–176.

Zhou, X., Jenkyns, H.C., Owens, J.D., Junium, C.K., Zheng, X.Y., Sageman, B.B., Hardisty, D.S., Lyons, T.W., Ridgwell, A., and Lu, Z., 2015, Upper ocean oxygenation dynamics from I/Ca ratios during the Cenomanian-Turonian OAE 2: Paleoceanography, v. 30, p. 510–526, doi:10.1002/2014PA002741.

Zhou, X., Thomas, E., Rickaby, R.E.M., Winguth, A.M.E., and Lu, Z., 2014, I/Ca evidence for upper ocean deoxygenation during the PETM: Paleoceanography, v. 29, p. 964–975, doi:10.1002/2014PA002702.

Supporting information for "Reduction in animal abundance and oxygen availability during and after the end-Triassic mass extinction"

Contents of this file

1. Figure S1
2. Figure S2
3. Figure S3

Additional supporting information (files uploaded separately)

1. Table S1: Point count values used in the study
2. Table S2: Diversity count values used in the study
3. Table S3: I/Ca ratios from Italcementi and Val Adrara sections

Figure S1: Plots of diversity changes in major taxa across the Triassic/Jurassic boundary in Lombardy Basin (sections Val Adrara and Italcementi combined) and Apennine platform (Mt. Cefalo section).

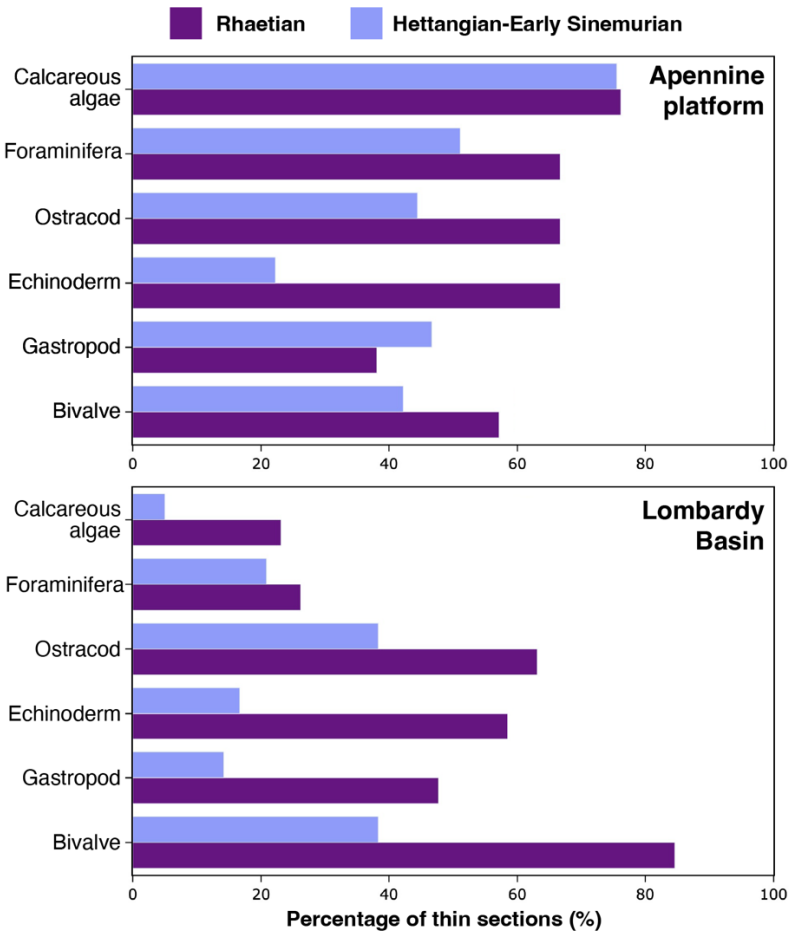

Figure S2: Plots of I/Ca vs $\delta^{18}O$, I/Ca vs Mg/Ca and I/Ca vs Mn/Sr in samples from Italcementi and Val Adrara sections.

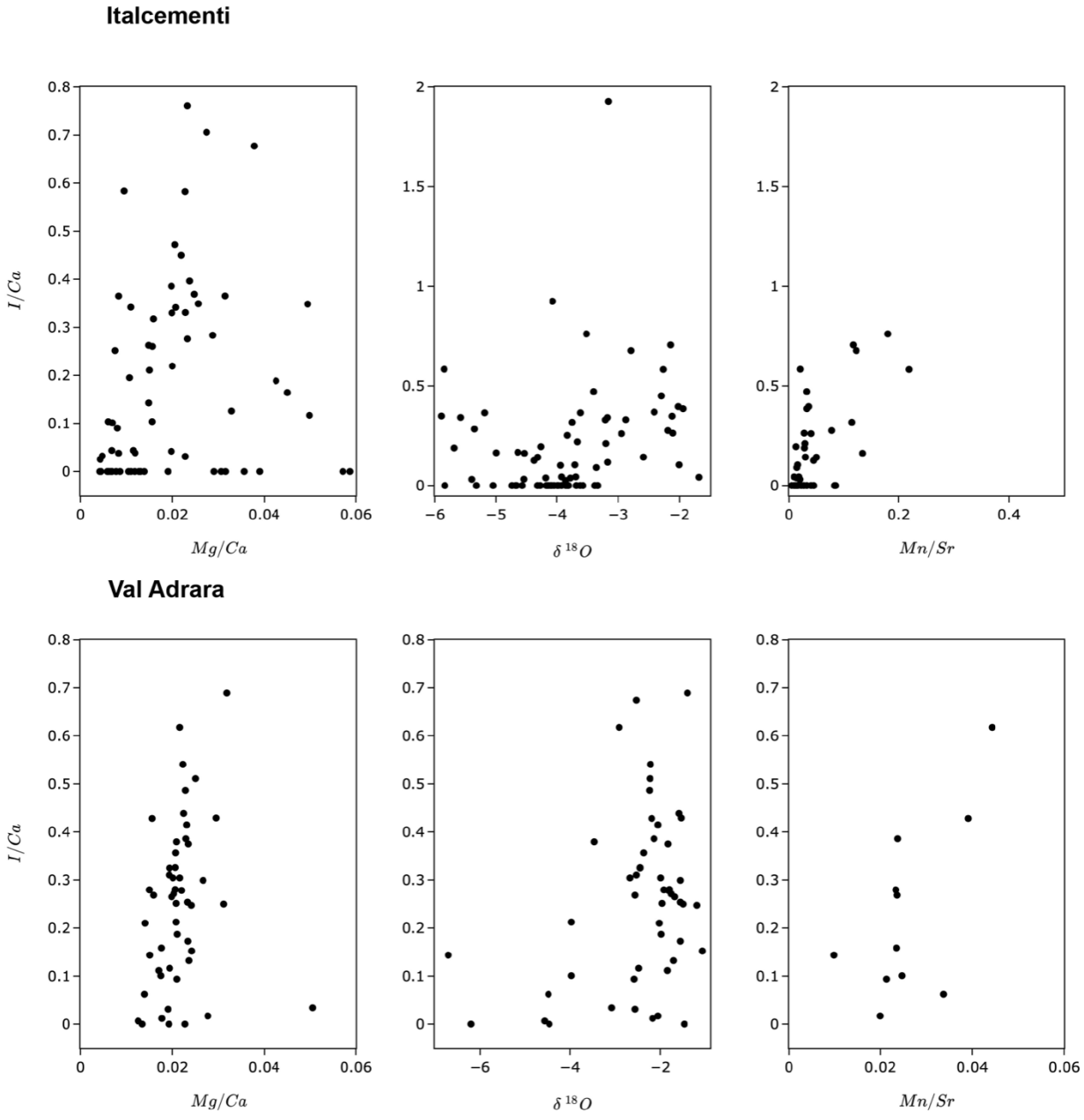

Figure S3: I/Ca ratios associated with every lithology in the Val Adrara and Italcementi sections.

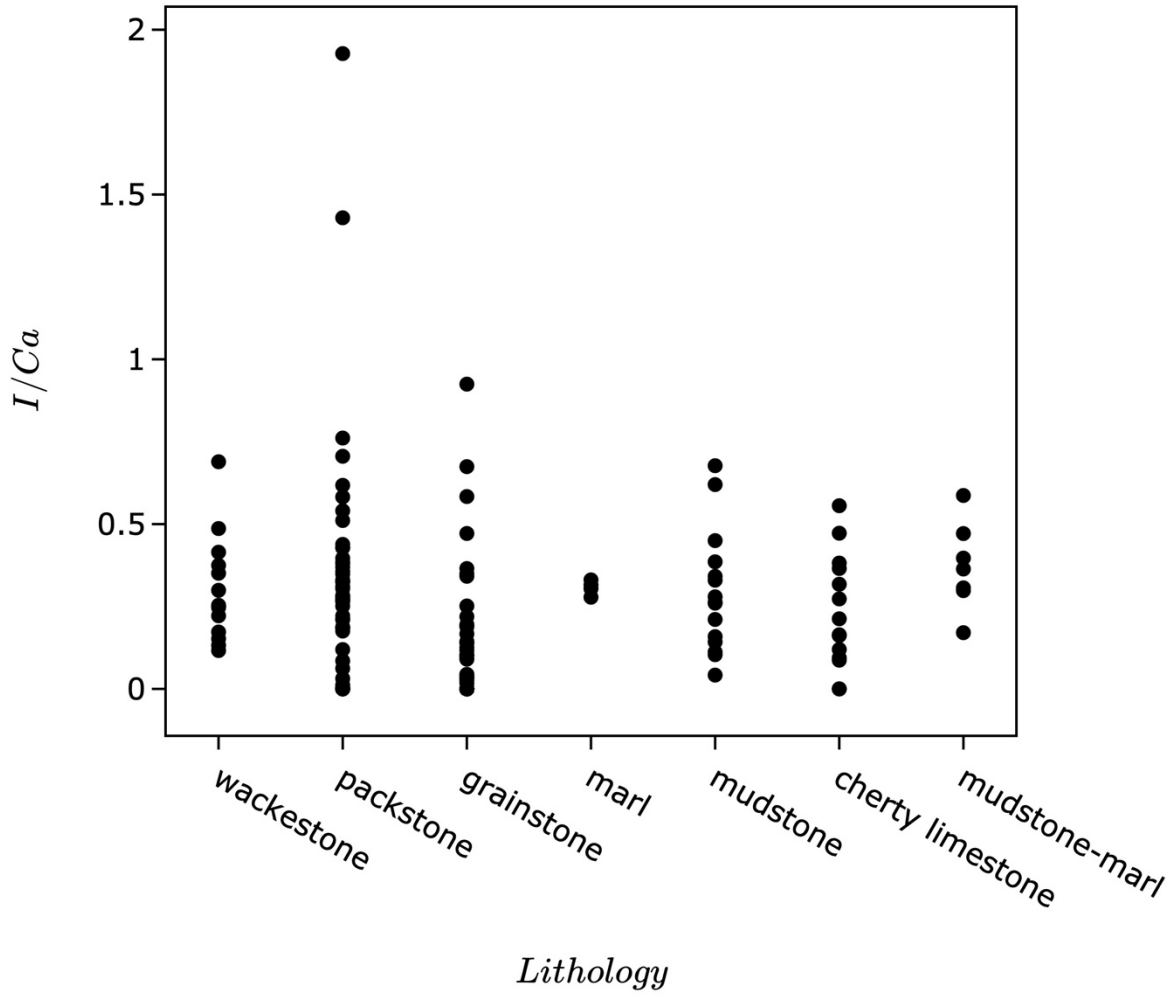

height	ganic_matte	icrosparite	obial_filame	robial_clott	micrite	sponges	peloid	ooids	ounter_stu	unid_biota	oraminifera	reen_algae	bivalves	chinoderm	problematic	ostracods	gastropods	t_blocky_ca	total	skeletal
2.8	0	0	0	0	239	0	3	0	0	5	0	6	19	4	0	12	0	12	300	15.3
9.8	0	0	0	0	298	0	0	0	0	0	0	0	1	1	0	0	0	0	300	0.7
30.8	0	0	0	0	275	0	0	0	0	3	0	0	6	12	0	4	0	0	300	8.3
33	0	0	0	0	298	0	0	0	0	1	0	0	0	1	0	0	0	0	300	0.7
46.9	0	0	0	0	258	0	0	0	0	5	5	2	7	5	0	8	2	8	300	11.3
49.9	0	0	0	0	286	0	0	0	0	0	0	0	6	0	0	3	0	5	300	3.0
52.2	0	9	0	0	236	0	12	0	0	3	2	0	16	6	3	2	0	11	300	10.7
64.7	0	0	0	0	300	0	0	0	0	0	0	0	0	0	0	0	0	0	300	0.0
69.3	0	0	0	0	297	0	0	0	0	2	0	0	1	0	0	0	0	0	300	1.0
71.8	0	4	0	0	288	0	0	0	0	2	0	0	3	0	1	0	0	2	300	2.0
80	0	190	0	0	3	0	95	12	0	0	0	0	0	0	0	0	0	0	300	0.0
81	0	34	0	0	15	0	8	233	0	0	0	0	1	0	0	0	0	9	300	0.3
82	0	13	0	0	64	0	73	122	0	1	0	2	1	0	0	0	0	24	300	1.3
85	0	59	0	0	0	0	74	40	0	7	0	33	28	0	2	0	0	57	300	23.3
86	0	31	0	0	3	0	48	173	0	0	0	16	2	0	0	0	0	27	300	6.0
87	0	25	0	0	27	0	24	180	0	2	0	3	5	0	0	0	1	33	300	3.7
88	0	34	0	0	16	0	63	65	0	7	0	35	5	0	0	0	2	73	300	16.3
89	0	40	0	0	10	0	103	89	0	1	1	20	3	0	1	0	2	30	300	9.3
91	0	7	0	0	0	0	53	152	0	0	0	8	1	0	0	0	0	79	300	3.0
92	0	39	0	0	0	0	28	168	0	0	0	5	0	0	0	0	0	60	300	1.7
93	0	27	0	0	120	0	76	28	0	5	0	6	1	3	14	0	0	20	300	9.7
95	0	123	0	0	51	0	79	31	0	2	0	9	0	1	0	0	0	4	300	4.0
97	0	18	0	0	98	0	174	2	1	1	0	2	0	3	1	0	0	0	300	2.3
98	0	124	0	0	62	0	107	0	0	2	0	2	0	0	1	0	0	2	300	1.7
100.6	0	24	0	0	202	0	41	4	0	2	0	1	0	0	1	0	0	25	300	1.3
101.4	0	0	0	0	279	0	1	0	0	0	0	0	1	0	0	0	0	19	300	0.3
102.5	0	0	0	0	279	0	0	0	0	0	0	0	0	1	0	0	0	20	300	0.3
103.5	0	0	0	0	292	0	0	0	0	0	0	0	0	0	0	0	0	8	300	0.0
108	0	0	0	0	300	0	0	0	0	0	0	0	0	0	0	0	0	0	300	0.0
114.4	10	0	0	7	282	0	0	0	0	0	0	0	0	0	0	0	0	1	300	0.0
119	0	0	0	0	300	0	0	0	0	0	0	0	0	0	0	0	0	0	300	0.0
128	0	0	0	5	293	0	0	0	0	0	0	0	0	0	0	0	0	2	300	0.0
134	0	0	0	0	0	0	0	0	0	0	0	0	0	0	0	0	0	300	300	0.0
140	0	0	0	0	300	0	0	0	0	0	0	0	0	0	0	0	0	0	300	0.0
150	0	0	0	0	300	0	0	0	0	0	0	0	0	0	0	0	0	0	300	0.0
158	0	0	0	0	292	0	0	0	0	1	0	0	3	0	0	1	0	3	300	1.7
167	0	0	0	0	1	0	0	0	0	0	0	0	0	0	0	0	0	299	300	0.0
168	0	1	0	0	299	0	0	0	0	0	0	0	0	0	0	0	0	1	301	0.0
169	0	0	0	0	8	0	0	0	0	0	0	0	0	0	0	0	0	292	300	0.0
173	0	0	0	0	293	0	0	0	0	5	0	0	2	0	0	0	0	0	300	2.3
180	0	92	0	0	151	0	56	0	0	0	0	0	0	0	0	1	0	0	300	0.3
198	0	60	0	0	232	0	8	0	0	0	0	0	0	0	0	0	0	0	300	0.0
202	0	128	0	0	159	0	11	0	0	1	0	0	0	0	0	0	0	1	300	0.3
210	0	1	0	0	264	0	0	0	0	6	0	0	0	1	0	2	0	26	300	3.0
214	0	4	0	0	294	0	1	0	0	1	0	0	0	0	0	0	0	0	300	0.3
219	0	27	0	0	1	0	269	0	0	0	0	0	0	0	0	3	0	0	300	1.0
226	0	50	0	0	96	0	154	0	0	0	0	0	0	0	0	0	0	0	300	0.0
231	1	1	0	0	292	0	4	0	0	1	0	0	1	0	0	0	0	0	300	0.7
238	0	22	0	0	275	0	0	0	0	0	0	0	0	0	0	3	0	0	300	1.0
240.75	0	147	0	0	7	0	80	45	0	2	5	0	0	0	0	1	0	13	300	2.7
242.9	0	6	0	0	283	0	6	0	0	0	2	0	0	0	0	2	0	1	300	1.3
245.6	0	0	0	0	291	0	0	0	0	6	0	0	1	0	0	1	0	0	299	2.7
250.3	0	1	0	0	274	0	0	0	1	3	2	0	2	0	0	7	2	7	299	5.3
255	0	6	0	0	268	0	0	0	0	23	0	0	0	0	0	0	0	3	300	7.7
259	0	0	0	0	278	0	0	0	0	6	0	0	2	0	0	12	0	2	300	6.7
260.4	0	2	0	0	280	4	0	0	0	13	0	0	0	0	0	1	0	0	300	6.0
262.5	0	1	0	0	277	0	2	0	0	18	0	0	1	0	0	1	0	0	300	6.7
264.5	0	0	0	0	285	0	15	0	0	0	0	0	0	0	0	0	0	0	300	0.0
269.5	0	1	0	0	279	0	0	0	0	13	0	0	2	0	0	2	0	3	300	5.7
271.5	0	4	3	0	134	0	148	0	1	2	0	0	8	0	0	0	0	0	300	3.3
272	0	21	0	0	201	0	63	0	0	13	0	0	1	0	0	1	0	0	300	5.0
277	0	6	0	0	261	18	2	0	0	10	0	0	1	0	0	0	0	2	300	9.7
278	0	13	0	0	255	4	22	0	0	5	0	0	0	0	0	1	0	0	300	3.3
296	0	5	0	0	265	11	2	0	0	3	0	0	2	0	0	1	0	11	300	5.7
306	0	28	0	0	185	16	63	0	0	3	0	0	4	0	0	0	0	1	300	7.7
324	1	15	0	0	175	3	0	31	0	8	5	0	2	0	0	5	2	52	299	8.3
333	0	2	0	0	207	87	1	0	0	0	0	0	0	0	0	1	0	2	300	29.3
348	0	12	0	0	213	33	0	0	0	3	1	0	1	0	0	0	0	37	300	12.7
363	0	6	0	0	247	45	0	0	0	0	0	0	1	0	0	1	0	0	300	15.7
378	0	13	0	0	203	81	0	0	0	0	3	0	0	0	0	0	0	0	300	28.0
390	0	15	0	0	252	31	0	0	0	2	0	0	0	0	0	0	0	0	300	11.0
417	0	19	0	0	236	41	0	0	0	0	0	0	0	0	0	1	0	3	300	14.0

height	bivalve	gastropod	ostracod	foram	greenalgae	echinoderm	peloid	ooid	sponge
1.5	1	0	1	0	0	0	0	0	0
3.5	1	1	1	1	0	0	0	0	0
4.6	1	1	1	1	0	0	0	1	0
6	1	1	1	1	0	0	0	1	0
6.7	1	0	1	0	0	0	0	0	0
7.5	0	0	0	0	0	0	0	0	0
8.31	1	0	1	0	0	0	0	0	0
8.6	1	0	1	0	0	0	0	0	0
9	1	1	1	0	0	1	0	0	0
9.6	1	0	1	0	0	0	0	0	0
11.5	1	0	0	0	0	1	0	0	0
12.5	1	0	1	1	0	0	0	0	0
13.2	1	0	0	0	0	0	0	0	0
14.1	0	0	1	1	0	0	0	0	0
14.5	1	0	1	0	0	0	1	0	0
15.3	1	1	1	0	1	1	0	0	0
16.5	1	0	0	0	0	0	0	0	0
17.8	1	0	1	0	0	0	0	0	0
20.6	1	0	1	0	0	1	0	0	0
21.6	0	0	0	1	0	0	0	0	0
22.9	1	0	0	0	0	0	0	0	0
23.3	1	1	1	0	0	1	0	0	0
24.3	1	0	1	1	0	1	0	0	0
25.2	0	1	0	0	0	1	0	0	0
26.1	1	0	1	1	0	0	0	0	0
26.9	0	0	1	0	0	0	0	0	0
27.5	1	0	1	0	0	0	0	0	0
27.9	1	1	0	0	1	1	0	0	0
28.3	1	1	1	0	0	1	0	1	0
29	1	1	1	0	1	1	0	0	0
30.3	1	0	0	0	0	0	1	0	0
31.5	1	0	0	0	0	0	0	0	0
32.8	0	0	0	0	0	1	0	0	0
33.8	1	1	0	1	0	1	0	0	0
34.7	1	1	0	0	0	0	0	0	0
35.6	0	0	0	0	0	0	0	0	0
36.5	1	0	0	0	0	0	1	0	0
37.3	1	1	1	0	0	1	0	0	0
38.7	1	1	0	0	0	1	1	0	0
39	1	1	1	0	0	1	1	0	0
40.3	1	1	0	0	0	1	1	0	0
40.7	1	1	1	0	0	1	1	0	0
41.1	1	1	0	0	0	1	1	0	0

41.51	1	0	1	0	1	1	1	0	0
42	0	0	0	0	0	0	0	0	0
42.5	1	1	1	0	1	1	1	0	0
43.1	1	1	1	0	0	1	0	0	0
43.6	1	1	1	0	1	1	1	0	0
43.7	1	0	0	1	0	1	1	0	0
43.8	1	1	1	0	1	1	1	0	0
43.9	1	1	1	1	1	1	1	0	0
44.2	1	1	1	0	1	1	0	0	1
44.5	1	1	1	1	1	1	1	0	1
44.9	0	0	0	0	0	0	0	0	0
45.5	1	1	0	1	1	1	1	0	1
46	1	0	1	0	0	1	0	0	1
46.5	0	0	0	0	0	0	0	0	0
47.6	0	0	0	0	0	0	0	0	0
47.8	0	0	0	0	0	0	0	0	0
48.2	0	0	0	0	0	0	0	0	0
49.2	0	0	0	0	0	0	0	0	0
49.5	0	0	0	0	0	0	0	0	0
50.2	0	0	0	0	0	0	0	0	0
52.5	0	0	0	0	0	0	0	0	0
54.5	0	0	0	0	0	0	0	0	0
55.7	0	0	0	0	0	0	0	0	0
56	0	0	0	0	0	0	0	0	0
57.2	0	0	0	0	0	0	0	0	0
58.6	0	0	0	0	0	0	0	0	0
58.9	0	0	0	0	0	0	0	0	0
60.7	0	0	0	0	0	0	0	0	0
62	0	0	0	0	0	0	0	0	0
64	0	0	0	0	0	0	0	0	0
64.6	0	0	0	0	0	0	0	0	0
65.1	0	0	0	0	0	0	0	0	0
66	1	0	1	0	0	0	0	0	0
68.6	1	0	1	0	0	0	0	0	0
70	1	0	1	0	0	0	0	0	0
71	0	0	0	0	0	0	0	0	0
72.2	1	0	1	0	0	0	1	0	0
73	0	1	1	1	0	0	1	0	0
74.4	1	0	1	0	0	0	1	0	0
75.4	0	0	0	0	0	0	0	0	0
77	0	0	0	0	0	0	0	0	0
77.3	0	0	1	1	0	0	1	0	0
78	1	1	1	0	0	1	1	0	0
79	1	1	1	1	0	0	1	0	0

79.2	1	0	1	0	0	1	1	0	0
80.5	1	1	1	1	0	1	1	0	0
81.5	1	0	1	0	0	1	0	0	0
82.5	1	0	1	1	0	1	1	0	0
84.2	1	0	1	0	0	1	0	0	0
86	0	0	1	1	0	0	1	1	0
86.9	0	0	1	0	0	0	0	0	0
87.4	0	0	0	1	0	0	1	1	0
89.1	0	0	0	0	0	0	0	0	0
90.2	1	0	0	1	1	0	1	1	0
91.2	0	0	0	0	0	0	1	1	0
92.4	1	0	0	1	0	0	1	1	0
93	1	0	0	0	0	0	0	1	0
93.6	0	0	0	0	0	0	0	0	0
93.9	1	0	0	1	0	0	1	1	0
95.4	0	0	0	0	0	0	0	0	0
95.9	1	0	0	0	1	0	0	0	0
96.4	1	1	1	1	1	1	1	1	0
97.6	0	0	0	0	0	0	0	0	0
97.9	1	0	0	0	0	0	1	1	0
99.2	0	0	0	0	0	0	0	0	0
100.6	1	0	1	0	1	0	1	1	0
103.4	0	0	0	0	0	0	0	0	0
105.1	0	0	0	0	0	0	0	0	0

Italcementi

height	bivalve	gastropod	brachiopod	echinoderm	ostracod	coral	bryozoan	sponge	foram
0	1	1	0	0	1	0	0	0	1
7	1	0	0	0	0	0	0	0	0
13	1	0	0	1	0	0	0	0	1
19	0	0	0	0	0	0	0	0	0
20	0	0	0	0	0	0	0	0	0
24	1	1	0	1	1	0	0	0	1
28	0	0	0	1	1	0	0	0	0
34	1	1	0	1	1	0	0	0	1
40	0	0	0	0	0	0	0	0	0
45	0	0	0	0	0	0	0	0	0
52	0	1	0	1	1	0	0	0	1
58	1	0	0	1	1	0	0	0	1
62	0	0	0	0	0	0	0	0	0
67	1	1	0	1	1	0	0	0	1
72	0	0	0	1	1	0	0	0	1
78	1	0	1	1	1	0	0	0	1
93	1	1	0	1	1	0	0	0	1
96	1	1	0	1	1	0	0	0	1
103	1	0	0	1	1	0	0	0	1
109	1	0	0	1	1	0	0	0	1
115	0	1	0	1	1	0	0	0	1
117	0	0	0	0	0	0	0	0	0
121	0	0	0	0	0	0	0	0	0
123	0	0	0	0	0	0	0	0	1
125	1	1	0	0	0	0	0	0	0
129	1	1	0	1	0	0	0	0	0
133	0	0	0	0	1	0	0	0	0
136	0	0	0	0	0	0	0	0	0
139	0	0	0	0	0	0	0	0	0
141	0	1	0	0	1	0	0	0	0
143	0	0	0	0	1	0	0	0	1
145	0	0	0	0	0	0	0	0	1
147	0	1	0	0	1	0	0	0	1
153	0	0	0	0	1	0	0	0	1
156	0	0	0	0	0	0	0	0	1
163	1	0	0	0	0	0	0	0	1
169	0	0	0	0	0	0	0	0	0
174	0	0	0	0	0	0	0	0	0
176	0	1	0	0	0	0	0	0	0
178	1	1	0	0	0	0	0	0	0
182	0	0	0	0	0	0	0	0	0
185	0	0	0	0	0	0	0	0	1
188	1	1	0	0	1	0	0	0	1

194	0	0	0	0	0	0	0	0	0
197	1	1	0	0	0	0	0	0	1
199	1	1	0	1	0	0	0	0	0
203	1	1	0	0	0	0	0	0	0
207	0	1	0	0	1	0	0	0	0
212	0	0	0	0	0	0	0	0	0
218	0	0	0	0	0	0	0	0	0
220	0	0	0	0	0	0	0	0	0
229	1	1	0	0	1	0	0	0	1
235	1	0	0	0	1	0	0	0	1
241	0	0	0	1	1	0	0	0	1
253	0	0	0	0	0	0	0	0	0
274	1	1	0	1	1	0	0	0	1
286	1	1	0	1	1	0	0	0	1
292	0	1	0	1	1	0	0	0	1
298	1	1	0	1	1	0	0	0	1
301	1	1	0	0	1	0	0	0	1
306	1	0	0	0	1	0	0	0	1
311	1	1	0	0	0	0	0	0	0
313	1	1	0	1	1	0	0	0	1
318	0	1	0	1	1	0	0	0	1
321	1	1	0	1	1	0	0	0	1
323	1	0	0	0	1	0	0	0	1

greenalga	redalga p	roblematic	Mt Cefalo
0	0	0	
1	0	1	
1	0	1	
0	0	1	
0	0	0	
1	0	1	
1	0	1	
1	0	1	
0	0	0	
0	0	0	
1	0	1	
1	0	1	
0	0	0	
1	0	1	
1	0	1	
1	0	0	
1	0	0	
1	0	1	
1	0	1	
1	0	1	
1	0	1	
0	0	0	
0	0	0	
0	0	1	
0	0	1	
0	0	1	
0	0	1	
0	0	0	
0	0	0	
0	0	1	
0	0	1	
0	0	1	
0	0	1	
0	0	1	
0	0	1	
0	0	0	
0	0	1	
0	0	1	
0	0	1	
0	0	1	
0	0	1	
0	0	1	
0	0	1	

0	0	0
1	0	0
1	0	1
1	0	1
0	0	1
0	0	1
0	0	1
0	0	1
0	0	1
0	0	1
0	0	1
0	0	0
1	0	0
1	0	0
0	0	0
1	0	0
0	0	0
0	0	0
1	0	0
0	0	1
0	0	1
0	0	0
0	0	1

height	bivalve	gastropod	brachiopod	echinoderm	ostracod	coral	bryozoan	sponge	foram
5.3	0	0	0	0	0	0	0	0	0
13.4	0	0	0	0	0	0	0	0	0
17.1	0	0	0	0	0	0	0	0	0
21	0	0	0	0	0	0	0	0	0
25.8	0	0	0	0	0	0	0	0	0
29	0	0	0	0	0	0	0	0	0
33.6	0	0	0	0	0	0	0	0	0
34	0	0	0	0	0	0	0	0	0
38	0	0	0	0	0	0	0	0	0
43.7	0	0	0	0	0	0	0	0	0
49.9	0	0	0	0	0	0	0	0	0
54.4	0	0	0	0	0	0	0	0	0
67	0	0	0	0	0	0	0	0	0
75	0	0	0	0	0	0	0	0	0
78.1	0	0	0	0	0	0	0	0	0
81.9	0	0	0	0	0	0	0	0	0
90.3	0	0	0	0	0	0	0	0	0
103.6	0	0	0	0	1	0	0	1	1
106.6	0	1	0	1	0	0	0	0	0
114.4	0	0	0	0	0	0	0	0	0
120	0	0	0	0	1	0	0	0	0
135.5	0	0	0	0	0	0	0	1	1
147.9	0	0	0	0	0	0	0	0	0
153.9	0	0	0	0	0	0	0	0	0
162.2	0	0	0	0	0	0	0	0	0
170	1	1	0	0	0	0	0	1	0
184.9	0	0	0	0	0	0	0	0	0
193.2	0	1	0	0	0	0	0	1	0
205.4	0	0	0	0	0	0	0	0	0
224.2	0	0	0	0	0	0	0	1	0
249.6	0	0	0	0	0	0	0	0	0
264.7	0	0	0	0	0	0	0	0	0
276.7	0	0	0	0	1	0	0	0	0
294	0	0	0	0	0	0	0	0	0
309.3	1	0	0	1	0	0	0	0	0
323.8	1	1	0	1	1	0	0	1	0
337.2	0	0	0	0	0	0	0	1	0
350	0	0	0	0	0	0	0	1	0
365	1	0	0	0	1	0	0	1	0
378.5	0	0	0	0	0	0	0	1	0
391	0	0	0	0	0	0	0	1	0
404.5	0	0	0	0	0	0	0	1	0

greenalga	redalga p	problemati	ozzo Glaciale
0	0	0	
0	0	0	
0	0	0	
0	0	0	
0	0	0	
0	0	0	
0	0	0	
0	0	0	
0	0	0	
0	0	0	
0	0	0	
0	0	0	
0	0	0	
0	0	0	
0	0	0	
0	0	0	
0	0	0	
0	0	0	
0	0	0	
0	0	0	
0	0	0	
0	0	0	
0	0	0	
0	0	0	
0	0	0	
0	0	0	
0	0	0	
0	0	0	
0	0	0	
0	0	0	
0	0	0	
0	0	0	
0	0	0	
0	0	0	
0	0	0	
0	0	0	
0	0	0	
0	0	0	
0	0	0	
0	0	0	
0	0	0	
0	0	0	

height	bivalve	gastropod	ostracod	foram	greenalga	sponge	echinoderm	peloid	ooid
2.8	1	1	1	1	1	0	1	1	0
9.8	1	0	0	0	0	0	1	0	0
20	0	0	0	0	0	0	1	0	0
30.8	1	0	1	0	0	0	1	1	0
40	1	0	1	0	0	0	1	1	0
46.9	1	1	1	1	1	0	1	1	0
49.9	1	1	1	1	1	0	1	0	0
51.2	1	1	1	1	1	0	1	0	0
52.2	1	1	1	0	0	0	1	0	0
64.7	0	0	0	0	0	0	0	0	0
69.3	1	0	1	1	0	0	0	0	0
71.8	0	0	1	0	0	0	0	1	0
80	0	0	0	0	0	0	0	0	0
80.8	0	0	0	0	0	0	0	1	0
81	0	1	0	1	0	0	0	1	1
85	1	0	0	1	0	0	0	1	1
87	1	1	0	0	0	0	0	1	1
88	1	1	0	1	1	0	1	0	0
89	0	0	0	1	0	0	1	1	1
91	1	0	0	0	0	0	0	1	1
92	1	0	0	0	0	0	0	0	0
93	1	0	0	1	1	0	0	1	1
95	1	0	0	0	0	0	0	1	1
98	1	0	1	0	0	0	0	1	1
100.6	0	0	0	0	0	0	0	1	1
101.4	0	0	0	0	0	0	0	0	0
102.5	0	0	0	0	0	0	0	1	1
103.5	0	0	0	0	0	0	0	0	0
108	0	0	0	0	0	0	0	0	0
114.4	0	0	0	0	0	0	0	0	0
119	0	0	0	0	0	0	0	0	0
128	0	0	0	0	0	0	0	0	0
134	0	0	0	0	0	0	0	0	0
140	0	0	0	0	0	0	0	0	0
145	0	0	0	0	0	0	0	1	0
150	0	0	0	0	0	0	0	0	0
158	0	0	1	0	0	0	0	0	0
167	0	0	0	0	0	0	0	0	0
168	1	0	0	0	0	0	0	0	1
169	0	0	0	0	0	0	0	0	0
173	0	0	1	0	0	0	0	0	0
180	0	0	0	0	0	0	0	0	0
185	0	0	0	0	0	0	0	0	0

198	0	0	0	0	0	0	0	0	0
202	0	0	0	0	0	0	0	0	0
210	0	0	0	0	0	0	0	0	0
214	0	0	0	0	0	0	0	0	0
219	0	0	0	0	0	0	0	0	0
226	0	0	0	0	0	0	0	0	1
231	0	0	1	0	0	0	0	0	0
238	0	0	1	0	0	0	0	0	0
240.75	1	0	0	0	0	0	0	1	1
242.9	0	0	1	0	0	0	0	0	0
245.6	1	0	1	0	0	0	1	0	0
250.3	1	1	1	0	0	0	1	0	0
255	1	1	1	1	0	0	1	1	0
259	1	1	1	1	0	0	1	0	0
260.4	1	1	1	0	0	1	0	1	0
262.5	1	1	1	0	0	0	1	0	0
264.5	0	0	1	0	0	0	0	1	0
269.5	1	0	1	0	0	0	1	0	0
271.5	1	0	1	0	0	0	0	0	0
272	1	1	1	0	0	0	1	0	0
277	0	0	1	0	0	1	0	0	0
278	0	0	1	1	0	1	0	0	0
296	1	1	1	1	0	1	0	1	0
306	1	1	1	0	0	1	1	0	0
324	1	1	1	1	0	1	1	1	0
333	1	0	1	0	0	1	0	0	0
348	1	0	1	1	0	1	0	0	0
363	0	0	1	1	0	1	0	0	0
378	0	0	0	0	0	1	0	0	0
390	1	0	1	1	0	1	1	0	0
417	0	0	1	0	0	1	1	1	0

Val Adrara

height	bivalve	gastropod	ostracod	foram	greenalgae	echinoderm	peloid	ooid	sponge
1.5	1	0	1	0	0	0	0	0	0
3.5	1	1	1	1	0	0	0	0	0
4.6	1	1	1	1	0	0	0	1	0
6	1	1	1	1	0	0	0	1	0
6.7	1	0	1	0	0	0	0	0	0
7.5	0	0	0	0	0	0	0	0	0
8.31	1	0	1	0	0	0	0	0	0
8.6	1	0	1	0	0	0	0	0	0
9	1	1	1	0	0	1	0	0	0
9.6	1	0	1	0	0	0	0	0	0
11.5	1	0	0	0	0	1	0	0	0
12.5	1	0	1	1	0	0	0	0	0
13.2	1	0	0	0	0	0	0	0	0
14.1	0	0	1	1	0	0	0	0	0
14.5	1	0	1	0	0	0	1	0	0
15.3	1	1	1	0	1	1	0	0	0
16.5	1	0	0	0	0	0	0	0	0
17.8	1	0	1	0	0	0	0	0	0
20.6	1	0	1	0	0	1	0	0	0
21.6	0	0	0	1	0	0	0	0	0
22.9	1	0	0	0	0	0	0	0	0
23.3	1	1	1	0	0	1	0	0	0
24.3	1	0	1	1	0	1	0	0	0
25.2	0	1	0	0	0	1	0	0	0
26.1	1	0	1	1	0	0	0	0	0
26.9	0	0	1	0	0	0	0	0	0
27.5	1	0	1	0	0	0	0	0	0
27.9	1	1	0	0	1	1	0	0	0
28.3	1	1	1	0	0	1	0	1	0
29	1	1	1	0	1	1	0	0	0
30.3	1	0	0	0	0	0	1	0	0
31.5	1	0	0	0	0	0	0	0	0
32.8	0	0	0	0	0	1	0	0	0
33.8	1	1	0	1	0	1	0	0	0
34.7	1	1	0	0	0	0	0	0	0
35.6	0	0	0	0	0	0	0	0	0
36.5	1	0	0	0	0	0	1	0	0
37.3	1	1	1	0	0	1	0	0	0
38.7	1	1	0	0	0	1	1	0	0
39	1	1	1	0	0	1	1	0	0
40.3	1	1	0	0	0	1	1	0	0
40.7	1	1	1	0	0	1	1	0	0
41.1	1	1	0	0	0	1	1	0	0

41.51	1	0	1	0	1	1	1	0	0
42	0	0	0	0	0	0	0	0	0
42.5	1	1	1	0	1	1	1	0	0
43.1	1	1	1	0	0	1	0	0	0
43.6	1	1	1	0	1	1	1	0	0
43.7	1	0	0	1	0	1	1	0	0
43.8	1	1	1	0	1	1	1	0	0
43.9	1	1	1	1	1	1	1	0	0
44.2	1	1	1	0	1	1	0	0	1
44.5	1	1	1	1	1	1	1	0	1
44.9	0	0	0	0	0	0	0	0	0
45.5	1	1	0	1	1	1	1	0	1
46	1	0	1	0	0	1	0	0	1
46.5	0	0	0	0	0	0	0	0	0
47.6	0	0	0	0	0	0	0	0	0
47.8	0	0	0	0	0	0	0	0	0
48.2	0	0	0	0	0	0	0	0	0
49.2	0	0	0	0	0	0	0	0	0
49.5	0	0	0	0	0	0	0	0	0
50.2	0	0	0	0	0	0	0	0	0
52.5	0	0	0	0	0	0	0	0	0
54.5	0	0	0	0	0	0	0	0	0
55.7	0	0	0	0	0	0	0	0	0
56	0	0	0	0	0	0	0	0	0
57.2	0	0	0	0	0	0	0	0	0
58.6	0	0	0	0	0	0	0	0	0
58.9	0	0	0	0	0	0	0	0	0
60.7	0	0	0	0	0	0	0	0	0
62	0	0	0	0	0	0	0	0	0
64	0	0	0	0	0	0	0	0	0
64.6	0	0	0	0	0	0	0	0	0
65.1	0	0	0	0	0	0	0	0	0
66	1	0	1	0	0	0	0	0	0
68.6	1	0	1	0	0	0	0	0	0
70	1	0	1	0	0	0	0	0	0
71	0	0	0	0	0	0	0	0	0
72.2	1	0	1	0	0	0	1	0	0
73	0	1	1	1	0	0	1	0	0
74.4	1	0	1	0	0	0	1	0	0
75.4	0	0	0	0	0	0	0	0	0
77	0	0	0	0	0	0	0	0	0
77.3	0	0	1	1	0	0	1	0	0
78	1	1	1	0	0	1	1	0	0
79	1	1	1	1	0	0	1	0	0

79.2	1	0	1	0	0	1	1	0	0
80.5	1	1	1	1	0	1	1	0	0
81.5	1	0	1	0	0	1	0	0	0
82.5	1	0	1	1	0	1	1	0	0
84.2	1	0	1	0	0	1	0	0	0
86	0	0	1	1	0	0	1	1	0
86.9	0	0	1	0	0	0	0	0	0
87.4	0	0	0	1	0	0	1	1	0
89.1	0	0	0	0	0	0	0	0	0
90.2	1	0	0	1	1	0	1	1	0
91.2	0	0	0	0	0	0	1	1	0
92.4	1	0	0	1	0	0	1	1	0
93	1	0	0	0	0	0	0	1	0
93.6	0	0	0	0	0	0	0	0	0
93.9	1	0	0	1	0	0	1	1	0
95.4	0	0	0	0	0	0	0	0	0
95.9	1	0	0	0	1	0	0	0	0
96.4	1	1	1	1	1	1	1	1	0
97.6	0	0	0	0	0	0	0	0	0
97.9	1	0	0	0	0	0	1	1	0
99.2	0	0	0	0	0	0	0	0	0
100.6	1	0	1	0	1	0	1	1	0
103.4	0	0	0	0	0	0	0	0	0
105.1	0	0	0	0	0	0	0	0	0

height	bivalve	gastropod	brachiopod	echinoderm	ostracod	coral	bryozoan	sponge	foram
0	1	1	0	0	1	0	0	0	1
7	1	0	0	0	0	0	0	0	0
13	1	0	0	1	0	0	0	0	1
19	0	0	0	0	0	0	0	0	0
20	0	0	0	0	0	0	0	0	0
24	1	1	0	1	1	0	0	0	1
28	0	0	0	1	1	0	0	0	0
34	1	1	0	1	1	0	0	0	1
40	0	0	0	0	0	0	0	0	0
45	0	0	0	0	0	0	0	0	0
52	0	1	0	1	1	0	0	0	1
58	1	0	0	1	1	0	0	0	1
62	0	0	0	0	0	0	0	0	0
67	1	1	0	1	1	0	0	0	1
72	0	0	0	1	1	0	0	0	1
78	1	0	1	1	1	0	0	0	1
93	1	1	0	1	1	0	0	0	1
96	1	1	0	1	1	0	0	0	1
103	1	0	0	1	1	0	0	0	1
109	1	0	0	1	1	0	0	0	1
115	0	1	0	1	1	0	0	0	1
117	0	0	0	0	0	0	0	0	0
121	0	0	0	0	0	0	0	0	0
123	0	0	0	0	0	0	0	0	1
125	1	1	0	0	0	0	0	0	0
129	1	1	0	1	0	0	0	0	0
133	0	0	0	0	1	0	0	0	0
136	0	0	0	0	0	0	0	0	0
139	0	0	0	0	0	0	0	0	0
141	0	1	0	0	1	0	0	0	0
143	0	0	0	0	1	0	0	0	1
145	0	0	0	0	0	0	0	0	1
147	0	1	0	0	1	0	0	0	1
153	0	0	0	0	1	0	0	0	1
156	0	0	0	0	0	0	0	0	1
163	1	0	0	0	0	0	0	0	1
169	0	0	0	0	0	0	0	0	0
174	0	0	0	0	0	0	0	0	0
176	0	1	0	0	0	0	0	0	0
178	1	1	0	0	0	0	0	0	0
182	0	0	0	0	0	0	0	0	0
185	0	0	0	0	0	0	0	0	1
188	1	1	0	0	1	0	0	0	1

194	0	0	0	0	0	0	0	0	0
197	1	1	0	0	0	0	0	0	1
199	1	1	0	1	0	0	0	0	0
203	1	1	0	0	0	0	0	0	0
207	0	1	0	0	1	0	0	0	0
212	0	0	0	0	0	0	0	0	0
218	0	0	0	0	0	0	0	0	0
220	0	0	0	0	0	0	0	0	0
229	1	1	0	0	1	0	0	0	1
235	1	0	0	0	1	0	0	0	1
241	0	0	0	1	1	0	0	0	1
253	0	0	0	0	0	0	0	0	0
274	1	1	0	1	1	0	0	0	1
286	1	1	0	1	1	0	0	0	1
292	0	1	0	1	1	0	0	0	1
298	1	1	0	1	1	0	0	0	1
301	1	1	0	0	1	0	0	0	1
306	1	0	0	0	1	0	0	0	1
311	1	1	0	0	0	0	0	0	0
313	1	1	0	1	1	0	0	0	1
318	0	1	0	1	1	0	0	0	1
321	1	1	0	1	1	0	0	0	1
323	1	0	0	0	1	0	0	0	1

greenalga	redalga p	roblematic	Mt Cefalo
0	0	0	
1	0	1	
1	0	1	
0	0	1	
0	0	0	
1	0	1	
1	0	1	
1	0	1	
0	0	0	
0	0	0	
1	0	1	
1	0	1	
0	0	0	
1	0	1	
1	0	1	
1	0	0	
1	0	0	
1	0	1	
1	0	1	
1	0	1	
1	0	1	
0	0	0	
0	0	0	
0	0	1	
0	0	1	
0	0	1	
0	0	1	
0	0	0	
0	0	0	
0	0	1	
0	0	1	
0	0	1	
0	0	1	
0	0	1	
0	0	1	
0	0	0	
0	0	1	
0	0	1	
0	0	1	
0	0	1	
0	0	1	
0	0	1	
0	0	1	

0	0	0
1	0	0
1	0	1
1	0	1
0	0	1
0	0	1
0	0	1
0	0	1
0	0	1
0	0	1
0	0	1
0	0	0
1	0	0
1	0	0
0	0	0
1	0	0
0	0	0
0	0	0
1	0	0
0	0	1
0	0	1
0	0	0
0	0	1

height	bivalve	gastropod	brachiopod	echinoderm	ostracod	coral	bryozoan	sponge	foram
5.3	0	0	0	0	0	0	0	0	0
13.4	0	0	0	0	0	0	0	0	0
17.1	0	0	0	0	0	0	0	0	0
21	0	0	0	0	0	0	0	0	0
25.8	0	0	0	0	0	0	0	0	0
29	0	0	0	0	0	0	0	0	0
33.6	0	0	0	0	0	0	0	0	0
34	0	0	0	0	0	0	0	0	0
38	0	0	0	0	0	0	0	0	0
43.7	0	0	0	0	0	0	0	0	0
49.9	0	0	0	0	0	0	0	0	0
54.4	0	0	0	0	0	0	0	0	0
67	0	0	0	0	0	0	0	0	0
75	0	0	0	0	0	0	0	0	0
78.1	0	0	0	0	0	0	0	0	0
81.9	0	0	0	0	0	0	0	0	0
90.3	0	0	0	0	0	0	0	0	0
103.6	0	0	0	0	1	0	0	1	1
106.6	0	1	0	1	0	0	0	0	0
114.4	0	0	0	0	0	0	0	0	0
120	0	0	0	0	1	0	0	0	0
135.5	0	0	0	0	0	0	0	1	1
147.9	0	0	0	0	0	0	0	0	0
153.9	0	0	0	0	0	0	0	0	0
162.2	0	0	0	0	0	0	0	0	0
170	1	1	0	0	0	0	0	1	0
184.9	0	0	0	0	0	0	0	0	0
193.2	0	1	0	0	0	0	0	1	0
205.4	0	0	0	0	0	0	0	0	0
224.2	0	0	0	0	0	0	0	1	0
249.6	0	0	0	0	0	0	0	0	0
264.7	0	0	0	0	0	0	0	0	0
276.7	0	0	0	0	1	0	0	0	0
294	0	0	0	0	0	0	0	0	0
309.3	1	0	0	1	0	0	0	0	0
323.8	1	1	0	1	1	0	0	1	0
337.2	0	0	0	0	0	0	0	1	0
350	0	0	0	0	0	0	0	1	0
365	1	0	0	0	1	0	0	1	0
378.5	0	0	0	0	0	0	0	1	0
391	0	0	0	0	0	0	0	1	0
404.5	0	0	0	0	0	0	0	1	0

greenalga	redalga p	problematic	ozzo Glaciale
0	0	0	
0	0	0	
0	0	0	
0	0	0	
0	0	0	
0	0	0	
0	0	0	
0	0	0	
0	0	0	
0	0	0	
0	0	0	
0	0	0	
0	0	0	
0	0	0	
0	0	0	
0	0	0	
0	0	0	
0	0	0	
0	0	0	
0	0	0	
0	0	0	
0	0	0	
0	0	0	
0	0	0	
0	0	0	
0	0	0	
0	0	0	
0	0	0	
0	0	0	
0	0	0	
0	0	0	
0	0	0	
0	0	0	
0	0	0	
0	0	0	
0	0	0	
0	0	0	
0	0	0	
0	0	0	
0	0	0	
0	0	0	
0	0	0	

height	bivalve	gastropod	ostracod	foram	greenalga	sponge	echinoderm	peloid	ooid
2.8	1	1	1	1	1	0	1	1	0
9.8	1	0	0	0	0	0	1	0	0
20	0	0	0	0	0	0	1	0	0
30.8	1	0	1	0	0	0	1	1	0
40	1	0	1	0	0	0	1	1	0
46.9	1	1	1	1	1	0	1	1	0
49.9	1	1	1	1	1	0	1	0	0
51.2	1	1	1	1	1	0	1	0	0
52.2	1	1	1	0	0	0	1	0	0
64.7	0	0	0	0	0	0	0	0	0
69.3	1	0	1	1	0	0	0	0	0
71.8	0	0	1	0	0	0	0	1	0
80	0	0	0	0	0	0	0	0	0
80.8	0	0	0	0	0	0	0	1	0
81	0	1	0	1	0	0	0	1	1
85	1	0	0	1	0	0	0	1	1
87	1	1	0	0	0	0	0	1	1
88	1	1	0	1	1	0	1	0	0
89	0	0	0	1	0	0	1	1	1
91	1	0	0	0	0	0	0	1	1
92	1	0	0	0	0	0	0	0	0
93	1	0	0	1	1	0	0	1	1
95	1	0	0	0	0	0	0	1	1
98	1	0	1	0	0	0	0	1	1
100.6	0	0	0	0	0	0	0	1	1
101.4	0	0	0	0	0	0	0	0	0
102.5	0	0	0	0	0	0	0	1	1
103.5	0	0	0	0	0	0	0	0	0
108	0	0	0	0	0	0	0	0	0
114.4	0	0	0	0	0	0	0	0	0
119	0	0	0	0	0	0	0	0	0
128	0	0	0	0	0	0	0	0	0
134	0	0	0	0	0	0	0	0	0
140	0	0	0	0	0	0	0	0	0
145	0	0	0	0	0	0	0	1	0
150	0	0	0	0	0	0	0	0	0
158	0	0	1	0	0	0	0	0	0
167	0	0	0	0	0	0	0	0	0
168	1	0	0	0	0	0	0	0	1
169	0	0	0	0	0	0	0	0	0
173	0	0	1	0	0	0	0	0	0
180	0	0	0	0	0	0	0	0	0
185	0	0	0	0	0	0	0	0	0

198	0	0	0	0	0	0	0	0	0
202	0	0	0	0	0	0	0	0	0
210	0	0	0	0	0	0	0	0	0
214	0	0	0	0	0	0	0	0	0
219	0	0	0	0	0	0	0	0	0
226	0	0	0	0	0	0	0	0	1
231	0	0	1	0	0	0	0	0	0
238	0	0	1	0	0	0	0	0	0
240.75	1	0	0	0	0	0	0	1	1
242.9	0	0	1	0	0	0	0	0	0
245.6	1	0	1	0	0	0	1	0	0
250.3	1	1	1	0	0	0	1	0	0
255	1	1	1	1	0	0	1	1	0
259	1	1	1	1	0	0	1	0	0
260.4	1	1	1	0	0	1	0	1	0
262.5	1	1	1	0	0	0	1	0	0
264.5	0	0	1	0	0	0	0	1	0
269.5	1	0	1	0	0	0	1	0	0
271.5	1	0	1	0	0	0	0	0	0
272	1	1	1	0	0	0	1	0	0
277	0	0	1	0	0	1	0	0	0
278	0	0	1	1	0	1	0	0	0
296	1	1	1	1	0	1	0	1	0
306	1	1	1	0	0	1	1	0	0
324	1	1	1	1	0	1	1	1	0
333	1	0	1	0	0	1	0	0	0
348	1	0	1	1	0	1	0	0	0
363	0	0	1	1	0	1	0	0	0
378	0	0	0	0	0	1	0	0	0
390	1	0	1	1	0	1	1	0	0
417	0	0	1	0	0	1	1	1	0

Val Adrara

height	bivalve	gastropod	ostracod	foram	greenalgae	echinoderm	peloid	ooid	sponge
1.5	1	0	1	0	0	0	0	0	0
3.5	1	1	1	1	0	0	0	0	0
4.6	1	1	1	1	0	0	0	1	0
6	1	1	1	1	0	0	0	1	0
6.7	1	0	1	0	0	0	0	0	0
7.5	0	0	0	0	0	0	0	0	0
8.31	1	0	1	0	0	0	0	0	0
8.6	1	0	1	0	0	0	0	0	0
9	1	1	1	0	0	1	0	0	0
9.6	1	0	1	0	0	0	0	0	0
11.5	1	0	0	0	0	1	0	0	0
12.5	1	0	1	1	0	0	0	0	0
13.2	1	0	0	0	0	0	0	0	0
14.1	0	0	1	1	0	0	0	0	0
14.5	1	0	1	0	0	0	1	0	0
15.3	1	1	1	0	1	1	0	0	0
16.5	1	0	0	0	0	0	0	0	0
17.8	1	0	1	0	0	0	0	0	0
20.6	1	0	1	0	0	1	0	0	0
21.6	0	0	0	1	0	0	0	0	0
22.9	1	0	0	0	0	0	0	0	0
23.3	1	1	1	0	0	1	0	0	0
24.3	1	0	1	1	0	1	0	0	0
25.2	0	1	0	0	0	1	0	0	0
26.1	1	0	1	1	0	0	0	0	0
26.9	0	0	1	0	0	0	0	0	0
27.5	1	0	1	0	0	0	0	0	0
27.9	1	1	0	0	1	1	0	0	0
28.3	1	1	1	0	0	1	0	1	0
29	1	1	1	0	1	1	0	0	0
30.3	1	0	0	0	0	0	1	0	0
31.5	1	0	0	0	0	0	0	0	0
32.8	0	0	0	0	0	1	0	0	0
33.8	1	1	0	1	0	1	0	0	0
34.7	1	1	0	0	0	0	0	0	0
35.6	0	0	0	0	0	0	0	0	0
36.5	1	0	0	0	0	0	1	0	0
37.3	1	1	1	0	0	1	0	0	0
38.7	1	1	0	0	0	1	1	0	0
39	1	1	1	0	0	1	1	0	0
40.3	1	1	0	0	0	1	1	0	0
40.7	1	1	1	0	0	1	1	0	0
41.1	1	1	0	0	0	1	1	0	0

41.51	1	0	1	0	1	1	1	0	0
42	0	0	0	0	0	0	0	0	0
42.5	1	1	1	0	1	1	1	0	0
43.1	1	1	1	0	0	1	0	0	0
43.6	1	1	1	0	1	1	1	0	0
43.7	1	0	0	1	0	1	1	0	0
43.8	1	1	1	0	1	1	1	0	0
43.9	1	1	1	1	1	1	1	0	0
44.2	1	1	1	0	1	1	0	0	1
44.5	1	1	1	1	1	1	1	0	1
44.9	0	0	0	0	0	0	0	0	0
45.5	1	1	0	1	1	1	1	0	1
46	1	0	1	0	0	1	0	0	1
46.5	0	0	0	0	0	0	0	0	0
47.6	0	0	0	0	0	0	0	0	0
47.8	0	0	0	0	0	0	0	0	0
48.2	0	0	0	0	0	0	0	0	0
49.2	0	0	0	0	0	0	0	0	0
49.5	0	0	0	0	0	0	0	0	0
50.2	0	0	0	0	0	0	0	0	0
52.5	0	0	0	0	0	0	0	0	0
54.5	0	0	0	0	0	0	0	0	0
55.7	0	0	0	0	0	0	0	0	0
56	0	0	0	0	0	0	0	0	0
57.2	0	0	0	0	0	0	0	0	0
58.6	0	0	0	0	0	0	0	0	0
58.9	0	0	0	0	0	0	0	0	0
60.7	0	0	0	0	0	0	0	0	0
62	0	0	0	0	0	0	0	0	0
64	0	0	0	0	0	0	0	0	0
64.6	0	0	0	0	0	0	0	0	0
65.1	0	0	0	0	0	0	0	0	0
66	1	0	1	0	0	0	0	0	0
68.6	1	0	1	0	0	0	0	0	0
70	1	0	1	0	0	0	0	0	0
71	0	0	0	0	0	0	0	0	0
72.2	1	0	1	0	0	0	1	0	0
73	0	1	1	1	0	0	1	0	0
74.4	1	0	1	0	0	0	1	0	0
75.4	0	0	0	0	0	0	0	0	0
77	0	0	0	0	0	0	0	0	0
77.3	0	0	1	1	0	0	1	0	0
78	1	1	1	0	0	1	1	0	0
79	1	1	1	1	0	0	1	0	0

79.2	1	0	1	0	0	1	1	0	0
80.5	1	1	1	1	0	1	1	0	0
81.5	1	0	1	0	0	1	0	0	0
82.5	1	0	1	1	0	1	1	0	0
84.2	1	0	1	0	0	1	0	0	0
86	0	0	1	1	0	0	1	1	0
86.9	0	0	1	0	0	0	0	0	0
87.4	0	0	0	1	0	0	1	1	0
89.1	0	0	0	0	0	0	0	0	0
90.2	1	0	0	1	1	0	1	1	0
91.2	0	0	0	0	0	0	1	1	0
92.4	1	0	0	1	0	0	1	1	0
93	1	0	0	0	0	0	0	1	0
93.6	0	0	0	0	0	0	0	0	0
93.9	1	0	0	1	0	0	1	1	0
95.4	0	0	0	0	0	0	0	0	0
95.9	1	0	0	0	1	0	0	0	0
96.4	1	1	1	1	1	1	1	1	0
97.6	0	0	0	0	0	0	0	0	0
97.9	1	0	0	0	0	0	1	1	0
99.2	0	0	0	0	0	0	0	0	0
100.6	1	0	1	0	1	0	1	1	0
103.4	0	0	0	0	0	0	0	0	0
105.1	0	0	0	0	0	0	0	0	0

height	bivalve	gastropod	brachiopod	echinoderm	ostracod	coral	bryozoan	sponge	foram
0	1	1	0	0	1	0	0	0	1
7	1	0	0	0	0	0	0	0	0
13	1	0	0	1	0	0	0	0	1
19	0	0	0	0	0	0	0	0	0
20	0	0	0	0	0	0	0	0	0
24	1	1	0	1	1	0	0	0	1
28	0	0	0	1	1	0	0	0	0
34	1	1	0	1	1	0	0	0	1
40	0	0	0	0	0	0	0	0	0
45	0	0	0	0	0	0	0	0	0
52	0	1	0	1	1	0	0	0	1
58	1	0	0	1	1	0	0	0	1
62	0	0	0	0	0	0	0	0	0
67	1	1	0	1	1	0	0	0	1
72	0	0	0	1	1	0	0	0	1
78	1	0	1	1	1	0	0	0	1
93	1	1	0	1	1	0	0	0	1
96	1	1	0	1	1	0	0	0	1
103	1	0	0	1	1	0	0	0	1
109	1	0	0	1	1	0	0	0	1
115	0	1	0	1	1	0	0	0	1
117	0	0	0	0	0	0	0	0	0
121	0	0	0	0	0	0	0	0	0
123	0	0	0	0	0	0	0	0	1
125	1	1	0	0	0	0	0	0	0
129	1	1	0	1	0	0	0	0	0
133	0	0	0	0	1	0	0	0	0
136	0	0	0	0	0	0	0	0	0
139	0	0	0	0	0	0	0	0	0
141	0	1	0	0	1	0	0	0	0
143	0	0	0	0	1	0	0	0	1
145	0	0	0	0	0	0	0	0	1
147	0	1	0	0	1	0	0	0	1
153	0	0	0	0	1	0	0	0	1
156	0	0	0	0	0	0	0	0	1
163	1	0	0	0	0	0	0	0	1
169	0	0	0	0	0	0	0	0	0
174	0	0	0	0	0	0	0	0	0
176	0	1	0	0	0	0	0	0	0
178	1	1	0	0	0	0	0	0	0
182	0	0	0	0	0	0	0	0	0
185	0	0	0	0	0	0	0	0	1
188	1	1	0	0	1	0	0	0	1

194	0	0	0	0	0	0	0	0	0
197	1	1	0	0	0	0	0	0	1
199	1	1	0	1	0	0	0	0	0
203	1	1	0	0	0	0	0	0	0
207	0	1	0	0	1	0	0	0	0
212	0	0	0	0	0	0	0	0	0
218	0	0	0	0	0	0	0	0	0
220	0	0	0	0	0	0	0	0	0
229	1	1	0	0	1	0	0	0	1
235	1	0	0	0	1	0	0	0	1
241	0	0	0	1	1	0	0	0	1
253	0	0	0	0	0	0	0	0	0
274	1	1	0	1	1	0	0	0	1
286	1	1	0	1	1	0	0	0	1
292	0	1	0	1	1	0	0	0	1
298	1	1	0	1	1	0	0	0	1
301	1	1	0	0	1	0	0	0	1
306	1	0	0	0	1	0	0	0	1
311	1	1	0	0	0	0	0	0	0
313	1	1	0	1	1	0	0	0	1
318	0	1	0	1	1	0	0	0	1
321	1	1	0	1	1	0	0	0	1
323	1	0	0	0	1	0	0	0	1

greenalga	redalga p	roblematica
0	0	0
1	0	1
1	0	1
0	0	1
0	0	0
1	0	1
1	0	1
1	0	1
0	0	0
0	0	0
1	0	1
1	0	1
0	0	0
1	0	1
1	0	1
1	0	0
1	0	0
1	0	1
1	0	1
1	0	1
1	0	1
0	0	0
0	0	0
0	0	1
0	0	1
0	0	1
0	0	1
0	0	0
0	0	0
0	0	1
0	0	1
0	0	1
0	0	1
0	0	1
0	0	1
0	0	0
0	0	1
0	0	1
0	0	1
0	0	1
0	0	1
0	0	1
0	0	1

0	0	0
1	0	0
1	0	1
1	0	1
0	0	1
0	0	1
0	0	1
0	0	1
0	0	1
0	0	1
0	0	1
0	0	0
1	0	0
1	0	0
0	0	0
1	0	0
0	0	0
0	0	0
1	0	0
0	0	1
0	0	1
0	0	0
0	0	1

height	bivalve	gastropod	brachiopod	echinoderm	ostracod	coral	bryozoan	sponge	foram
5.3	0	0	0	0	0	0	0	0	0
13.4	0	0	0	0	0	0	0	0	0
17.1	0	0	0	0	0	0	0	0	0
21	0	0	0	0	0	0	0	0	0
25.8	0	0	0	0	0	0	0	0	0
29	0	0	0	0	0	0	0	0	0
33.6	0	0	0	0	0	0	0	0	0
34	0	0	0	0	0	0	0	0	0
38	0	0	0	0	0	0	0	0	0
43.7	0	0	0	0	0	0	0	0	0
49.9	0	0	0	0	0	0	0	0	0
54.4	0	0	0	0	0	0	0	0	0
67	0	0	0	0	0	0	0	0	0
75	0	0	0	0	0	0	0	0	0
78.1	0	0	0	0	0	0	0	0	0
81.9	0	0	0	0	0	0	0	0	0
90.3	0	0	0	0	0	0	0	0	0
103.6	0	0	0	0	1	0	0	1	1
106.6	0	1	0	1	0	0	0	0	0
114.4	0	0	0	0	0	0	0	0	0
120	0	0	0	0	1	0	0	0	0
135.5	0	0	0	0	0	0	0	1	1
147.9	0	0	0	0	0	0	0	0	0
153.9	0	0	0	0	0	0	0	0	0
162.2	0	0	0	0	0	0	0	0	0
170	1	1	0	0	0	0	0	1	0
184.9	0	0	0	0	0	0	0	0	0
193.2	0	1	0	0	0	0	0	1	0
205.4	0	0	0	0	0	0	0	0	0
224.2	0	0	0	0	0	0	0	1	0
249.6	0	0	0	0	0	0	0	0	0
264.7	0	0	0	0	0	0	0	0	0
276.7	0	0	0	0	1	0	0	0	0
294	0	0	0	0	0	0	0	0	0
309.3	1	0	0	1	0	0	0	0	0
323.8	1	1	0	1	1	0	0	1	0
337.2	0	0	0	0	0	0	0	1	0
350	0	0	0	0	0	0	0	1	0
365	1	0	0	0	1	0	0	1	0
378.5	0	0	0	0	0	0	0	1	0
391	0	0	0	0	0	0	0	1	0
404.5	0	0	0	0	0	0	0	1	0

greenalga	redalga p	problematic	ozzo Glaciale
0	0	0	
0	0	0	
0	0	0	
0	0	0	
0	0	0	
0	0	0	
0	0	0	
0	0	0	
0	0	0	
0	0	0	
0	0	0	
0	0	0	
0	0	0	
0	0	0	
0	0	0	
0	0	0	
0	0	0	
0	0	0	
0	0	0	
0	0	0	
0	0	0	
0	0	0	
0	0	0	
0	0	0	
0	0	0	
0	0	0	
0	0	0	
0	0	0	
0	0	0	
0	0	0	
0	0	0	
0	0	0	
0	0	0	
0	0	0	
0	0	0	
0	0	0	
0	0	0	
0	0	0	
0	0	0	
0	0	0	
0	0	0	
0	0	0	

height	bivalve	gastropod	ostracod	foram	greenalga	sponge	echinoderm	peloid	ooid
2.8	1	1	1	1	1	0	1	1	0
9.8	1	0	0	0	0	0	1	0	0
20	0	0	0	0	0	0	1	0	0
30.8	1	0	1	0	0	0	1	1	0
40	1	0	1	0	0	0	1	1	0
46.9	1	1	1	1	1	0	1	1	0
49.9	1	1	1	1	1	0	1	0	0
51.2	1	1	1	1	1	0	1	0	0
52.2	1	1	1	0	0	0	1	0	0
64.7	0	0	0	0	0	0	0	0	0
69.3	1	0	1	1	0	0	0	0	0
71.8	0	0	1	0	0	0	0	1	0
80	0	0	0	0	0	0	0	0	0
80.8	0	0	0	0	0	0	0	1	0
81	0	1	0	1	0	0	0	1	1
85	1	0	0	1	0	0	0	1	1
87	1	1	0	0	0	0	0	1	1
88	1	1	0	1	1	0	1	0	0
89	0	0	0	1	0	0	1	1	1
91	1	0	0	0	0	0	0	1	1
92	1	0	0	0	0	0	0	0	0
93	1	0	0	1	1	0	0	1	1
95	1	0	0	0	0	0	0	1	1
98	1	0	1	0	0	0	0	1	1
100.6	0	0	0	0	0	0	0	1	1
101.4	0	0	0	0	0	0	0	0	0
102.5	0	0	0	0	0	0	0	1	1
103.5	0	0	0	0	0	0	0	0	0
108	0	0	0	0	0	0	0	0	0
114.4	0	0	0	0	0	0	0	0	0
119	0	0	0	0	0	0	0	0	0
128	0	0	0	0	0	0	0	0	0
134	0	0	0	0	0	0	0	0	0
140	0	0	0	0	0	0	0	0	0
145	0	0	0	0	0	0	0	1	0
150	0	0	0	0	0	0	0	0	0
158	0	0	1	0	0	0	0	0	0
167	0	0	0	0	0	0	0	0	0
168	1	0	0	0	0	0	0	0	1
169	0	0	0	0	0	0	0	0	0
173	0	0	1	0	0	0	0	0	0
180	0	0	0	0	0	0	0	0	0
185	0	0	0	0	0	0	0	0	0

198	0	0	0	0	0	0	0	0	0
202	0	0	0	0	0	0	0	0	0
210	0	0	0	0	0	0	0	0	0
214	0	0	0	0	0	0	0	0	0
219	0	0	0	0	0	0	0	0	0
226	0	0	0	0	0	0	0	0	1
231	0	0	1	0	0	0	0	0	0
238	0	0	1	0	0	0	0	0	0
240.75	1	0	0	0	0	0	0	1	1
242.9	0	0	1	0	0	0	0	0	0
245.6	1	0	1	0	0	0	1	0	0
250.3	1	1	1	0	0	0	1	0	0
255	1	1	1	1	0	0	1	1	0
259	1	1	1	1	0	0	1	0	0
260.4	1	1	1	0	0	1	0	1	0
262.5	1	1	1	0	0	0	1	0	0
264.5	0	0	1	0	0	0	0	1	0
269.5	1	0	1	0	0	0	1	0	0
271.5	1	0	1	0	0	0	0	0	0
272	1	1	1	0	0	0	1	0	0
277	0	0	1	0	0	1	0	0	0
278	0	0	1	1	0	1	0	0	0
296	1	1	1	1	0	1	0	1	0
306	1	1	1	0	0	1	1	0	0
324	1	1	1	1	0	1	1	1	0
333	1	0	1	0	0	1	0	0	0
348	1	0	1	1	0	1	0	0	0
363	0	0	1	1	0	1	0	0	0
378	0	0	0	0	0	1	0	0	0
390	1	0	1	1	0	1	1	0	0
417	0	0	1	0	0	1	1	1	0

Val Adrara

height	bivalve	gastropod	ostracod	foram	greenalgae	echinoderm	peloid	ooid	sponge
1.5	1	0	1	0	0	0	0	0	0
3.5	1	1	1	1	0	0	0	0	0
4.6	1	1	1	1	0	0	0	1	0
6	1	1	1	1	0	0	0	1	0
6.7	1	0	1	0	0	0	0	0	0
7.5	0	0	0	0	0	0	0	0	0
8.31	1	0	1	0	0	0	0	0	0
8.6	1	0	1	0	0	0	0	0	0
9	1	1	1	0	0	1	0	0	0
9.6	1	0	1	0	0	0	0	0	0
11.5	1	0	0	0	0	1	0	0	0
12.5	1	0	1	1	0	0	0	0	0
13.2	1	0	0	0	0	0	0	0	0
14.1	0	0	1	1	0	0	0	0	0
14.5	1	0	1	0	0	0	1	0	0
15.3	1	1	1	0	1	1	0	0	0
16.5	1	0	0	0	0	0	0	0	0
17.8	1	0	1	0	0	0	0	0	0
20.6	1	0	1	0	0	1	0	0	0
21.6	0	0	0	1	0	0	0	0	0
22.9	1	0	0	0	0	0	0	0	0
23.3	1	1	1	0	0	1	0	0	0
24.3	1	0	1	1	0	1	0	0	0
25.2	0	1	0	0	0	1	0	0	0
26.1	1	0	1	1	0	0	0	0	0
26.9	0	0	1	0	0	0	0	0	0
27.5	1	0	1	0	0	0	0	0	0
27.9	1	1	0	0	1	1	0	0	0
28.3	1	1	1	0	0	1	0	1	0
29	1	1	1	0	1	1	0	0	0
30.3	1	0	0	0	0	0	1	0	0
31.5	1	0	0	0	0	0	0	0	0
32.8	0	0	0	0	0	1	0	0	0
33.8	1	1	0	1	0	1	0	0	0
34.7	1	1	0	0	0	0	0	0	0
35.6	0	0	0	0	0	0	0	0	0
36.5	1	0	0	0	0	0	1	0	0
37.3	1	1	1	0	0	1	0	0	0
38.7	1	1	0	0	0	1	1	0	0
39	1	1	1	0	0	1	1	0	0
40.3	1	1	0	0	0	1	1	0	0
40.7	1	1	1	0	0	1	1	0	0
41.1	1	1	0	0	0	1	1	0	0

41.51	1	0	1	0	1	1	1	0	0
42	0	0	0	0	0	0	0	0	0
42.5	1	1	1	0	1	1	1	0	0
43.1	1	1	1	0	0	1	0	0	0
43.6	1	1	1	0	1	1	1	0	0
43.7	1	0	0	1	0	1	1	0	0
43.8	1	1	1	0	1	1	1	0	0
43.9	1	1	1	1	1	1	1	0	0
44.2	1	1	1	0	1	1	0	0	1
44.5	1	1	1	1	1	1	1	0	1
44.9	0	0	0	0	0	0	0	0	0
45.5	1	1	0	1	1	1	1	0	1
46	1	0	1	0	0	1	0	0	1
46.5	0	0	0	0	0	0	0	0	0
47.6	0	0	0	0	0	0	0	0	0
47.8	0	0	0	0	0	0	0	0	0
48.2	0	0	0	0	0	0	0	0	0
49.2	0	0	0	0	0	0	0	0	0
49.5	0	0	0	0	0	0	0	0	0
50.2	0	0	0	0	0	0	0	0	0
52.5	0	0	0	0	0	0	0	0	0
54.5	0	0	0	0	0	0	0	0	0
55.7	0	0	0	0	0	0	0	0	0
56	0	0	0	0	0	0	0	0	0
57.2	0	0	0	0	0	0	0	0	0
58.6	0	0	0	0	0	0	0	0	0
58.9	0	0	0	0	0	0	0	0	0
60.7	0	0	0	0	0	0	0	0	0
62	0	0	0	0	0	0	0	0	0
64	0	0	0	0	0	0	0	0	0
64.6	0	0	0	0	0	0	0	0	0
65.1	0	0	0	0	0	0	0	0	0
66	1	0	1	0	0	0	0	0	0
68.6	1	0	1	0	0	0	0	0	0
70	1	0	1	0	0	0	0	0	0
71	0	0	0	0	0	0	0	0	0
72.2	1	0	1	0	0	0	1	0	0
73	0	1	1	1	0	0	1	0	0
74.4	1	0	1	0	0	0	1	0	0
75.4	0	0	0	0	0	0	0	0	0
77	0	0	0	0	0	0	0	0	0
77.3	0	0	1	1	0	0	1	0	0
78	1	1	1	0	0	1	1	0	0
79	1	1	1	1	0	0	1	0	0

79.2	1	0	1	0	0	1	1	0	0
80.5	1	1	1	1	0	1	1	0	0
81.5	1	0	1	0	0	1	0	0	0
82.5	1	0	1	1	0	1	1	0	0
84.2	1	0	1	0	0	1	0	0	0
86	0	0	1	1	0	0	1	1	0
86.9	0	0	1	0	0	0	0	0	0
87.4	0	0	0	1	0	0	1	1	0
89.1	0	0	0	0	0	0	0	0	0
90.2	1	0	0	1	1	0	1	1	0
91.2	0	0	0	0	0	0	1	1	0
92.4	1	0	0	1	0	0	1	1	0
93	1	0	0	0	0	0	0	1	0
93.6	0	0	0	0	0	0	0	0	0
93.9	1	0	0	1	0	0	1	1	0
95.4	0	0	0	0	0	0	0	0	0
95.9	1	0	0	0	1	0	0	0	0
96.4	1	1	1	1	1	1	1	1	0
97.6	0	0	0	0	0	0	0	0	0
97.9	1	0	0	0	0	0	1	1	0
99.2	0	0	0	0	0	0	0	0	0
100.6	1	0	1	0	1	0	1	1	0
103.4	0	0	0	0	0	0	0	0	0
105.1	0	0	0	0	0	0	0	0	0

height	bivalve	gastropod	brachiopod	echinoderm	ostracod	coral	bryozoan	sponge	foram
0	1	1	0	0	1	0	0	0	1
7	1	0	0	0	0	0	0	0	0
13	1	0	0	1	0	0	0	0	1
19	0	0	0	0	0	0	0	0	0
20	0	0	0	0	0	0	0	0	0
24	1	1	0	1	1	0	0	0	1
28	0	0	0	1	1	0	0	0	0
34	1	1	0	1	1	0	0	0	1
40	0	0	0	0	0	0	0	0	0
45	0	0	0	0	0	0	0	0	0
52	0	1	0	1	1	0	0	0	1
58	1	0	0	1	1	0	0	0	1
62	0	0	0	0	0	0	0	0	0
67	1	1	0	1	1	0	0	0	1
72	0	0	0	1	1	0	0	0	1
78	1	0	1	1	1	0	0	0	1
93	1	1	0	1	1	0	0	0	1
96	1	1	0	1	1	0	0	0	1
103	1	0	0	1	1	0	0	0	1
109	1	0	0	1	1	0	0	0	1
115	0	1	0	1	1	0	0	0	1
117	0	0	0	0	0	0	0	0	0
121	0	0	0	0	0	0	0	0	0
123	0	0	0	0	0	0	0	0	1
125	1	1	0	0	0	0	0	0	0
129	1	1	0	1	0	0	0	0	0
133	0	0	0	0	1	0	0	0	0
136	0	0	0	0	0	0	0	0	0
139	0	0	0	0	0	0	0	0	0
141	0	1	0	0	1	0	0	0	0
143	0	0	0	0	1	0	0	0	1
145	0	0	0	0	0	0	0	0	1
147	0	1	0	0	1	0	0	0	1
153	0	0	0	0	1	0	0	0	1
156	0	0	0	0	0	0	0	0	1
163	1	0	0	0	0	0	0	0	1
169	0	0	0	0	0	0	0	0	0
174	0	0	0	0	0	0	0	0	0
176	0	1	0	0	0	0	0	0	0
178	1	1	0	0	0	0	0	0	0
182	0	0	0	0	0	0	0	0	0
185	0	0	0	0	0	0	0	0	1
188	1	1	0	0	1	0	0	0	1

194	0	0	0	0	0	0	0	0	0
197	1	1	0	0	0	0	0	0	1
199	1	1	0	1	0	0	0	0	0
203	1	1	0	0	0	0	0	0	0
207	0	1	0	0	1	0	0	0	0
212	0	0	0	0	0	0	0	0	0
218	0	0	0	0	0	0	0	0	0
220	0	0	0	0	0	0	0	0	0
229	1	1	0	0	1	0	0	0	1
235	1	0	0	0	1	0	0	0	1
241	0	0	0	1	1	0	0	0	1
253	0	0	0	0	0	0	0	0	0
274	1	1	0	1	1	0	0	0	1
286	1	1	0	1	1	0	0	0	1
292	0	1	0	1	1	0	0	0	1
298	1	1	0	1	1	0	0	0	1
301	1	1	0	0	1	0	0	0	1
306	1	0	0	0	1	0	0	0	1
311	1	1	0	0	0	0	0	0	0
313	1	1	0	1	1	0	0	0	1
318	0	1	0	1	1	0	0	0	1
321	1	1	0	1	1	0	0	0	1
323	1	0	0	0	1	0	0	0	1

greenalga	redalga p	roblematica
0	0	0
1	0	1
1	0	1
0	0	1
0	0	0
1	0	1
1	0	1
1	0	1
0	0	0
0	0	0
1	0	1
1	0	1
0	0	0
1	0	1
1	0	1
1	0	0
1	0	0
1	0	1
1	0	1
1	0	1
1	0	1
0	0	0
0	0	0
0	0	1
0	0	1
0	0	1
0	0	1
0	0	0
0	0	0
0	0	1
0	0	1
0	0	1
0	0	1
0	0	1
0	0	1
0	0	0
0	0	1
0	0	1
0	0	1
0	0	1
0	0	1
0	0	1
0	0	1

0	0	0
1	0	0
1	0	1
1	0	1
0	0	1
0	0	1
0	0	1
0	0	1
0	0	1
0	0	1
0	0	1
0	0	0
1	0	0
1	0	0
0	0	0
1	0	0
0	0	0
0	0	0
1	0	0
0	0	1
0	0	1
0	0	0
0	0	1

height	bivalve	gastropod	brachiopod	echinoderm	ostracod	coral	bryozoan	sponge	foram
5.3	0	0	0	0	0	0	0	0	0
13.4	0	0	0	0	0	0	0	0	0
17.1	0	0	0	0	0	0	0	0	0
21	0	0	0	0	0	0	0	0	0
25.8	0	0	0	0	0	0	0	0	0
29	0	0	0	0	0	0	0	0	0
33.6	0	0	0	0	0	0	0	0	0
34	0	0	0	0	0	0	0	0	0
38	0	0	0	0	0	0	0	0	0
43.7	0	0	0	0	0	0	0	0	0
49.9	0	0	0	0	0	0	0	0	0
54.4	0	0	0	0	0	0	0	0	0
67	0	0	0	0	0	0	0	0	0
75	0	0	0	0	0	0	0	0	0
78.1	0	0	0	0	0	0	0	0	0
81.9	0	0	0	0	0	0	0	0	0
90.3	0	0	0	0	0	0	0	0	0
103.6	0	0	0	0	1	0	0	1	1
106.6	0	1	0	1	0	0	0	0	0
114.4	0	0	0	0	0	0	0	0	0
120	0	0	0	0	1	0	0	0	0
135.5	0	0	0	0	0	0	0	1	1
147.9	0	0	0	0	0	0	0	0	0
153.9	0	0	0	0	0	0	0	0	0
162.2	0	0	0	0	0	0	0	0	0
170	1	1	0	0	0	0	0	1	0
184.9	0	0	0	0	0	0	0	0	0
193.2	0	1	0	0	0	0	0	1	0
205.4	0	0	0	0	0	0	0	0	0
224.2	0	0	0	0	0	0	0	1	0
249.6	0	0	0	0	0	0	0	0	0
264.7	0	0	0	0	0	0	0	0	0
276.7	0	0	0	0	1	0	0	0	0
294	0	0	0	0	0	0	0	0	0
309.3	1	0	0	1	0	0	0	0	0
323.8	1	1	0	1	1	0	0	1	0
337.2	0	0	0	0	0	0	0	1	0
350	0	0	0	0	0	0	0	1	0
365	1	0	0	0	1	0	0	1	0
378.5	0	0	0	0	0	0	0	1	0
391	0	0	0	0	0	0	0	1	0
404.5	0	0	0	0	0	0	0	1	0

greenalga	redalga	problematica
0	0	0
0	0	0
0	0	0
0	0	0
0	0	0
0	0	0
0	0	0
0	0	0
0	0	0
0	0	0
0	0	0
0	0	0
0	0	0
0	0	0
0	0	0
0	0	0
0	0	0
0	0	0
0	0	0
0	0	0
0	0	0
0	0	0
0	0	0
0	0	0
0	0	0
0	0	0
0	0	0
0	0	0
0	0	0
0	0	0
0	0	0
0	0	0
0	0	0
0	0	0
0	0	0
0	0	0
0	0	0
0	0	0
0	0	0
0	0	0
0	0	0
0	0	0

height	bivalve	gastropod	ostracod	foram	greenalga	sponge	echinoderm	peloid	ooid
2.8	1	1	1	1	1	0	1	1	0
9.8	1	0	0	0	0	0	1	0	0
20	0	0	0	0	0	0	1	0	0
30.8	1	0	1	0	0	0	1	1	0
40	1	0	1	0	0	0	1	1	0
46.9	1	1	1	1	1	0	1	1	0
49.9	1	1	1	1	1	0	1	0	0
51.2	1	1	1	1	1	0	1	0	0
52.2	1	1	1	0	0	0	1	0	0
64.7	0	0	0	0	0	0	0	0	0
69.3	1	0	1	1	0	0	0	0	0
71.8	0	0	1	0	0	0	0	1	0
80	0	0	0	0	0	0	0	0	0
80.8	0	0	0	0	0	0	0	1	0
81	0	1	0	1	0	0	0	1	1
85	1	0	0	1	0	0	0	1	1
87	1	1	0	0	0	0	0	1	1
88	1	1	0	1	1	0	1	0	0
89	0	0	0	1	0	0	1	1	1
91	1	0	0	0	0	0	0	1	1
92	1	0	0	0	0	0	0	0	0
93	1	0	0	1	1	0	0	1	1
95	1	0	0	0	0	0	0	1	1
98	1	0	1	0	0	0	0	1	1
100.6	0	0	0	0	0	0	0	1	1
101.4	0	0	0	0	0	0	0	0	0
102.5	0	0	0	0	0	0	0	1	1
103.5	0	0	0	0	0	0	0	0	0
108	0	0	0	0	0	0	0	0	0
114.4	0	0	0	0	0	0	0	0	0
119	0	0	0	0	0	0	0	0	0
128	0	0	0	0	0	0	0	0	0
134	0	0	0	0	0	0	0	0	0
140	0	0	0	0	0	0	0	0	0
145	0	0	0	0	0	0	0	1	0
150	0	0	0	0	0	0	0	0	0
158	0	0	1	0	0	0	0	0	0
167	0	0	0	0	0	0	0	0	0
168	1	0	0	0	0	0	0	0	1
169	0	0	0	0	0	0	0	0	0
173	0	0	1	0	0	0	0	0	0
180	0	0	0	0	0	0	0	0	0
185	0	0	0	0	0	0	0	0	0

198	0	0	0	0	0	0	0	0	0
202	0	0	0	0	0	0	0	0	0
210	0	0	0	0	0	0	0	0	0
214	0	0	0	0	0	0	0	0	0
219	0	0	0	0	0	0	0	0	0
226	0	0	0	0	0	0	0	0	1
231	0	0	1	0	0	0	0	0	0
238	0	0	1	0	0	0	0	0	0
240.75	1	0	0	0	0	0	0	1	1
242.9	0	0	1	0	0	0	0	0	0
245.6	1	0	1	0	0	0	1	0	0
250.3	1	1	1	0	0	0	1	0	0
255	1	1	1	1	0	0	1	1	0
259	1	1	1	1	0	0	1	0	0
260.4	1	1	1	0	0	1	0	1	0
262.5	1	1	1	0	0	0	1	0	0
264.5	0	0	1	0	0	0	0	1	0
269.5	1	0	1	0	0	0	1	0	0
271.5	1	0	1	0	0	0	0	0	0
272	1	1	1	0	0	0	1	0	0
277	0	0	1	0	0	1	0	0	0
278	0	0	1	1	0	1	0	0	0
296	1	1	1	1	0	1	0	1	0
306	1	1	1	0	0	1	1	0	0
324	1	1	1	1	0	1	1	1	0
333	1	0	1	0	0	1	0	0	0
348	1	0	1	1	0	1	0	0	0
363	0	0	1	1	0	1	0	0	0
378	0	0	0	0	0	1	0	0	0
390	1	0	1	1	0	1	1	0	0
417	0	0	1	0	0	1	1	1	0

Val Adrara

height	I/Ca ratios	stage	Italcementi
1.5	0.11638436	Rhaetian	
2.5	0.4147545	Rhaetian	
3.5	0.48662269	Rhaetian	
4.5	0.21234732	Rhaetian	
4.6	0.22124713	Rhaetian	
4.8	0.18699916	Rhaetian	
5	0.28009251	Rhaetian	
5.2	0.18705932	Rhaetian	
6	0.2511927	Rhaetian	
6.4	0.35096098	Rhaetian	
6.7	0.37493768	Rhaetian	
7.4	0.68923119	Rhaetian	
7.5	0.24974417	Rhaetian	
7.6	0.15222062	Rhaetian	
7.7	0.17262048	Rhaetian	
7.9	0.22184572	Rhaetian	
8.3	0.25365962	Rhaetian	
8.4	0.29917112	Rhaetian	
8.5	0.24714651	Rhaetian	
15	0.13219031	Rhaetian	
20.5	0.03130065	Rhaetian	
23.9	0.42906931	Rhaetian	
30.1	0	Rhaetian	
35.4	0.43851522	Rhaetian	
40.1	0.00652526	Rhaetian	
41.1	0.06208281	Rhaetian	
43.1	0.61769158	Rhaetian	
43.5	0.51095725	Rhaetian	
43.6	0.3043029	Rhaetian	
43.7	0.37933989	Rhaetian	
43.8	0.32461183	Rhaetian	
43.9	0.32562269	Rhaetian	
44.2	0.31032334	Rhaetian	
44.5	0.35676672	Rhaetian	
45.5	1.4293723	Rhaetian	
46	0.54052791	Rhaetian	
46.1	0.278198	Hettangian	
46.5	0.30434453	Hettangian	
46.8	0.3156856	Hettangian	
47	0.33077032	Hettangian	
47.8	0.27103742	Hettangian	
48	0.26484055	Hettangian	
49.9	0.1585904	Hettangian	
53	0.11168259	Hettangian	
56.6	0.27941121	Hettangian	
60.7	0.21001301	Hettangian	

61	0.42809386	Hettangian
65.3	0.26825504	Hettangian
70	0.01185157	Hettangian
72.9	0.38574635	Hettangian
77	0.01708235	Hettangian
80	0.67437623	Hettangian
84.8	0.03429122	Hettangian
86.5	0.09389566	Hettangian
90.2	0	Hettangian
93	0.10102217	Hettangian
95.1	0	Hettangian
98.3	0.14356164	Hettangian
100.6	0	Hettangian

height	I/Ca ratios	stage
0.5	0.17553944	Rhaetian
2.8	0.70584274	Rhaetian
6.8	0.33071266	Rhaetian
9.8	0.27584429	Rhaetian
16	1.92757485	Rhaetian
20	0.58230292	Rhaetian
24	0	Rhaetian
30.8	0.76108244	Rhaetian
34	0.34825307	Rhaetian
41.9	0.18360507	Rhaetian
46.9	0.39625049	Rhaetian
48	0.36897473	Rhaetian
50.3	0.34138592	Rhaetian
51.3	0.32985263	Rhaetian
53.5	0.44993818	Rhaetian
55	0.67721403	Rhaetian
57	0.61993325	Rhaetian
57.6	0.38564853	Rhaetian
57.9	0.04191127	Rhaetian
60.7	0.10373532	Rhaetian
64.7	0.26250336	lower-Hettangian
66.2	0.21074568	lower-Hettangian
67.7	0.26016131	lower-Hettangian
71.4	0.14259066	lower-Hettangian
79	0.47159107	lower-Hettangian
86	0	lower-Hettangian
90	0.34901169	lower-Hettangian
95	0	lower-Hettangian
100.6	0.18866823	lower-Hettangian
103.5	0.34182784	lower-Hettangian
106.5	0.36518116	lower-Hettangian
108	0.03116112	lower-Hettangian
110	0.58361463	lower-Hettangian
112	0	lower-Hettangian
115	0.92470904	lower-Hettangian
118	0.03855055	lower-Hettangian
122	0.12578035	lower-Hettangian
126	0.02515991	lower-Hettangian
129	0	lower-Hettangian
132	0	lower-Hettangian
135	0	lower-Hettangian
138	0	lower-Hettangian
141	0	lower-Hettangian
144	0	lower-Hettangian
147	0	lower-Hettangian
150	0.03213083	lower-Hettangian

154	0.25153159	lower-Hettangian
157	0.04376268	lower-Hettangian
160	0.03796047	lower-Hettangian
163	0.16692414	lower-Hettangian
166	0	lower-Hettangian
169	0	lower-Hettangian
172	0	lower-Hettangian
175	0	lower-Hettangian
178	0	lower-Hettangian
181	0	lower-Hettangian
184	0.13907046	lower-Hettangian
186.8	0	lower-Hettangian
190	0	lower-Hettangian
193	0	lower-Hettangian
196	0	lower-Hettangian
200	0	lower-Hettangian
203	0	lower-Hettangian
206	0.09016142	lower-Hettangian
209	0.10369134	lower-Hettangian
212	0.1417996	lower-Hettangian
215	0.11684494	lower-Hettangian
218	0.19509616	lower-Hettangian
222	0.1011641	lower-Hettangian
227	0	lower-Hettangian
230	0.04381678	lower-Hettangian
233	0.21926847	lower-Hettangian
236	0	lower-Hettangian
239	0	lower-Hettangian
241.03	0.19148491	lower-Hettangian
245	0.08528757	lower-Hettangian
249.1	0	lower-Hettangian
252	0.28336275	lower-Hettangian
255	0	lower-Hettangian
259.5	0	lower-Hettangian
263.2	0.11941185	lower-Hettangian
267.1	0	lower-Hettangian
271	0	lower-Hettangian
275	0	lower-Hettangian
279	0.36533796	lower-Hettangian
282	0.09414858	upper-Hettangian
286	0.5558097	upper-Hettangian
290	0.38184862	upper-Hettangian
294	0.1641992	upper-Hettangian
298	0.11979282	upper-Hettangian
302	0.16174032	upper-Hettangian
312	0	upper-Hettangian
322	0.21270885	upper-Hettangian

333	0.08711916	upper-Hettangian
342	0.27298681	upper-Hettangian
348	0.47240743	upper-Hettangian
356	0.31754261	upper-Hettangian
366	0.2982428	upper-Hettangian
375	0.39690318	upper-Hettangian
384	0.47134035	upper-Hettangian
393	0.36377763	upper-Hettangian
402	0.17061947	upper-Hettangian
411	0.30656529	upper-Hettangian
420	0.58691452	upper-Hettangian

height	I/Ca ratios	stage	Italcementi
1.5	0.11638436	Rhaetian	
2.5	0.4147545	Rhaetian	
3.5	0.48662269	Rhaetian	
4.5	0.21234732	Rhaetian	
4.6	0.22124713	Rhaetian	
4.8	0.18699916	Rhaetian	
5	0.28009251	Rhaetian	
5.2	0.18705932	Rhaetian	
6	0.2511927	Rhaetian	
6.4	0.35096098	Rhaetian	
6.7	0.37493768	Rhaetian	
7.4	0.68923119	Rhaetian	
7.5	0.24974417	Rhaetian	
7.6	0.15222062	Rhaetian	
7.7	0.17262048	Rhaetian	
7.9	0.22184572	Rhaetian	
8.3	0.25365962	Rhaetian	
8.4	0.29917112	Rhaetian	
8.5	0.24714651	Rhaetian	
15	0.13219031	Rhaetian	
20.5	0.03130065	Rhaetian	
23.9	0.42906931	Rhaetian	
30.1	0	Rhaetian	
35.4	0.43851522	Rhaetian	
40.1	0.00652526	Rhaetian	
41.1	0.06208281	Rhaetian	
43.1	0.61769158	Rhaetian	
43.5	0.51095725	Rhaetian	
43.6	0.3043029	Rhaetian	
43.7	0.37933989	Rhaetian	
43.8	0.32461183	Rhaetian	
43.9	0.32562269	Rhaetian	
44.2	0.31032334	Rhaetian	
44.5	0.35676672	Rhaetian	
45.5	1.4293723	Rhaetian	
46	0.54052791	Rhaetian	
46.1	0.278198	Hettangian	
46.5	0.30434453	Hettangian	
46.8	0.3156856	Hettangian	
47	0.33077032	Hettangian	
47.8	0.27103742	Hettangian	
48	0.26484055	Hettangian	
49.9	0.1585904	Hettangian	
53	0.11168259	Hettangian	
56.6	0.27941121	Hettangian	
60.7	0.21001301	Hettangian	

61	0.42809386	Hettangian
65.3	0.26825504	Hettangian
70	0.01185157	Hettangian
72.9	0.38574635	Hettangian
77	0.01708235	Hettangian
80	0.67437623	Hettangian
84.8	0.03429122	Hettangian
86.5	0.09389566	Hettangian
90.2	0	Hettangian
93	0.10102217	Hettangian
95.1	0	Hettangian
98.3	0.14356164	Hettangian
100.6	0	Hettangian

height	I/Ca ratios	stage
0.5	0.17553944	Rhaetian
2.8	0.70584274	Rhaetian
6.8	0.33071266	Rhaetian
9.8	0.27584429	Rhaetian
16	1.92757485	Rhaetian
20	0.58230292	Rhaetian
24	0	Rhaetian
30.8	0.76108244	Rhaetian
34	0.34825307	Rhaetian
41.9	0.18360507	Rhaetian
46.9	0.39625049	Rhaetian
48	0.36897473	Rhaetian
50.3	0.34138592	Rhaetian
51.3	0.32985263	Rhaetian
53.5	0.44993818	Rhaetian
55	0.67721403	Rhaetian
57	0.61993325	Rhaetian
57.6	0.38564853	Rhaetian
57.9	0.04191127	Rhaetian
60.7	0.10373532	Rhaetian
64.7	0.26250336	lower-Hettangian
66.2	0.21074568	lower-Hettangian
67.7	0.26016131	lower-Hettangian
71.4	0.14259066	lower-Hettangian
79	0.47159107	lower-Hettangian
86	0	lower-Hettangian
90	0.34901169	lower-Hettangian
95	0	lower-Hettangian
100.6	0.18866823	lower-Hettangian
103.5	0.34182784	lower-Hettangian
106.5	0.36518116	lower-Hettangian
108	0.03116112	lower-Hettangian
110	0.58361463	lower-Hettangian
112	0	lower-Hettangian
115	0.92470904	lower-Hettangian
118	0.03855055	lower-Hettangian
122	0.12578035	lower-Hettangian
126	0.02515991	lower-Hettangian
129	0	lower-Hettangian
132	0	lower-Hettangian
135	0	lower-Hettangian
138	0	lower-Hettangian
141	0	lower-Hettangian
144	0	lower-Hettangian
147	0	lower-Hettangian
150	0.03213083	lower-Hettangian

154	0.25153159	lower-Hettangian
157	0.04376268	lower-Hettangian
160	0.03796047	lower-Hettangian
163	0.16692414	lower-Hettangian
166	0	lower-Hettangian
169	0	lower-Hettangian
172	0	lower-Hettangian
175	0	lower-Hettangian
178	0	lower-Hettangian
181	0	lower-Hettangian
184	0.13907046	lower-Hettangian
186.8	0	lower-Hettangian
190	0	lower-Hettangian
193	0	lower-Hettangian
196	0	lower-Hettangian
200	0	lower-Hettangian
203	0	lower-Hettangian
206	0.09016142	lower-Hettangian
209	0.10369134	lower-Hettangian
212	0.1417996	lower-Hettangian
215	0.11684494	lower-Hettangian
218	0.19509616	lower-Hettangian
222	0.1011641	lower-Hettangian
227	0	lower-Hettangian
230	0.04381678	lower-Hettangian
233	0.21926847	lower-Hettangian
236	0	lower-Hettangian
239	0	lower-Hettangian
241.03	0.19148491	lower-Hettangian
245	0.08528757	lower-Hettangian
249.1	0	lower-Hettangian
252	0.28336275	lower-Hettangian
255	0	lower-Hettangian
259.5	0	lower-Hettangian
263.2	0.11941185	lower-Hettangian
267.1	0	lower-Hettangian
271	0	lower-Hettangian
275	0	lower-Hettangian
279	0.36533796	lower-Hettangian
282	0.09414858	upper-Hettangian
286	0.5558097	upper-Hettangian
290	0.38184862	upper-Hettangian
294	0.1641992	upper-Hettangian
298	0.11979282	upper-Hettangian
302	0.16174032	upper-Hettangian
312	0	upper-Hettangian
322	0.21270885	upper-Hettangian

333	0.08711916	upper-Hettangian
342	0.27298681	upper-Hettangian
348	0.47240743	upper-Hettangian
356	0.31754261	upper-Hettangian
366	0.2982428	upper-Hettangian
375	0.39690318	upper-Hettangian
384	0.47134035	upper-Hettangian
393	0.36377763	upper-Hettangian
402	0.17061947	upper-Hettangian
411	0.30656529	upper-Hettangian
420	0.58691452	upper-Hettangian